Design of Ultra wideband Microwave Antenna Array for Detection of Breast Cancer Tumours

by

Alistair Johnson

Electrical and Biomedical Engineering
Faculty Advisor: Prof. Nikolova

Electrical and Biomedical Engineering Project Report
submitted in partial fulfillment of the degree of
Bachelor of Engineering

McMaster University
Hamilton, Ontario, Canada
April 27th, 2009

Abstract

The capabilities of current medical devices to detect breast cancer are agreeably insufficient for society's needs. As such it is desirable for a new more reliable detection system to be fabricated. It has been reported in literature that cancerous tissue in the breast exhibits separate dielectric properties when compared to normal breast tissue at microwave frequencies. This report overviews the design and optimization of a novel microwave antenna which must serve as an element in a sensor array for early-stage breast-cancer detection. Specifically, the sensor detection limits will be ascertained. This includes determining the antenna sensitivity to tissue contrast between the suspect malignant growth and the surrounding healthy tissue in terms of permittivity and conductivity as well as the sensitivity limits in terms of the size of the malignant region and its depth under the skin (i.e., distance from the sensor). A two antenna system in which the antennas were opposing each other and co-polarized was used to determine these sensitivity limits. This set up was analyzed in both frequency domain simulations and experiments, using breast phantoms whose specific fabrication and properties are discussed in the report.

Keywords: microwave imaging, microwave tomography, breast cancer detection, breast phantom, phantom fabrication

Acknowledgements

The author would like to acknowledge the gracious help of Natalia Nikolova, PhD, for her invaluable guidance and unwavering support in designing the methodology, procedure, and final documentation for this project. The author would also like to thank Aastha Trehan, Reza Khalaj Amineh, and Li Liu for their assistance in the countless simulations and experiments performed.

Table of Contents

List of Tables

List of Figures

Nomenclature

True positive – Occurs when an imaging modality has detected a potential cancer which was later confirmed to be a true tumour.

False positive – Occurs when an imaging modality has detected a potential cancer which was later disregarded as it was not an actual tumour.

True negative – Occurs when an imaging modality detects nothing abnormal in a tissue which does not contain any cancerous tumours.

False negative – Occurs when an imaging modality detects nothing in a tissue which does contain a cancerous tumour.

Specificity – Specificity is a measure of an imaging modality's capability of discerning healthy tissue. It is measured clinically by taking the ratio of true negative cancers to the total number of cases where cancer was not present.

Sensitivity – Sensitivity is a measure of an imaging modality's capability of detecting a cancerous tumour. It is measured clinically by taking the ratio of true positive cancers to the total number of cancers. In this report, the sensitivity relates to the ability of the antenna to detect an abnormal presence in the host tissue compared to the same measurements when no abnormal tissue is present.

Contrast – The factor by which one medium's dielectric properties are higher than another's. For example, a tumour with a permittivity contrast of 5 indicates that it's permittivity, ε, is five times greater than the host medium.

Phantom – A fabricated substance intended to act as an equivalent model of some form of biological tissue.

Introduction

Currently cancer is one of the leading causes of mortality, with more deaths per year than heart disease in those under 85 years of age [5]. Breast cancer, the most frequently occurring cancer with an estimated 182,460 new cases in 2008, accounted for approximately 26% of all newly diagnosed cancers in 2008 in America [5]. Its relative frequency in relationship to other cancers in females is most readily observed in Figure 1. Furthermore, although statistics from the US mortality data project breast cancer deaths to be decreasing for the past decade, in 2004 they still accounted for 15.5% of all female cancer deaths [3]. A graphical comparison of the cancer death rates can be seen in Figure 2. In 2002, it was estimated that 103.7 per 100,000 persons in the more developed countries worldwide were diagnosed with breast cancer [3]. In Canada, this rate increased to 124.0 per 100,000 persons, with 33.7 per 100,000 persons dying due to the disease [3]. Clearly there exists a strong need for more effective breast cancer detection systems in order to further decrease the mortality rate of this disease.

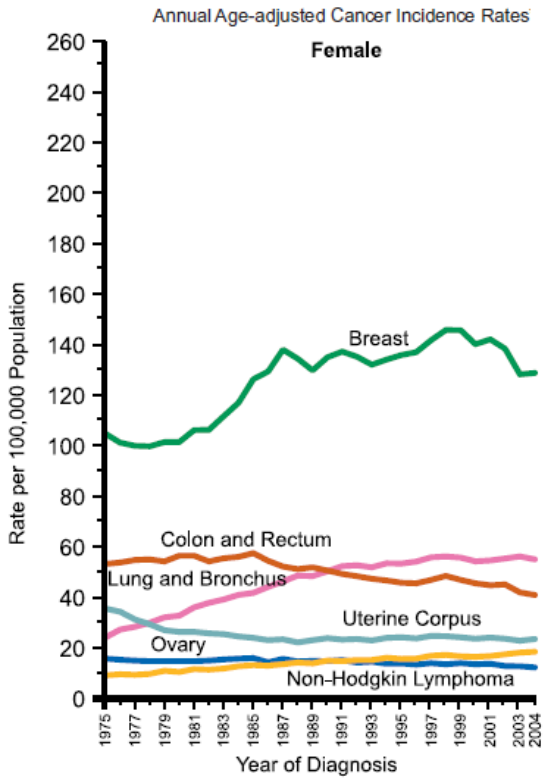

Figure 1: Annual Age-adjusted Cancer Incidence Rates.

Source: US Mortality Data, 1960 to 2004, US Mortality Volumes, 1930 to 1959, National Center for Health Statistics, Centers for Disease Control and Prevention, 2006.

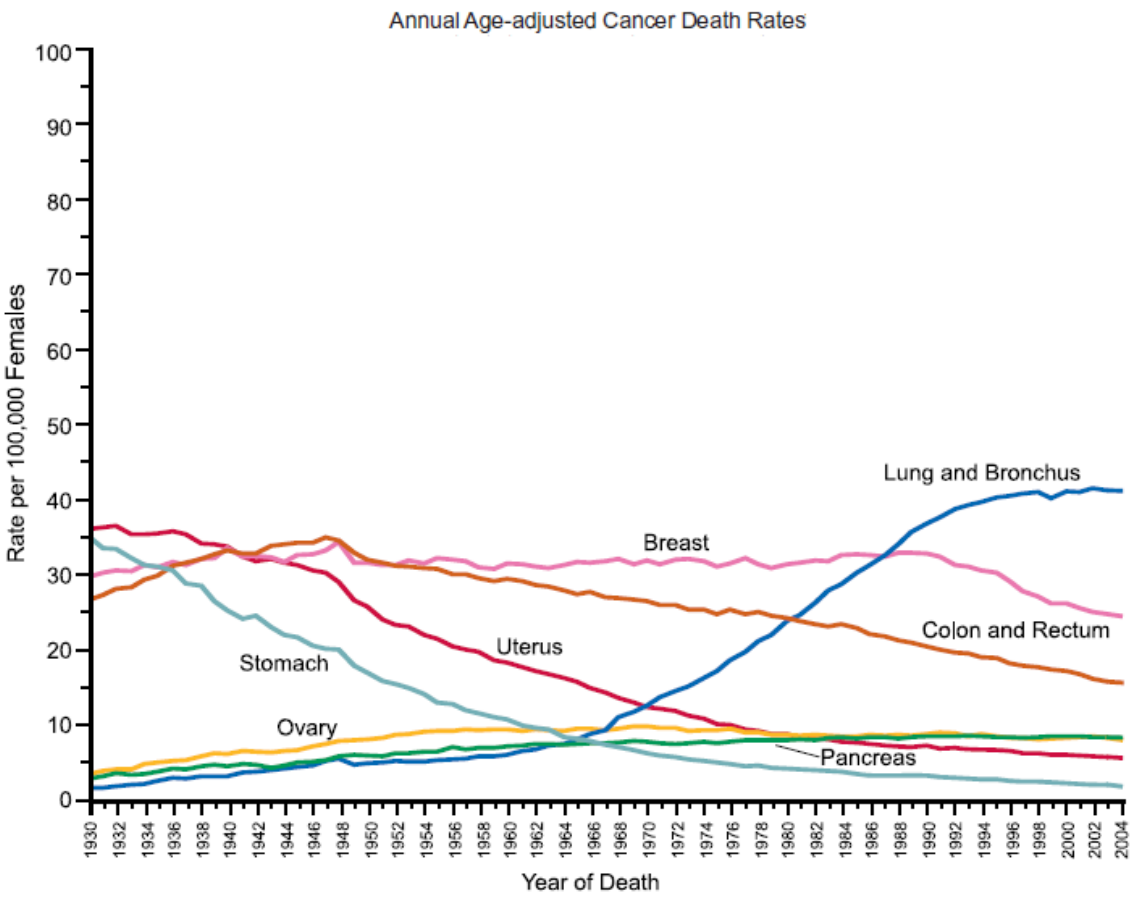

Figure 2: Annual Age-adjusted Cancer Death Rates.

Source: US Mortality Data, 1960 to 2004, US Mortality Volumes 1930 to 1959, National Center for Health Statistics, Centers for Disease Control and Prevention, 2006.

There currently exist three ulterior methods for detecting breast cancer clinically. The first, mammography, is the most common method and relied on the most by practitioners. The second, breast palpation, is used frequently by physicians as a non-invasive method of detecting breast cancer but it is mainly used to supplement other detection systems rather than replace them. The third and least frequently used system is breast MRI, which although effective in detecting the cancer is very expensive and not practical for wide spread breast cancer screening.

Mammography is currently the gold-standard method for breast cancer screening in clinical use today. Mammography involves the use of breast compression followed by high intensity x-rays in order to obtain a 2D image of the breast. Aside from the lack of comfort provided for the patient in the extreme compression phase, mammography has

the significant disadvantage of using ionizing radiation in order to image the breast. The National Research Council has reported many potential risks to ionizing radiation exposure, ranging from potential genetic alterations to newly generated cancerous tumours [5]. Although studies show the risk of these ionizing procedures to be acceptable, one such study finding a rate of 36.5 lives saved per life lost [7]; it is very much desired to reduce this risk as much as possible. The stigma alone of a cancer detection system causing cancer may lead to a reduction in the frequency of use of said imaging modality [2]. Furthermore, the accuracy of modern day mammography leaves much to be desired in terms of detection rates. The sensitivity of a Mammography to invasive breast cancers was shown in one study to be as low as 33.3% [8]. A whopping two thirds of the women screened by mammography currently had some form of a breast cancer tumour but were unaware due to the lack of detection by mammography. This is a huge disadvantage of mammography, and the area in which Microwave Imaging may provide the most utility in potential future clinical applications.

Breast palpation, both performed clinically and by individually, has been a long standing method of attempting to detect any malignancies in breast cancer tissue. However, it suffers many crippling drawbacks. The first of which is the lack of standardization in the method of clinical breast examination. There exist a wide variety of techniques that are used to attempt to detect breast cancer, and as such it is difficult to estimate the efficacy of this specific technique. Keeping this factor in mind, studies have shown breast examination to have a sensitivity of 17.6-21.6% [8][16]. In comparing it with mammography, three recent studies have shown that clinical breast examination was able to detect 4.6% to 5.7% of cancers that mammography was not able to detect alone [9][10][11]. However, clinical breast examination has also been shown to suffer from a false positive rate of 13.4%, causing immeasurable psychological trauma [12]. Furthermore, studies have shown breast self examination, even when the woman is sufficiently and rigorously trained in her methodology, to be ineffective at altering cancer mortality rates, even though physician visits and benign breast tumour biopsies increased in the control grouped educated in BSE [13][14][15]. As such, although clinical breast examination may be effective in some cases in detecting cancer in conjunction with mammography, it cannot be solely relied on to accurately detect breast cancer tumours.

The third and final imaging modality used for detecting breast cancer, MRI, has shown the most effectiveness at performing its task, however still remains the least used method for breast cancer screening. In a study performed on women with a high risk factor for cancer, over 15%, the sensitivity of MRI was estimated to be 71.1%, compared to 40% for mammography and 17.8% for clinical breast examination [8]. The problem with MRI, however, is its associated cost and relative low amount of units globally. Specifically in Canada, the number of MRI units present in 2007 was estimated to be 222, a sharp increase from its previous number of 30 in 1993 [19]. However, even with the large increase in units, waiting times for MRI scans are still very lengthy, and the number of MRIs is a measly 6.74 per million people residing in Canada [19]. Furthermore, the number of MRIs per Canadian female, whose risk of breast cancer is far greater than their respective gender counterpart, rises to 13.33 MRIs per million persons, which still remains as a wholly unimpressive figure. Clearly, widespread screening of breast cancer using MRI is completely infeasible and a new, lower cost alternative must be developed in order to meet the demand for such a large target population.

This brief introduction to the severity of breast cancer and the lack of effectiveness of the current detection methods, be it due to sensitivity or availability, has strongly outlined a need for a novel imaging modality that is both relatively inexpensive to construct and at the same time remains sensitive to malignant tumours in the tissue. Microwave Imaging of the breast has the promise of fulfilling both of these desired criteria. It has been shown in literature that there is a contrast in the dielectric properties of tumours when compared to normal tissue [1][1]. It is thus theoretically possible to use this dielectric property shift as a signature of cancerous tissue, and consequently with proper development of microwave antennas detect breast cancer. One antenna, which has been designed to meet this goal, has been chosen to be tested in regards to its sensitivity. Specifically, the goal of this report is to analyze how sensitive this antenna is to a variety of tumour sizes, contrasts, and locations when placed in a co-polarized dual antenna set up. This will be accomplished through both simulations and experimental analysis of in lab fabricated antennas. It will be ascertained whether or not the antenna could practically serve as a detector for breast cancer tumours, and the limits of its sensitivity will be presented. The antenna's sensitivity will be qualified in regards to the size of the tumour, the contrast of

the tumour with respect to the host medium, and the location of the tumour within the host medium. This sensitivity determined in this report is dependent on the complex S-parameters present in a dual antenna system. More specifically, the complex S-parameters of a situation where a tumour is present will be compared to the complex S-parameters of a situation where no tumour is present. Analysis of these two sets of S-parameters will be used in order to ascertain whether they are indicative of a change of the dielectric properties in the tissue, which is analogous to the presence of a tumour. This comparison is known as the tumour signature. Multiple tumour signatures will be compared in this report in order to determine which most can most accurately and effectively detect the presence of a tumour. The S-parameters will be analyzed with respect to both their magnitudes and phases.

Literature Review

Microwave detection of breast cancer is a relatively new and promising field. As a result, much of the research that has been performed shows a potential for detecting a tumour but no commercialized product has been released insofar. As well, due to the wide variety of antenna designs, it can be difficult to compare two methods as they may have all together completely separate approaches. However, it is necessary to provide an overall idea of the preliminary state of this study.

One example antenna that has been designed by a group working in the same field is shown in Figure 3 [25]. The antenna is of a bowtie design, chosen because its cross-polarization allows for effective removal of the backscatter due to the chest wall while axially unsymmetrical tumours were permitted [25]. The group eventually were able to detect 1.5 cm long ellipsoidal tumour with a depth of 1 cm [25]. Although this shows that the overall method of microwave detection is feasible, an improvement in the sensitivity with regards to tumour depth and size is sought after. It is desirable to have sub centimetre detection of breast cancer tumours, as these tumours usually have not metastasized. Detection of the tumour before it has a chance to metastasize is critical in extending the life span of those afflicted with breast cancer.

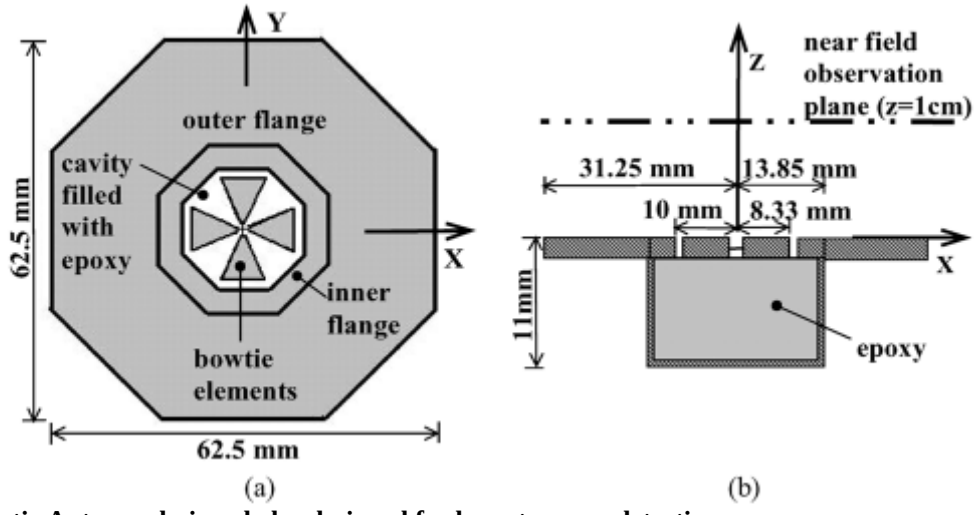

Figure 3: Bowtie Antenna designed also designed for breast cancer detection

Other groups have had more success using a CPW-fed elliptical slot antenna on LCP, an antenna whose design is more accurately detailed in [26]. The antenna's sensitivity was

tested on a heterogeneous breast simulation using the commercial software "Microstripes". The model is shown in Figure 4.

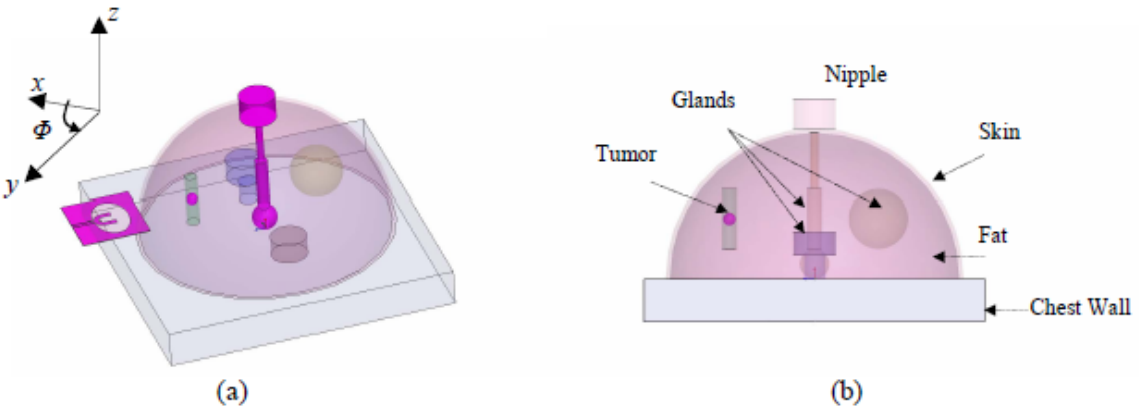

Figure 4: Breast phantom model. A) Isometric view b) Side view

The specific details of the model are detailed in [27]. In their simulations, they rotated the antenna about the breast and examined the power reflected by the tissue. Their results are shown in Figure 5.

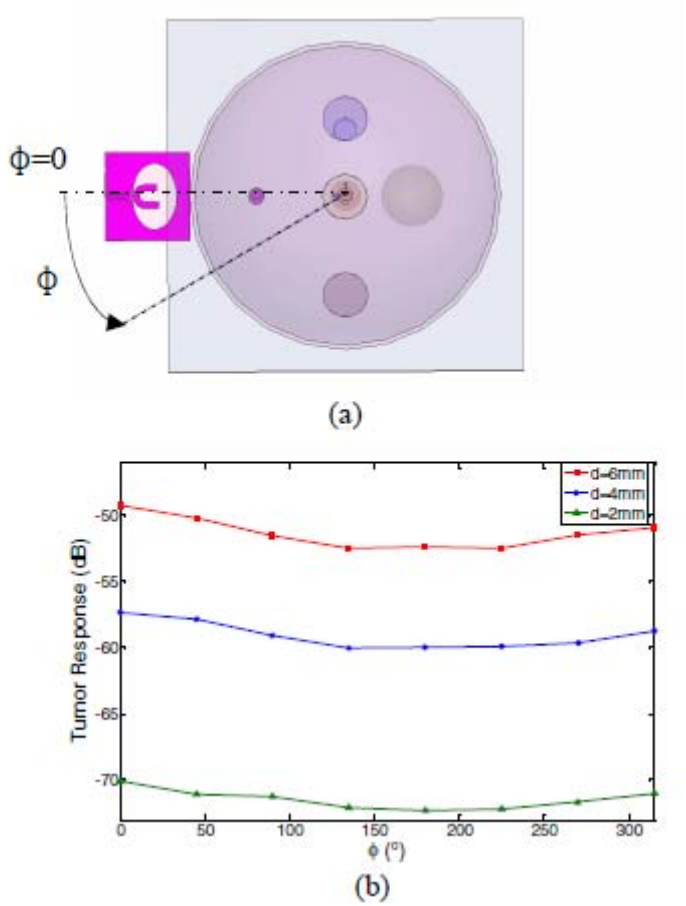

Figure 5: a) Cross section of model showing the rotational direction. The antenna is rotated by 45° for each iteration. b) Tumour response levels for 3 sizes of the tumour

It appears as if their tumour does show some sensitivity in regards to relative size. However, the paper fails to detail how the tumour response is calculated and differentiated from the other glands present in the breast. As well, there is very little difference in the tumour response with regard to its distance from the antenna. As a result, the antenna may not be capable to accurately predict the general location of the tumour. This would make clinical biopsies, an excellent confirmation of a potential cancer diagnosis, a virtual impossibility. Although their antenna shows great promise with regards to its sensitivity to the presence of a tumour, its sensitivity to the location of the tumour leaves much to be desired. The antenna analyzed in this paper will be used in a similar sweeping fashion, however it is designed such that any signals received that are indicative of a tumour will be localized, and as such specifying the location of any potential tumours will be greatly simplified.

In reviewing two of the works it can be observed that although the different antennas proposed each have their unique advantages, none of them are able to maintain collective sensitivity to the size, location, and depth of the tumour. It is here that the antenna analyzed in this paper hopes to improve upon previous works. Due to its special design, detailed in the next section, it is capable of localizing the power generated to the front aperture. This will allow for a better tumour contrast, as more power is emitted into the tissue of interest, while at the same time providing localization of the received signal, as the sections of the tissue not directly in front of the antenna front face do not receive much power.

Statement of Problem and Methodology of Solution

Before outlining the procedure used in determining the sensitivity of the antenna it is necessary to detail the construction of the antenna itself. The formal paper outlining the construction of the antenna can be found at [20], and a summary of the critical aspects of the design as they apply to this analysis follows.

The antenna used in these experiments is a TEM horn antenna. This specific type of antenna was chosen for three main reasons. The first was in order to direct all of the radiated power through the aperture, and consequently through the tissue. The second was to allow for an enclosure consisting of copper sheets and microwave absorbing sheets which effectively eliminate outside electromagnetic interference. The third and final reason was the removal of the need for a coupling liquid, which has many disadvantages outlined in previous papers [21][22].

The antenna consists of two flared plates with a balun in order to match the impedance of the antenna to that of the coaxial cable, set at 50 ohms. A micro-strip balun is used due to its effectiveness in ultra wide-band antennae [23]. The upper plate of the balun is connected to the coaxial core, and the lower plate of the balun is connected to the coaxial shield. Both of the widths of these plates are tapered, which allows for the impedance of the coaxial cable to gradually change to the impedance of the antenna. The antenna itself can be seen in Figure 6.

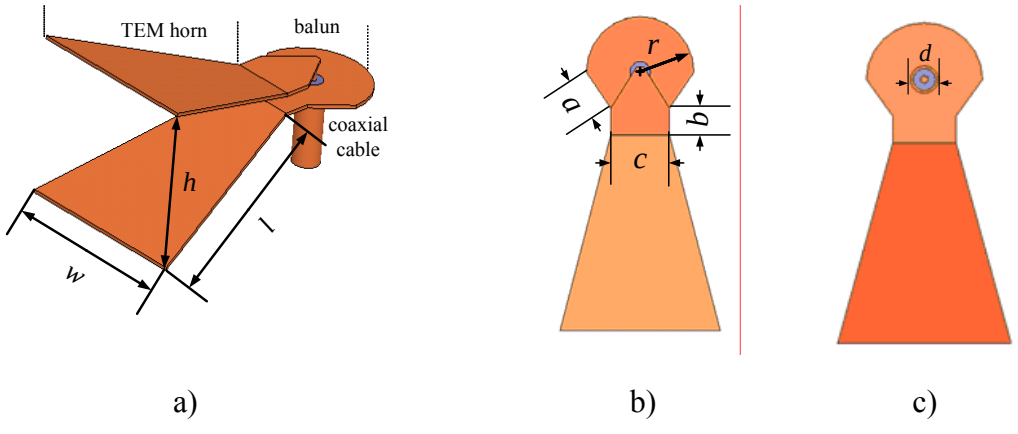

Figure 6: a) TEM horn antenna. b) Top view of the antenna. c) Bottom view of the antenna.

The TEM horn is then placed into a dielectric medium with $\varepsilon' = 10$ and $\tan\delta = 0.01$. This medium is solid state and acts to couple the antenna with the target tissue, negating the need of a coupling medium.

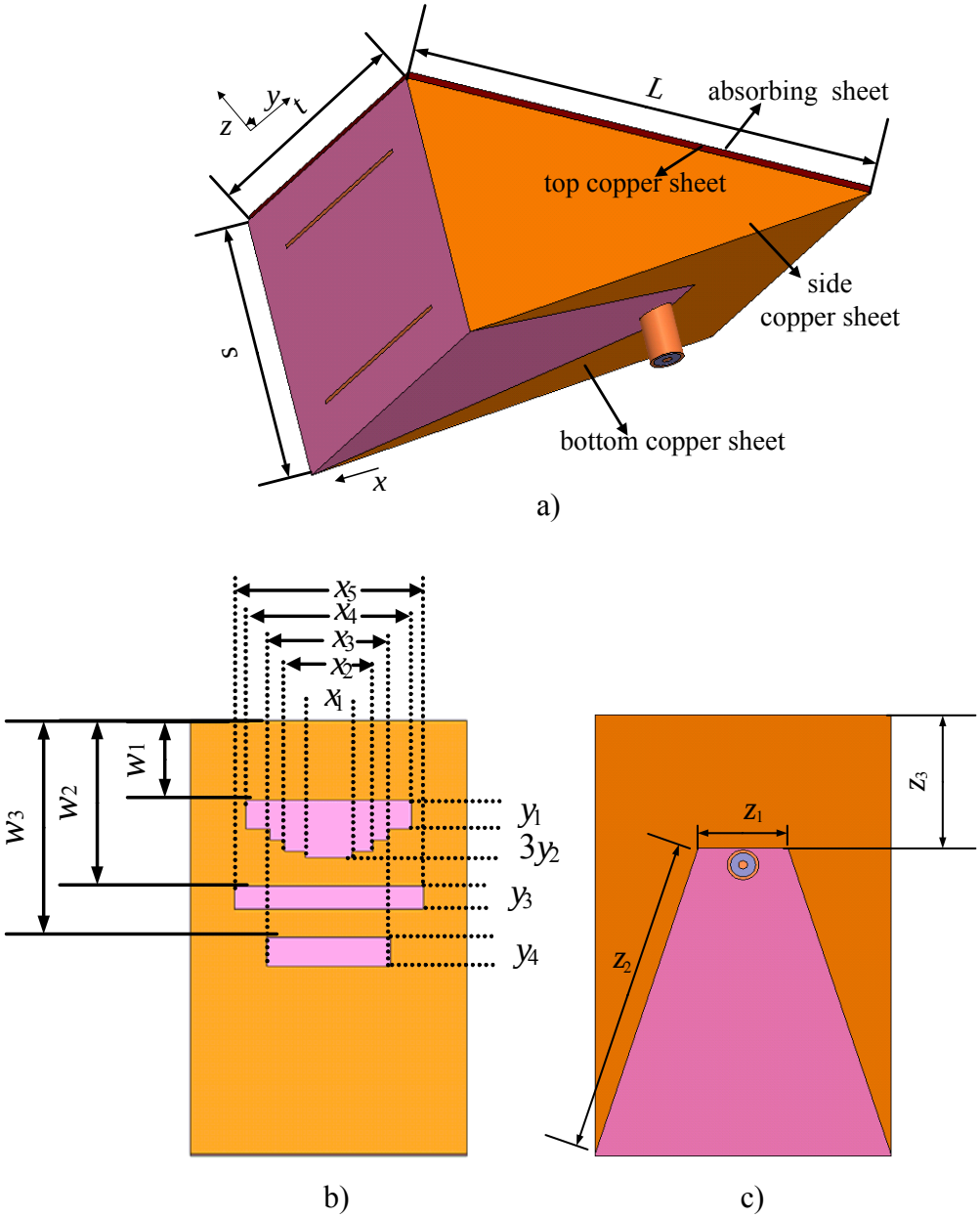

Figure 7: a) The TEM horn antenna placed in a dielectric medium. b) The copper sheet design on the top surface of the dielectric medium. C) The copper sheet design on the bottom surface of the dielectric medium, with the protruding coaxial cable connection visible.

The top side of this medium has specially designed copper sheets placed on both the top and bottom faces. It also has a microwave absorbing sheet placed on top of the

copper sheets on the top surface, which has $\varepsilon' \approx 30$, $\varepsilon'' \approx 2$, $\mu' \approx 1.7$, and $\mu'' \approx 2.7$. The medium is visualized in Figure 7.

There are a large number of parameters to be considered and optimized in order to improve the performance of the antenna. For the analysis performed in this report, the values of these parameters used are located in the appendix, Table 8.

This antenna was fabricated and tested using the experimental procedures outlined in its respective section. In addendum, the antenna was also modelled in a high frequency simulation software created by Ansoft; HFSS version 11. This software was used to rigorously analyze the sensitivity of the antenna due to the ease it allowed in accurately changing the simulation set up. As a result, the experimental tests were used in an attempt to verify the simulation results. Such a verification would then allow us to reasonably assume that the simulations accurately predict the results in a practical situation.

A final note is on the relation between the complex permittivity and the effective conductivity and relative permittivity. In the lab, when measuring the dielectric properties of the tissue, two frequency dependent variables are recorded: $\varepsilon'(\omega)$ and $\varepsilon''(\omega)$. These equations are related to the relative permittivity and the effective conductivity through the relationships in (1).

$$\sigma_{eff} = \varepsilon''(\omega) \times \varepsilon_0 \times \omega \tag{1}$$

Simulation Design Procedures

The antenna was modelled using the tools available in HFSS v. 11. A dual antenna system was the focal point of this study, and an example simulation design is shown in Figure 8 and Figure 9.

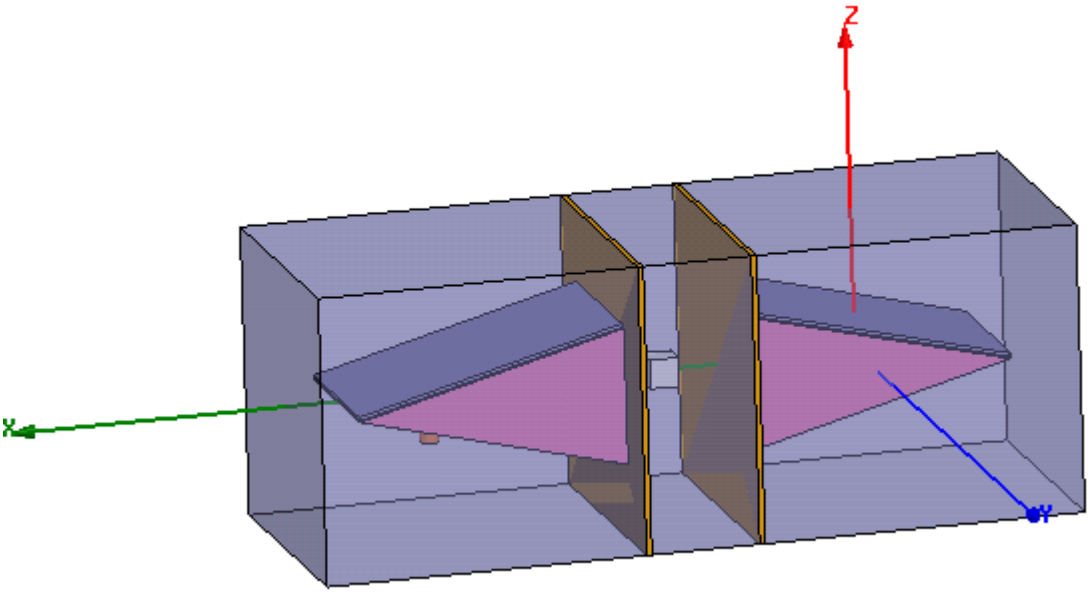

Figure 8: Example HFSS window with antenna simulation set up visible.

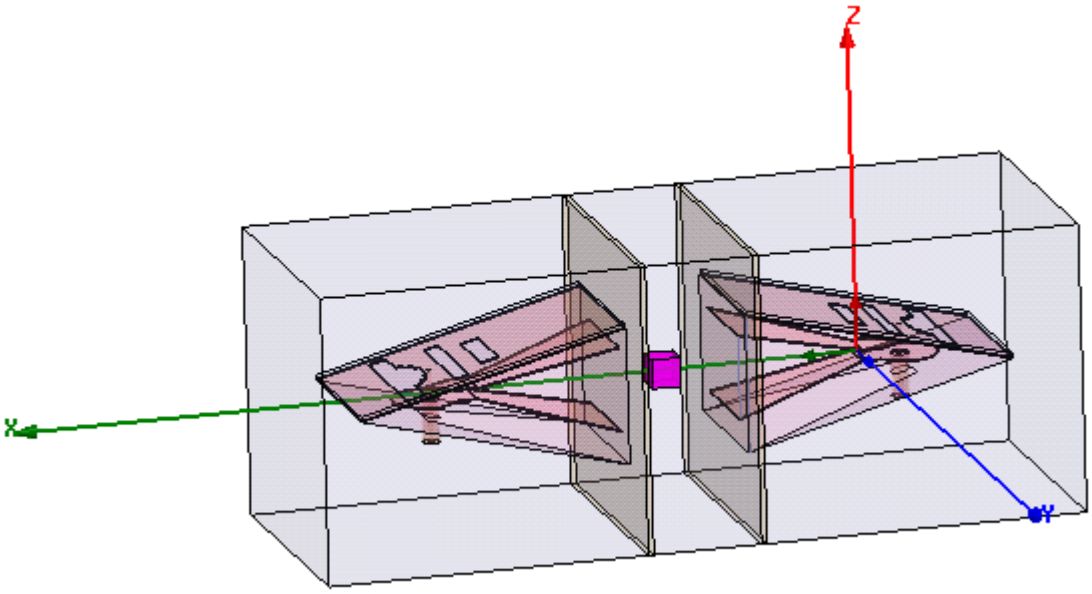

Figure 9: Example HFSS window with details of antennae exposed.

A simulation is performed by sweeping the frequency spectrum from 3 to 11 GHz and acquiring the S-parameters at each frequency with a maximum allowable error of 0.02. A large number of these simulations were performed for the three categories of sensitivity to the presence of a tumour: size, contrast, and location. The tumour was represented in all cases by a cuboid with varying side lengths and dielectric contrasts. The dielectric properties of the tumour were defined to be close to actual breast cancer tissue and frequency dependent. For the permittivity, values of 14, 10, 9, 8, and 7 were set for frequencies of 3, 5, 7, 9, and 11 GHz, respectively. For the conductivity, values of 2, 2.5, 2.7, 3.2, and 3.4 were set for frequencies of 3, 5, 7, 9, and 11 GHz. For the frequencies between the predefined set, the permittivity and conductivity were determined using linear interpolation of the two nearest frequencies. Plots of the two properties can be seen in Figure 10

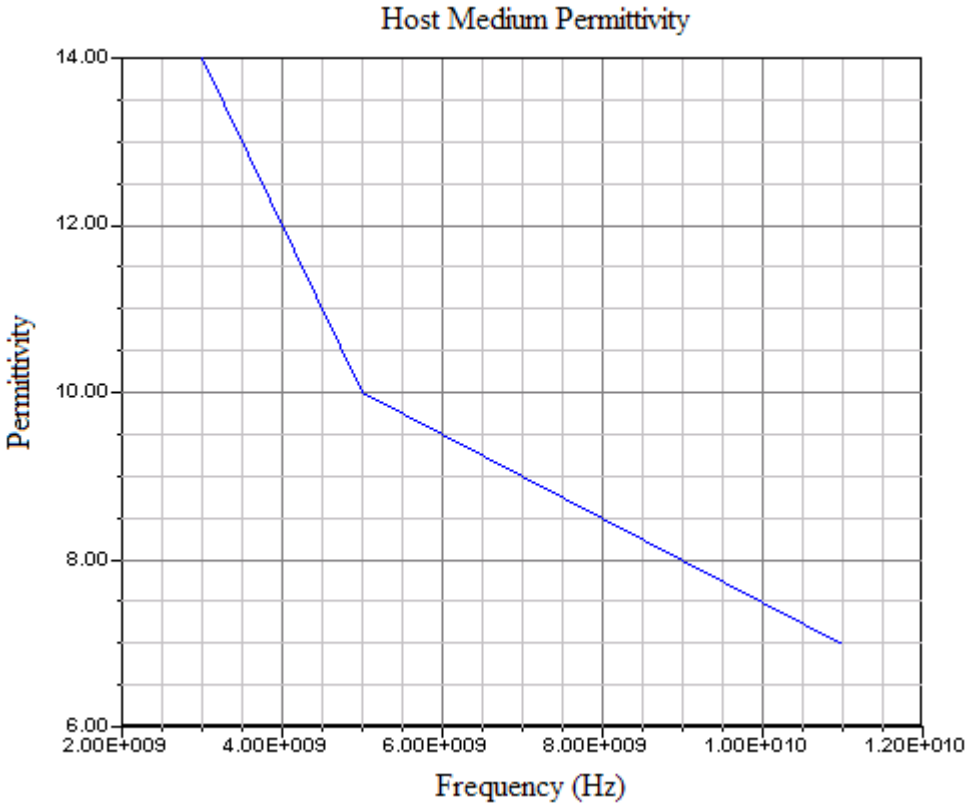

a)

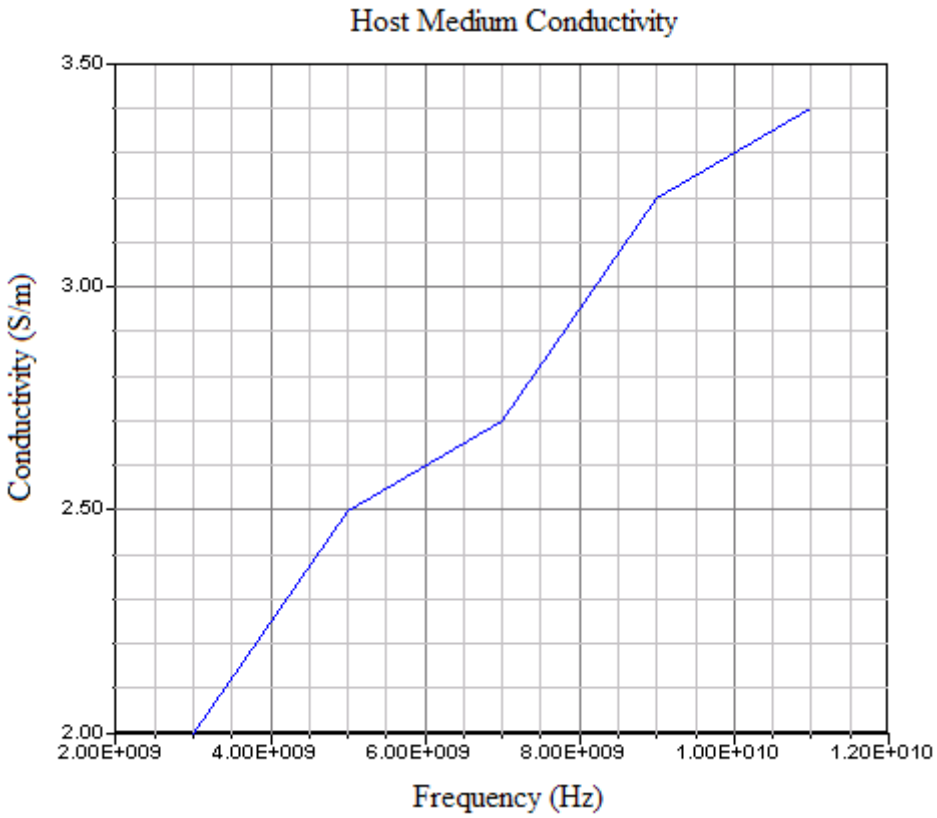

b)

Figure 10: a) Graph of the host medium's permittivity plotted against frequency b) Graph of the host medium's conductivity plotted against frequency

The size of the tumour was quantified by the length of its side dimensions. This dimension was varied from 2mm to 6mm. The tumour's location was fixed to be at the center of the antenna's aperture, and its contrast was varied. The conductivity contrast was fixed at 1 for all of these simulations, and the permittivity contrast was varied from 2 to 4.

The location of the tumour was varied in the x, y, and z directions, as assigned to the antenna array by HFSS, seen in either Figure 8 or Figure 9. In some cases, the radiation boundaries in the simulation had to be extended in order to ensure that they did not negatively affect the solutions. The size of the tumour was kept constant at 8mm by 8mm by 8mm. For the variation in the x direction, the tumour was kept at a fixed permittivity of 50 and a fixed conductivity of 0.4. For the variation in the z direction, the conductivity contrast of the tumour was kept at 3, whilst the permittivity contrast

remained at 1. This was then repeated for a permittivity contrast of 3, and a conductivity contrast of 1. It was decided that the prior procedure was redundant, and only one set of simulations were performed for the final variation in the y direction. In this set up, the contrast was kept at 3 for the conductivity and 1 for the permittivity.

For specifically determining the sensitivity of the antenna to different contrasts, a multitude of simulations were configured in which the contrast of the tumour was varied from 1 to 5. These two parameters were varied with the size of the tumour remaining constant at 8mm by 8mm by 8mm and the location of the tumour being at the center of the tissue.

Experimental Design Procedures

In order to assure that the simulation results are applicable to practical situations, there arises a need to conduct an experimental analog to the computerized set up. This first involves fabricating the antennas whose sensitivities are currently being ascertained.

The antenna was fabricated using two moulds which had already been created. Liquid dielectric, which would eventually act as the dielectric coupling medium, was poured into the first mold. Two copper sheets were cut out according to specification for the internal antenna. These two copper sheets were then attached to the large faces of the dielectric as shown in Figure 6. A hole was drilled through the locus of the semi-circle at the base of the antenna to allow the coaxial cable connector to be placed in the antenna in the proper position. Some solder was placed on either side of the connector to help ensure a good connection was made. The protruding end of the connector was cut such that it extended to the second mold's surface. This half fabricated antenna was then placed inside the larger mold and more liquid dielectric was poured to surround it. Careful consideration was taken in ensuring that the antenna was properly positioned in the center of this second mold. Once solidified, the copper sheets and microwave power absorption later were added on to the appropriate faces, as detailed in Figure 7.

With the two required antenna produced, the next step in the creation process was a suitable phantom to experiment upon. In order to ensure accuracy and reliability in the experiment, a proper breast phantom must be fabricated in accordance with the parameters used in the prior simulations. Such parameters, namely the conductivity and permittivity, were chosen based upon large scale studies conducted on real breast tissue, such as the work performed by Lazebnik *et al* [1].

There are a wide variety of methods used to create breast phantoms. Upon a thorough review, it was eventually decided to use the method outlined by Okano *et al*. [24]. The materials used to create the phantom were agar, deionised water, glycerol, and polyethylene. The advantage of this method is the use of glycerine phantoms, known for their longer shelf life. Also, the materials used are completely non-toxic, removing any potential safety hazards and complications that may have risen otherwise. However, the disadvantage of using this method was the lack of data on the permittivities and conductivities across the 3 to 11 GHz band. In order to obtain a proper phantom, the

recipe had to be adjusted until the correct proportions had finally been discovered. The method of fabrication follows.

First, the deionised water and glycerol were combined in a ratio of four grams of glycerol for every three grams of deionised water. This solution was heated over a hot plate or open flame on medium heat for approximately ten minutes. The solution was slowly stirred throughout the heating process in order to reduce the amount of air bubbles present. Agar and polyethylene powder were combined in a separate container in a ratio of six grams of agar for every 5 grams of polyethylene. This powder combination was then slowly added to the glycerol and water solution while constantly stirring, at a rate of approximately one gram per minute. After the addition of all the powder, the solution's viscosity will have transitioned from that of a liquid to that of a highly viscous custard. This solution was then poured into a container with the desired shape of the phantom. It was then placed into the refrigerator and allowed to cool and solidify overnight.

This was the methodology for the standard breast phantom that acted as the host medium in the experiments, representing non-cancerous breast tissue. In order to properly compare the experimental results to that of the simulation, an additional phantom was created to represent the cancerous tissue. The only alteration to the methodology in creating this phantom was the addition of one tablespoon of salt for every 100 mL of deionised water. This created a conductivity contrast between this new phantom and the original host medium. A third new breast phantom was created using the original methodology, except for the insertion of an 8mm by 8mm by 8mm piece of the cancerous tissue inside the new phantom just prior to it being placed in the refrigerator for cooling. The result of these three creation trials was the production of three breast phantoms: the first representing normal healthy breast tissue, the second representing breast tissue with an 8mm by 8mm by 8mm tumour inserted, and the final tissue phantom used to determine the exact permittivity and conductivity of the cancerous tumour that was earlier inserted into the otherwise normal breast phantom. The phantoms created can be seen in Figure 11.

a) b)

c)

Figure 11: Three phantoms created. a) The original phantom with standard properties; b) The new phantom with an 8mm by 8mm by 8mm tumour inserted inside; c) The phantom from which the tumour was extracted

In order to perform the experiments, a VNA was used to accurately acquire and display the complex S-parameters of the system. The VNA was automatically calibrated

for the frequency band 3 to 11 GHz through use of a calibration kit, and connected to the antennas through coaxial cables connected to ports one and two. The VNA was set to average the recordings over 16 samples, and output its maximum power possible of 8 dBm. Signal smoothing was disabled for the readings. An example set up of the experimental apparatus is shown in Figure 12. The phantom was held in place by a clamp, while the two antennas used were also held in place by separate clamps. This set up was repeated for the other phantoms.

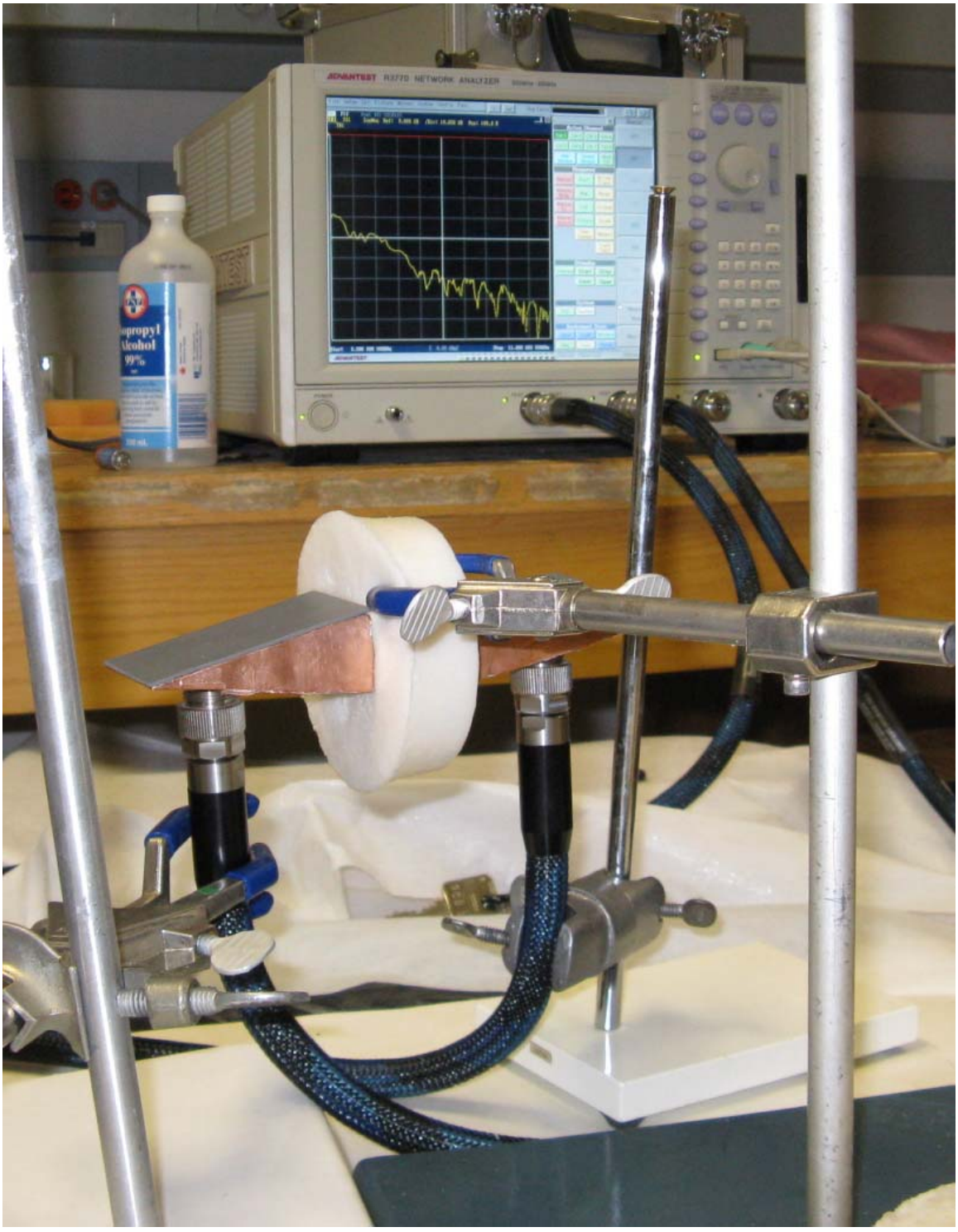

Figure 12: Experimental set up.

The actual permittivity and conductivity of the phantoms used were determined using a single port probe which was also set up in the lab. Prior to use, this probe must

also be calibrated for the frequency range of 3 to 11 GHz. This was done using the designated calibration procedure outlined by the software on the probe. The probe performed a scan when first exposed to air, then when shorted through use of a special shorting block, and then finally when immersed in deionised water at a temperature of 25°C. Once this was performed the probe was placed on the surface of a phantom and a measurement was manually triggered. This measurement was repeated multiple times in order to obtain an average recording and reduce noise's impact on the data. An example set up is shown in

Figure 13.

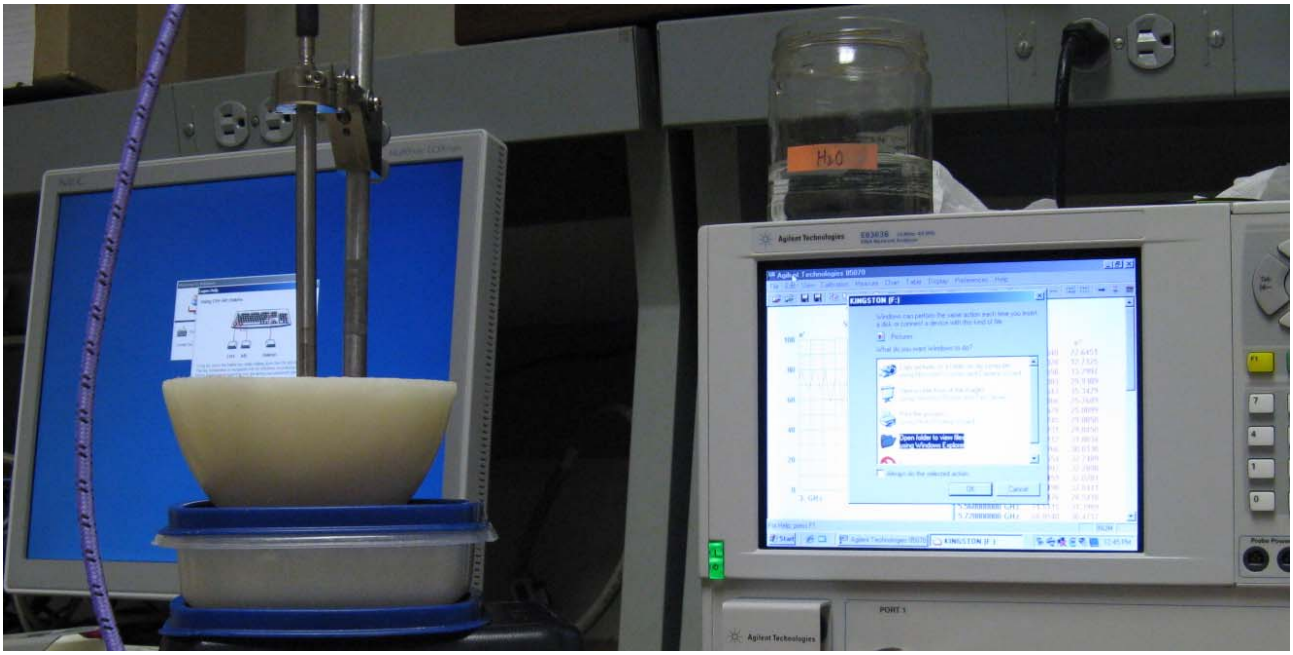

Figure 13: One port probe used for determining dielectric properties of the phantoms.

Results

Simulations

The results of the simulations will be grouped in the following three categories: contrast, size, and location.

The results were quantified by separating the complex S-parameters into their respective magnitudes and phases, i.e.

$$S_{ij} = \left|S_{ij}\right| e^{\angle S_{ij}} \tag{2}$$

This allowed for a separate analysis of the sensitivity of the antenna's magnitude to potential tumours, and the sensitivity of the antenna's phase to potential tumours. In order to assess the sensitivity, a tumour signature must first be generated and compared to the signal generated by normal tissue. This was done by first simulating healthy tumour free tissue and extracting the S-parameters from this simulation. An example of such a tissue is shown in Figure 14.

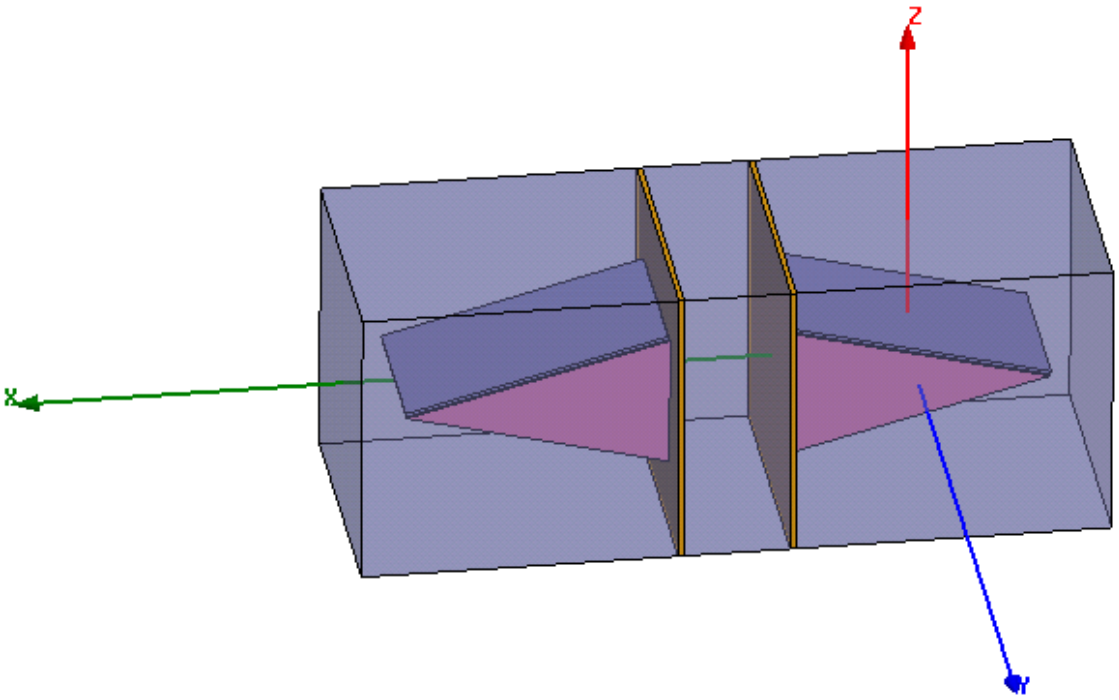

Figure 14: Healthy Tissue.

After these parameters were acquired, the simulation testing the sensitivity of the antenna to a tumour was performed. An example set up is shown in Figure 15.

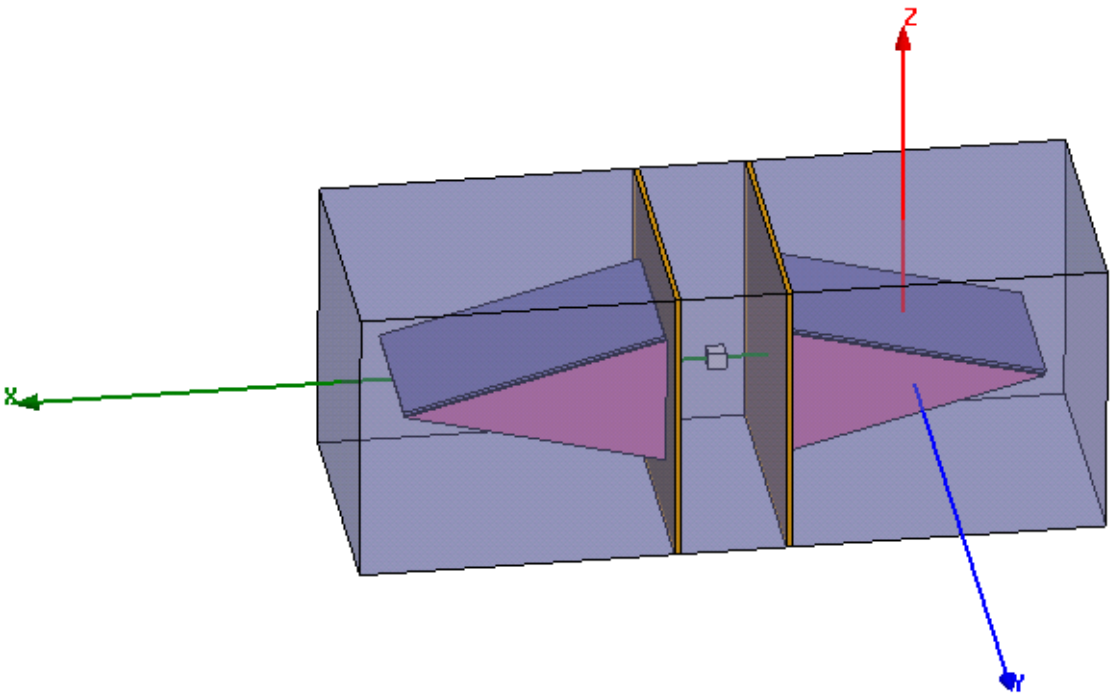

Figure 15: Example simulation set up with tumour present.

Then, a variety of signatures were used in order to quantify the data and determine which signature was most effective at accurately portraying a change in the S-parameters caused by the presence of a tumour. The signatures for the magnitudes are shown in equations (3)(4) for magnitude.

$$\text{Signature} = 20 \times \log_{10}\left(\frac{|S_{ij}|}{|S_{ij_{NT}}|}\right) \tag{3}$$

$$\text{Signature} = \frac{|S_{ij} - S_{ij_{NT}}|}{|S_{ij_{NT}}|} \tag{4}$$

In order to help avoid confusion, the signatures used will be specified using the above equations.

Contrast

The first signature used is a comparison between the S11 parameter of the tissue with a tumour related to the S11 parameter of the tissue without a tumour, as seen in equation (4) If we take the case with relatively strong contrasts, a permittivity contrast of 5 and a conductivity contrast of 5, and look at the S11 parameter, we observe the

following results, seen in Figure 16, Figure 17, Figure 18, Figure 19, Figure 20, Figure 21, Figure 22, Figure 23, Figure 24.

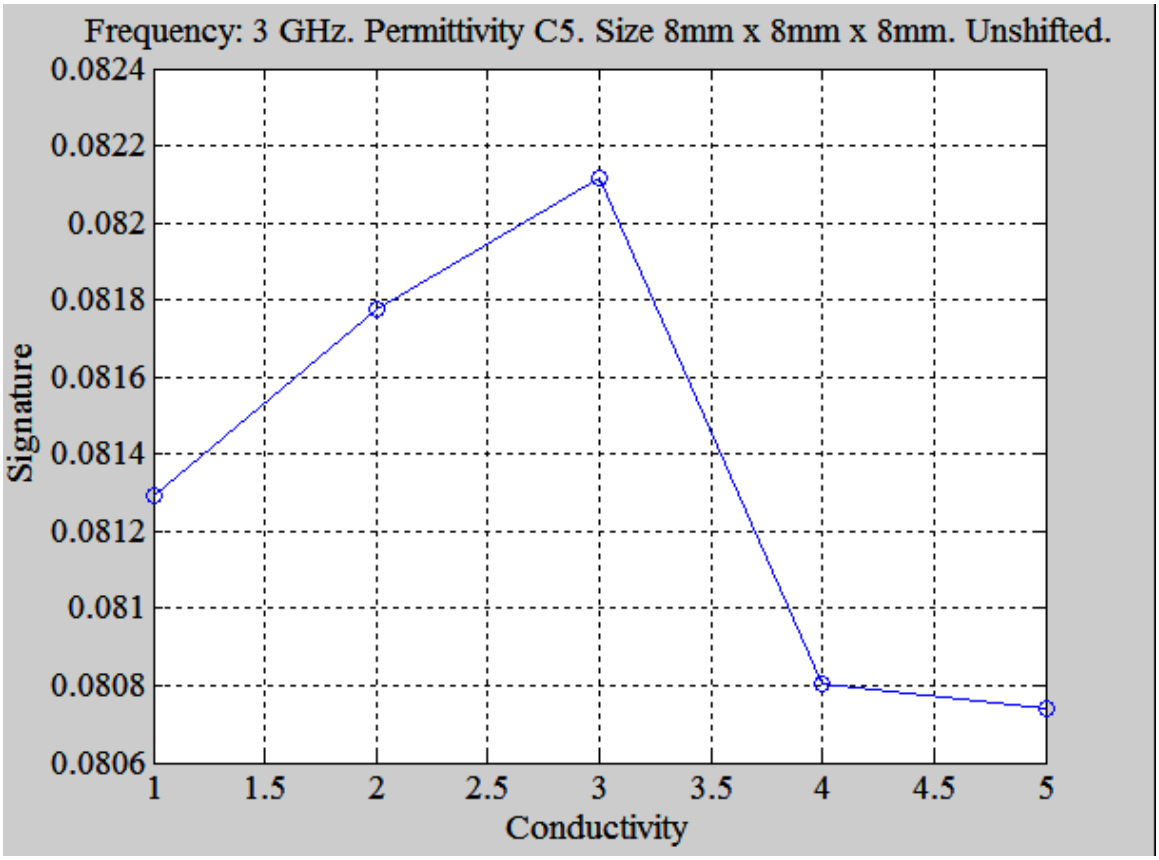

Figure 16: S11 signature as it appears in equation (4). Specific details of plot listed in plot title.

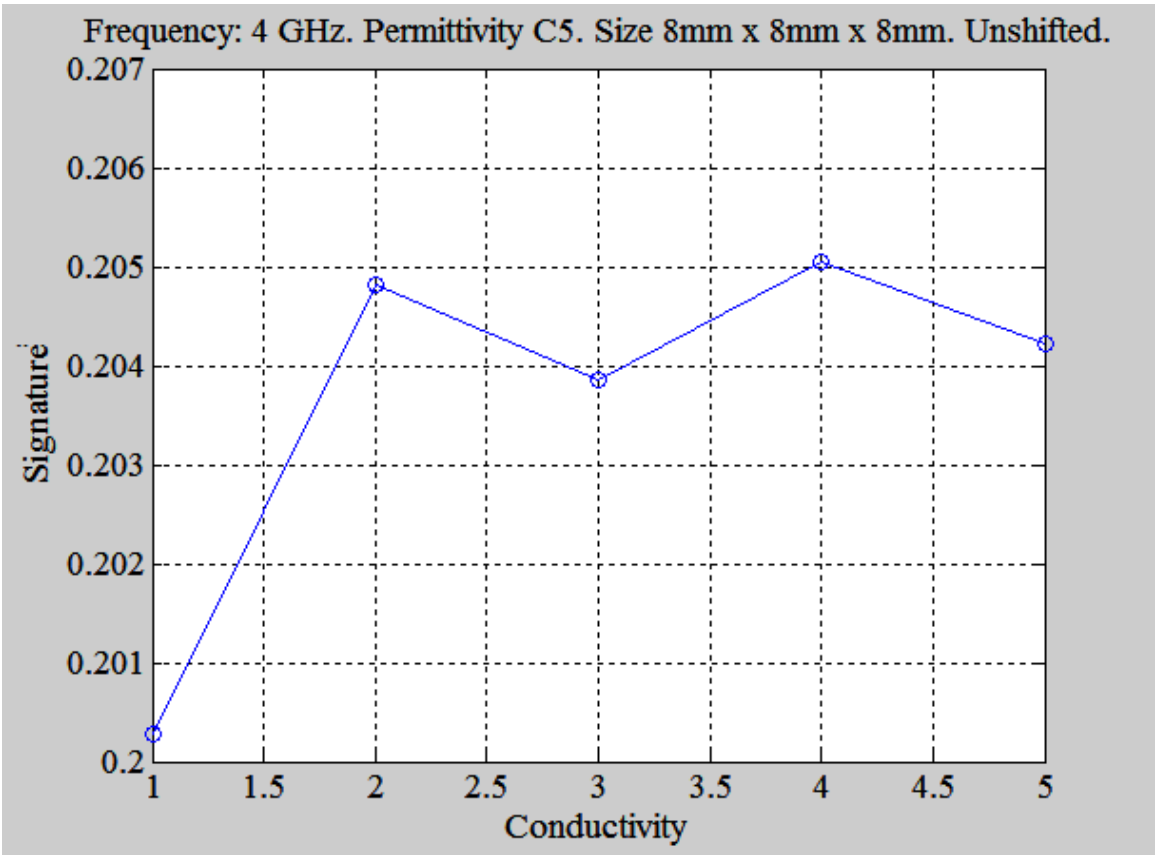

Figure 17: S11 signature as it appears in equation (4). Specific details of plot listed in plot title.

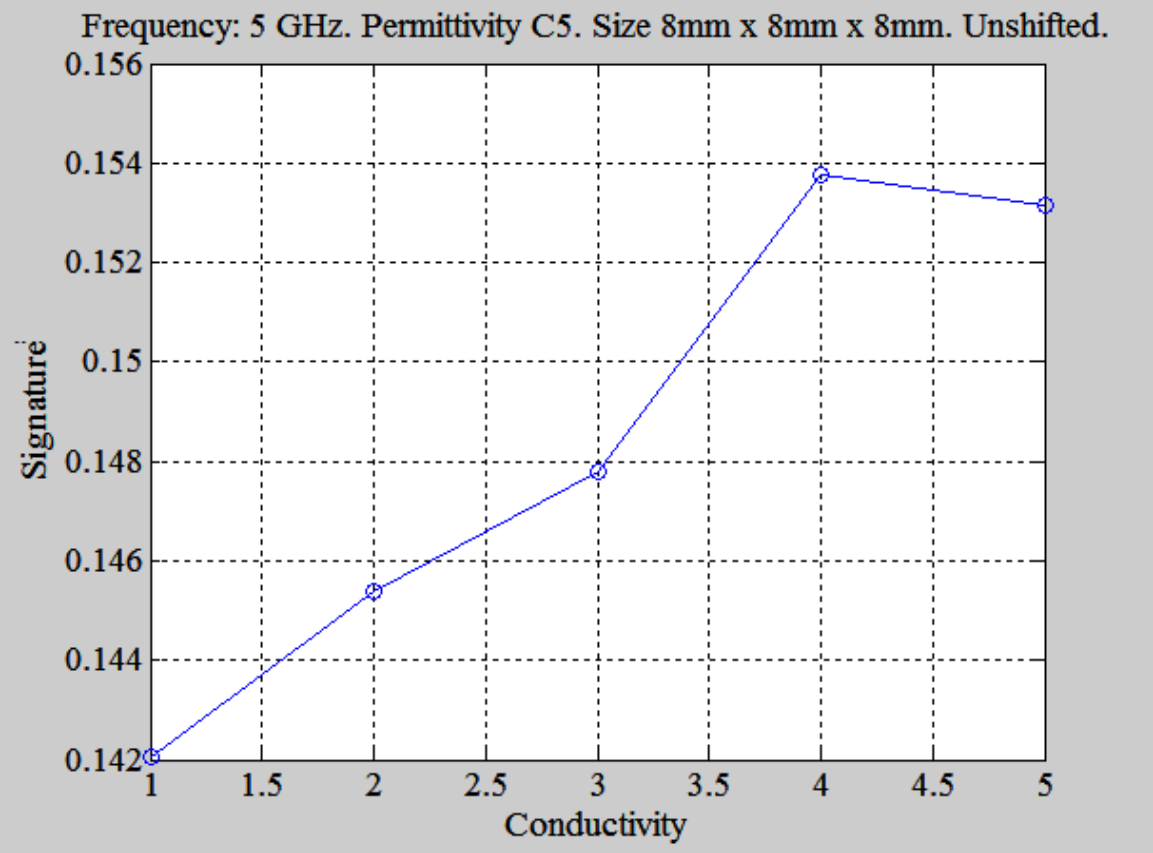

Figure 18: S11 signature as it appears in equation (4). Specific details of plot listed in plot title.

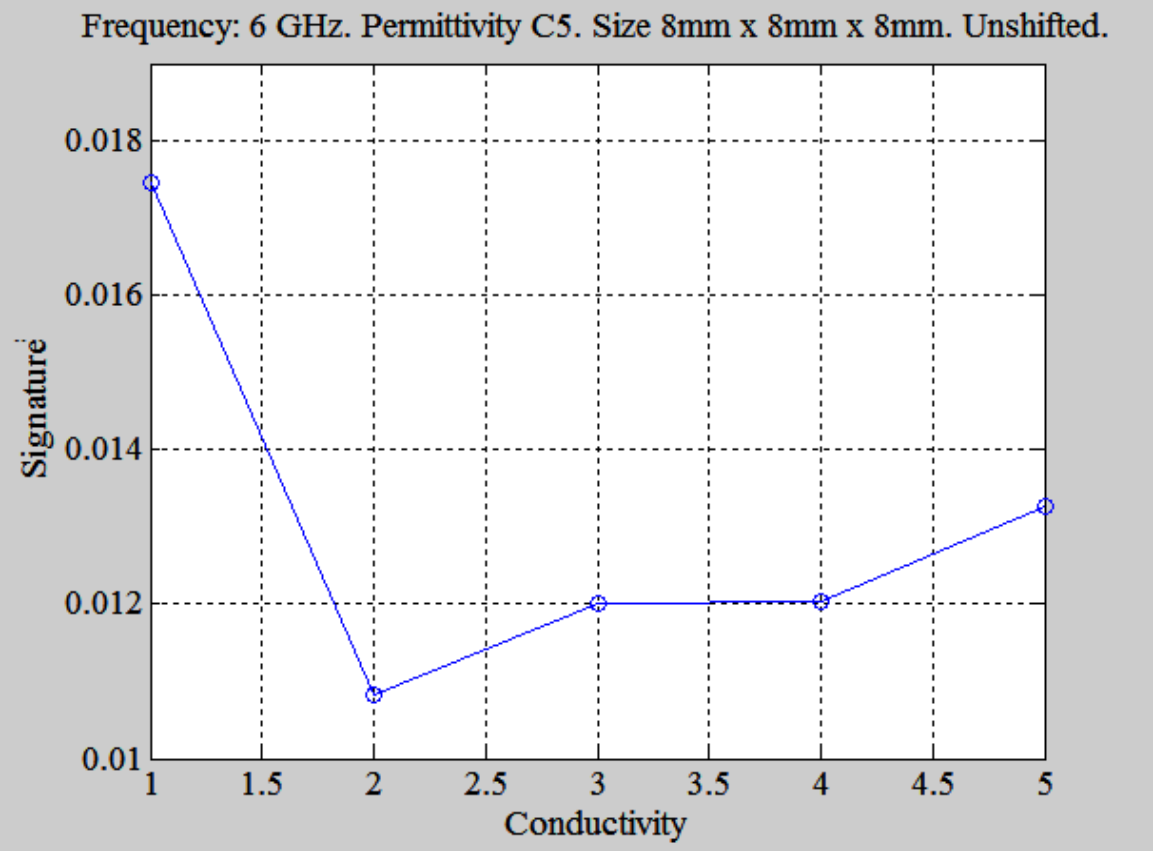

Figure 19: S11 signature as it appears in equation (4). Specific details of plot listed in plot title.

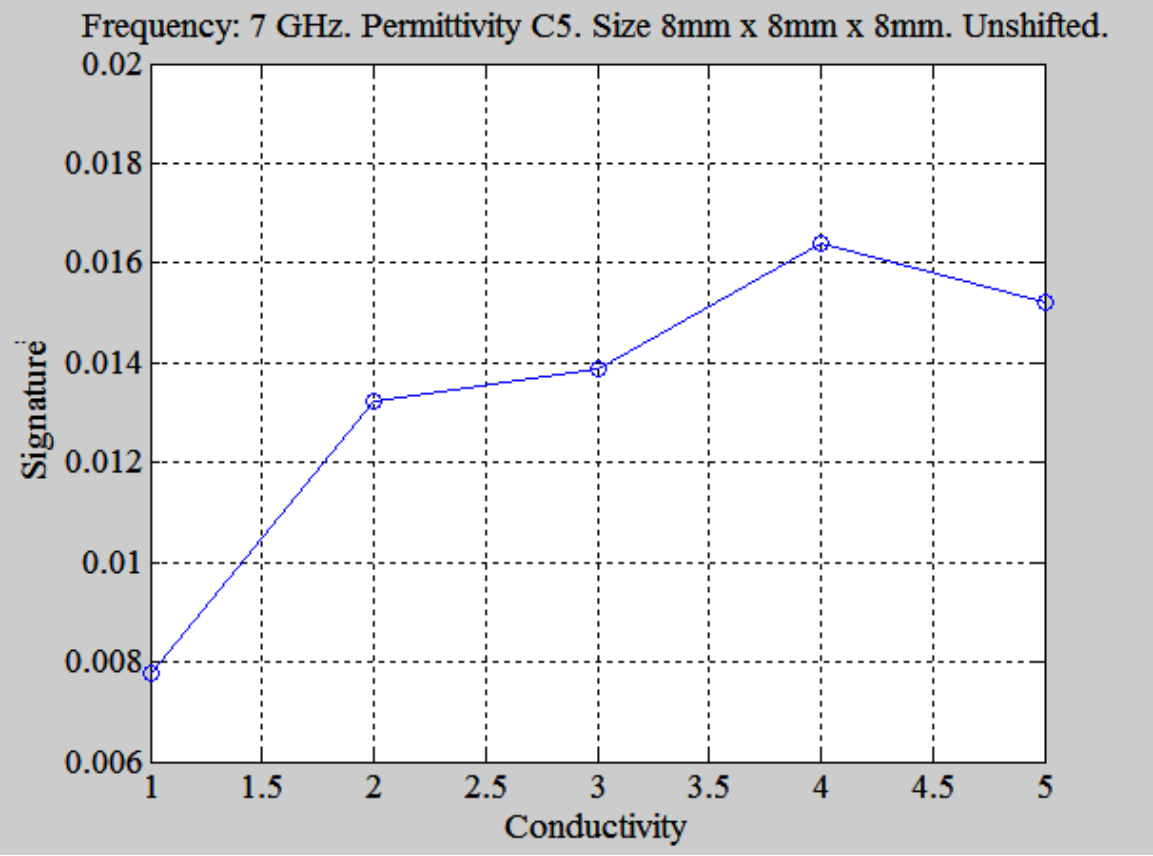

Figure 20: S11 signature as it appears in equation (4). Specific details of plot listed in plot title.

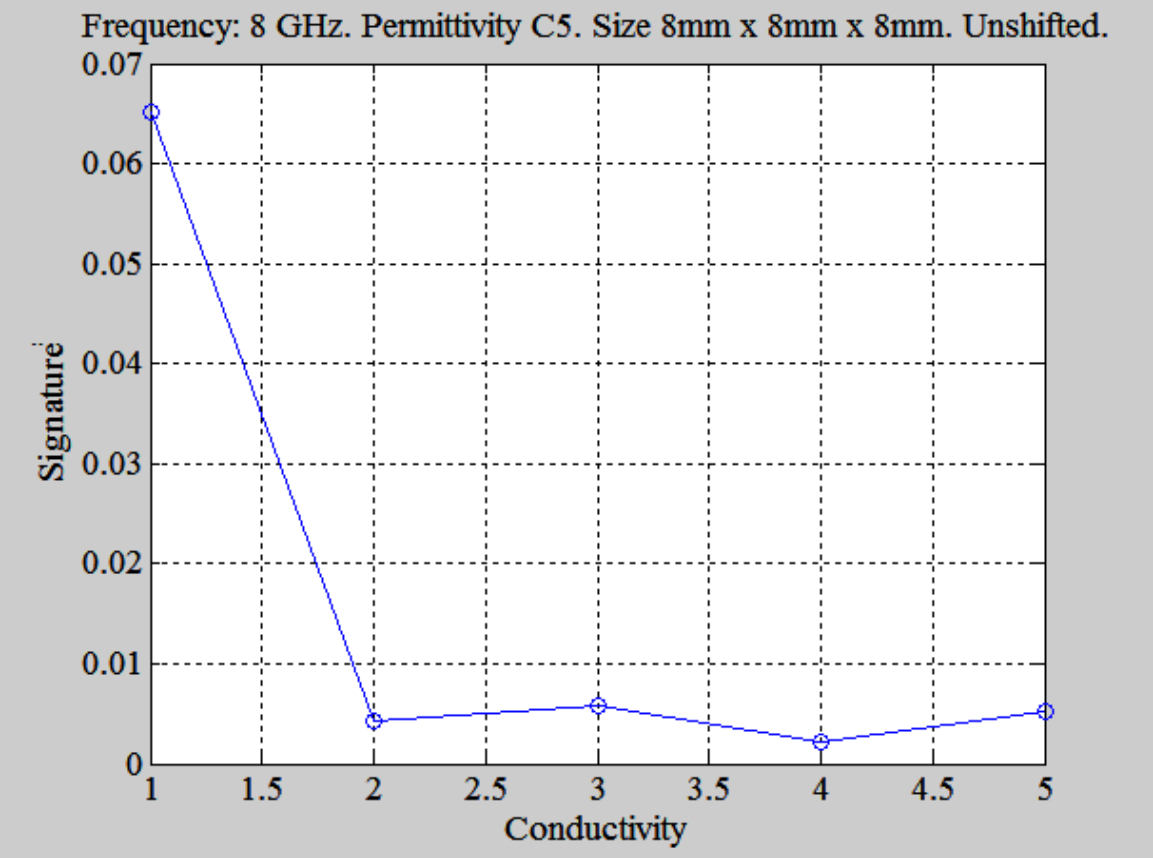

Figure 21: S11 signature as it appears in equation (4). Specific details of plot listed in plot title.

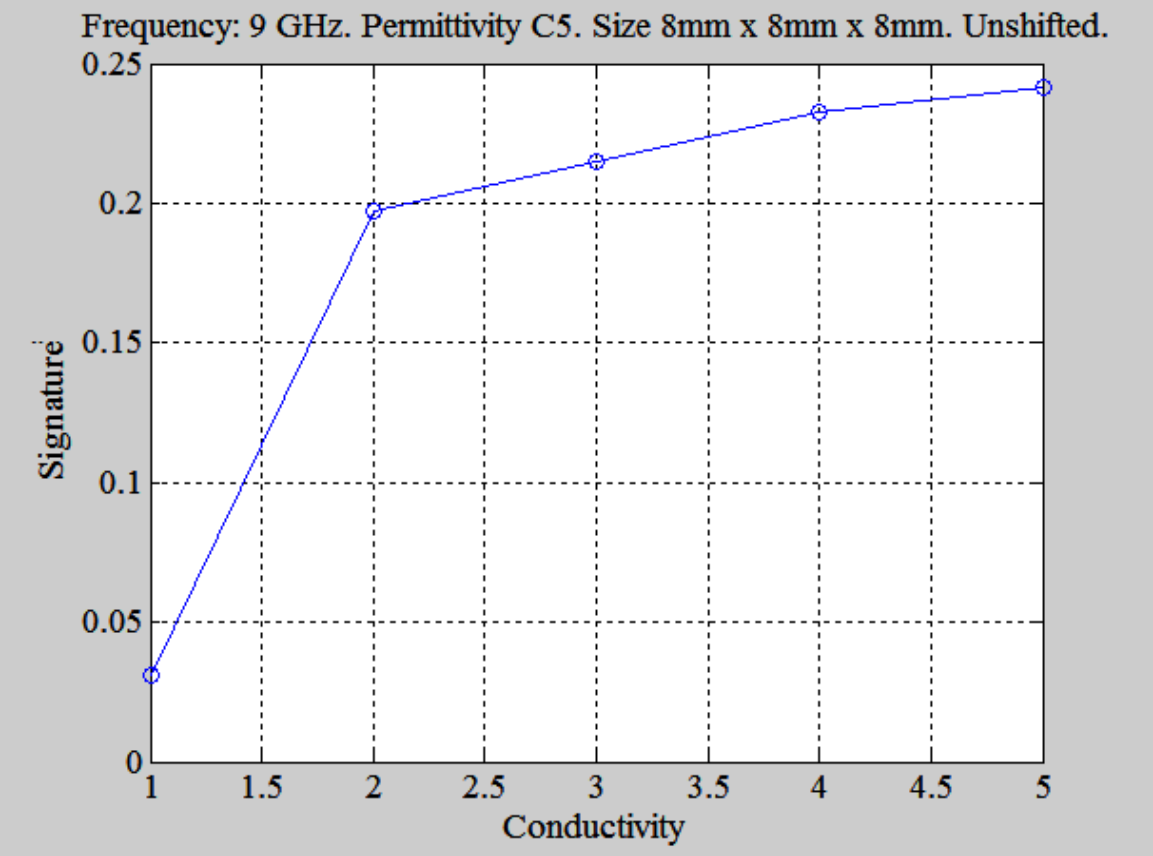

Figure 22: S11 signature as it appears in equation (4). Specific details of plot listed in plot title.

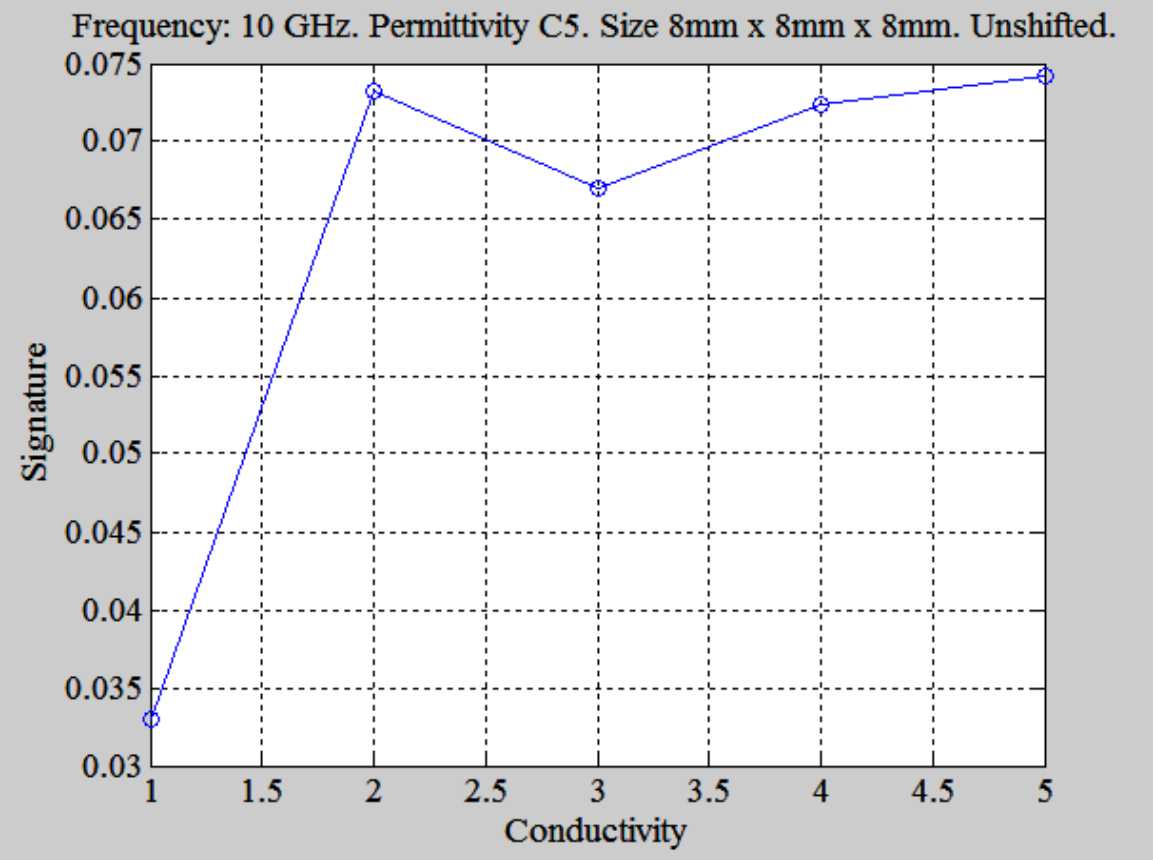

Figure 23: S11 signature as it appears in equation (4). Specific details of plot listed in plot title.

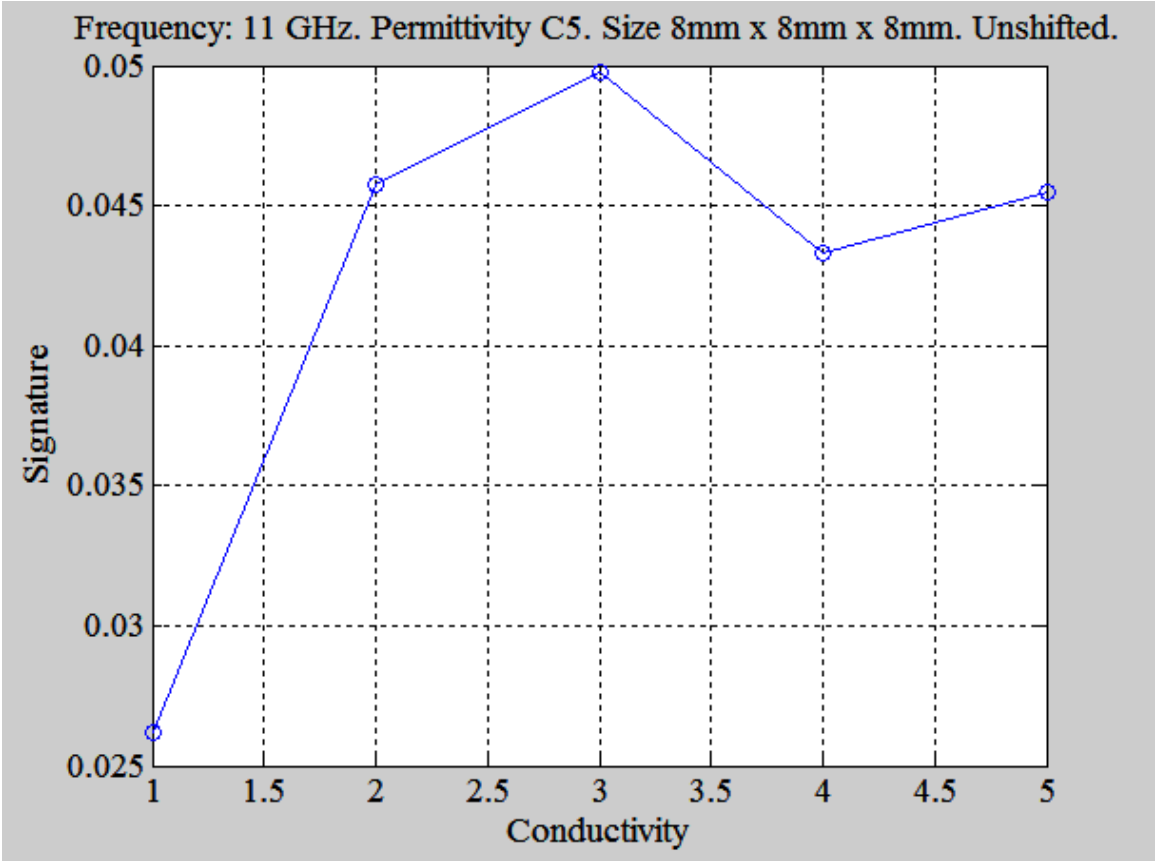

Figure 24: S11 signature as it appears in equation (4). Specific details of plot listed in plot title.

As we can see, the S11 signature appears to have little value except in the higher frequency ranges of 9-11 GHz. However, at this frequency, the acquired simulations have become relatively noisy due to numerical noise in the simulator. Throughout most of the simulations and experiments, the values at approximately 7 GHz and higher were forced to be disregarded due to numerical errors. This will be given further justification later in the report.

The other parameters available, the S21 parameters, show more promise.

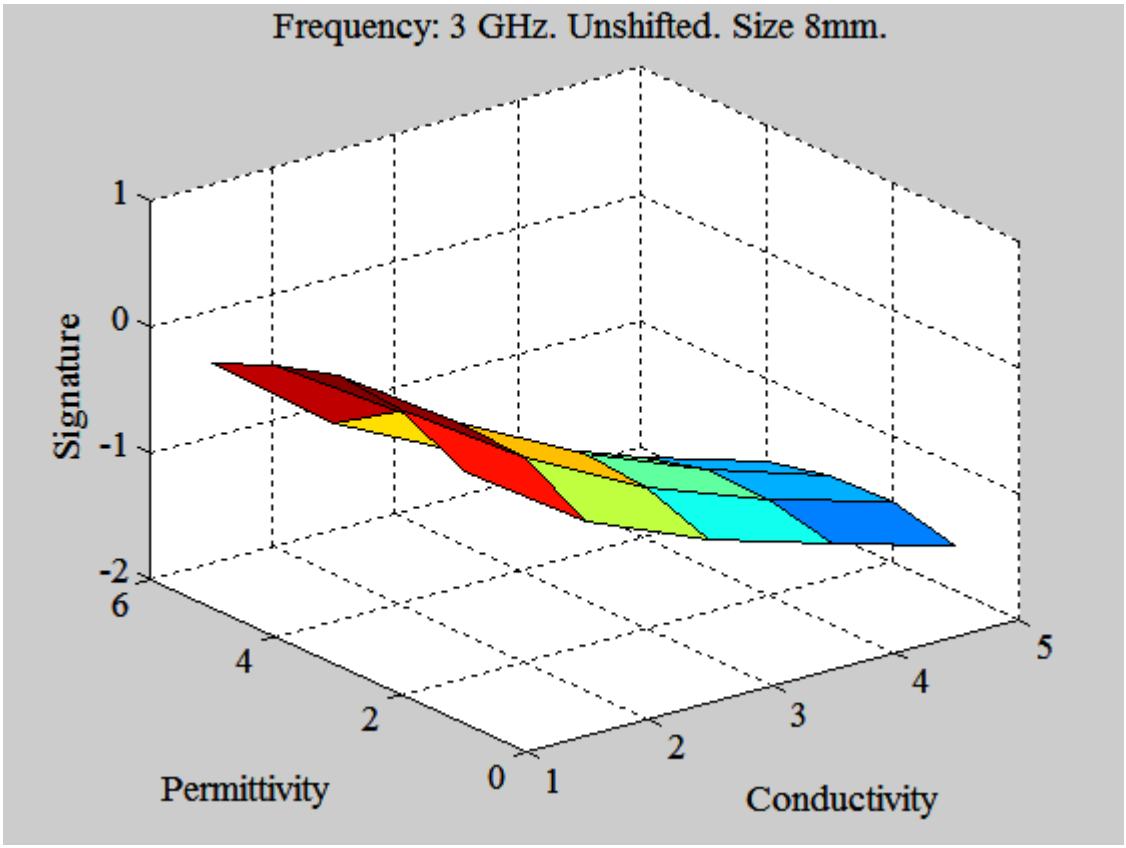

Figure 25: S21 signature as it appears in equation (3). The details of the plot are specified in the title. A "size" of 8mm indicates a side length of 8mm, i.e., a cuboid with dimensions 8mm by 8mm by 8mm.

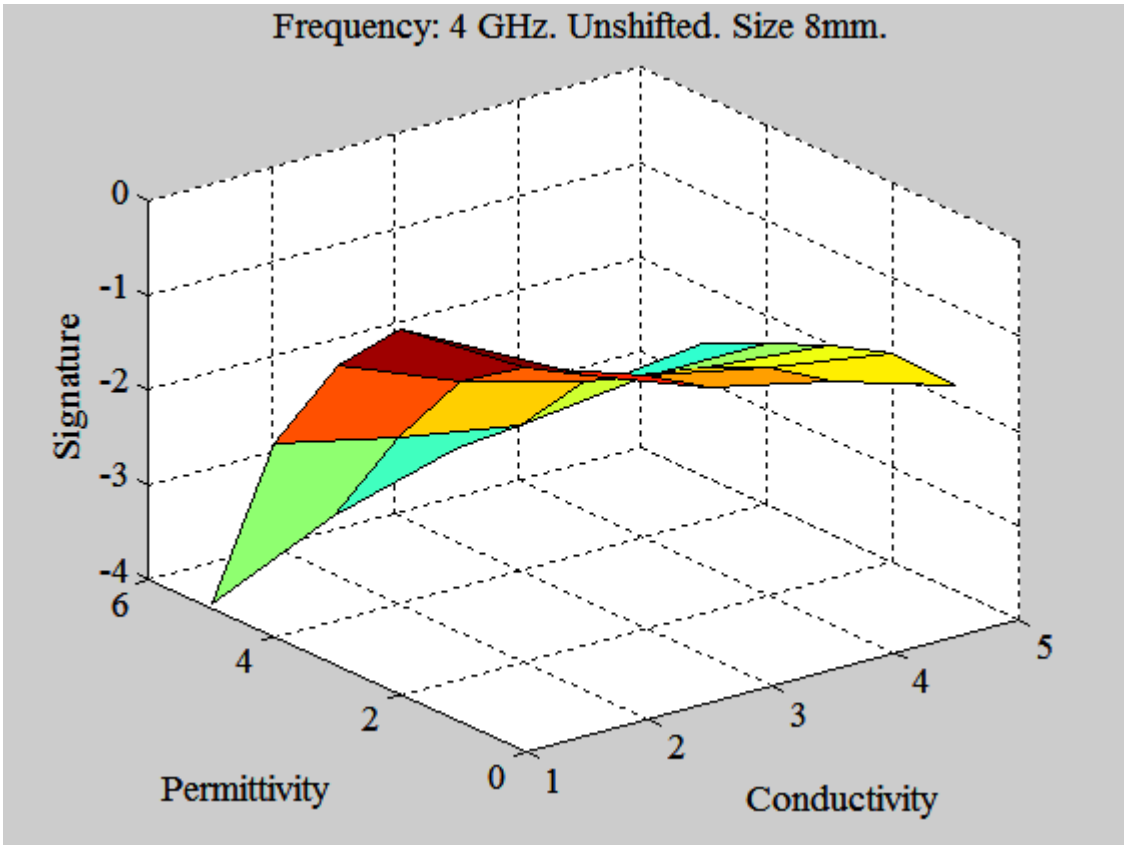

Figure 26: S21 signature as it appears in equation (3). The details of the plot are specified in the title. A "size" of 8mm indicates a side length of 8mm, i.e., a cuboid with dimensions 8mm by 8mm by 8mm.

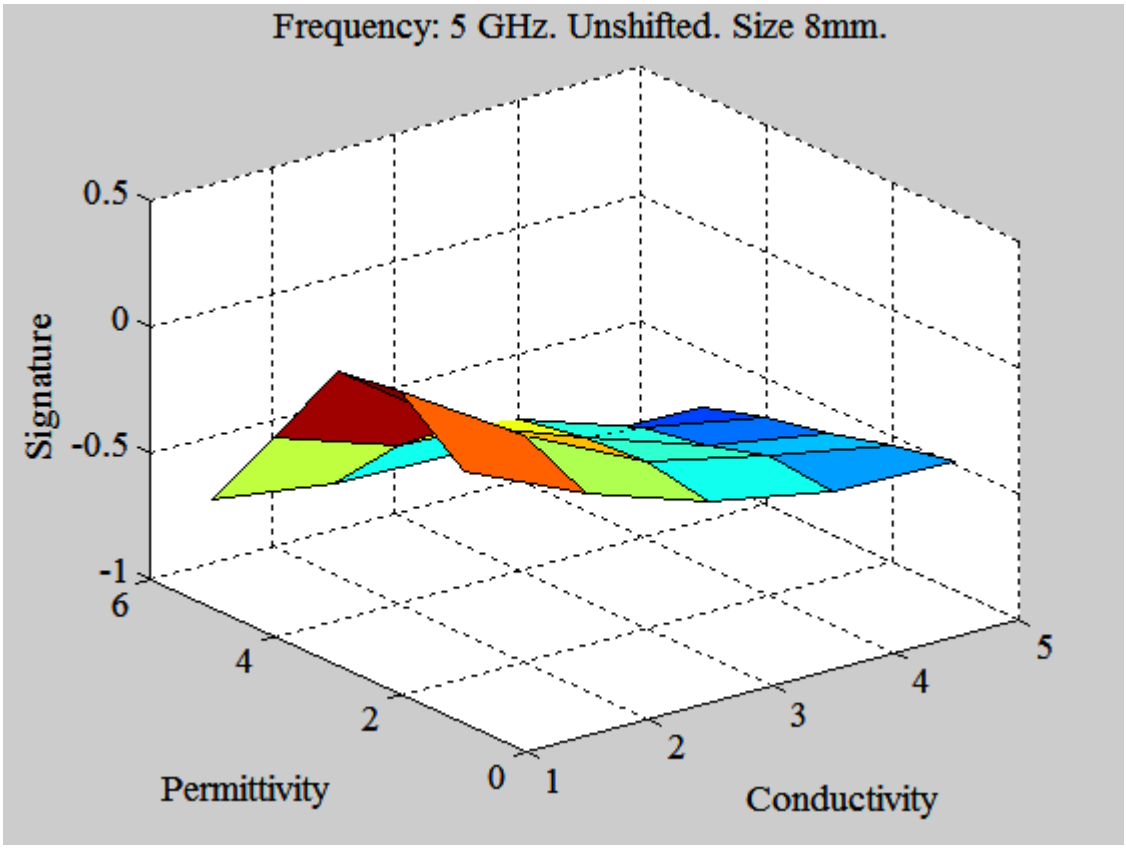

Figure 27: S21 signature as it appears in equation (3). The details of the plot are specified in the title. A "size" of 8mm indicates a side length of 8mm, i.e., a cuboid with dimensions 8mm by 8mm by 8mm.

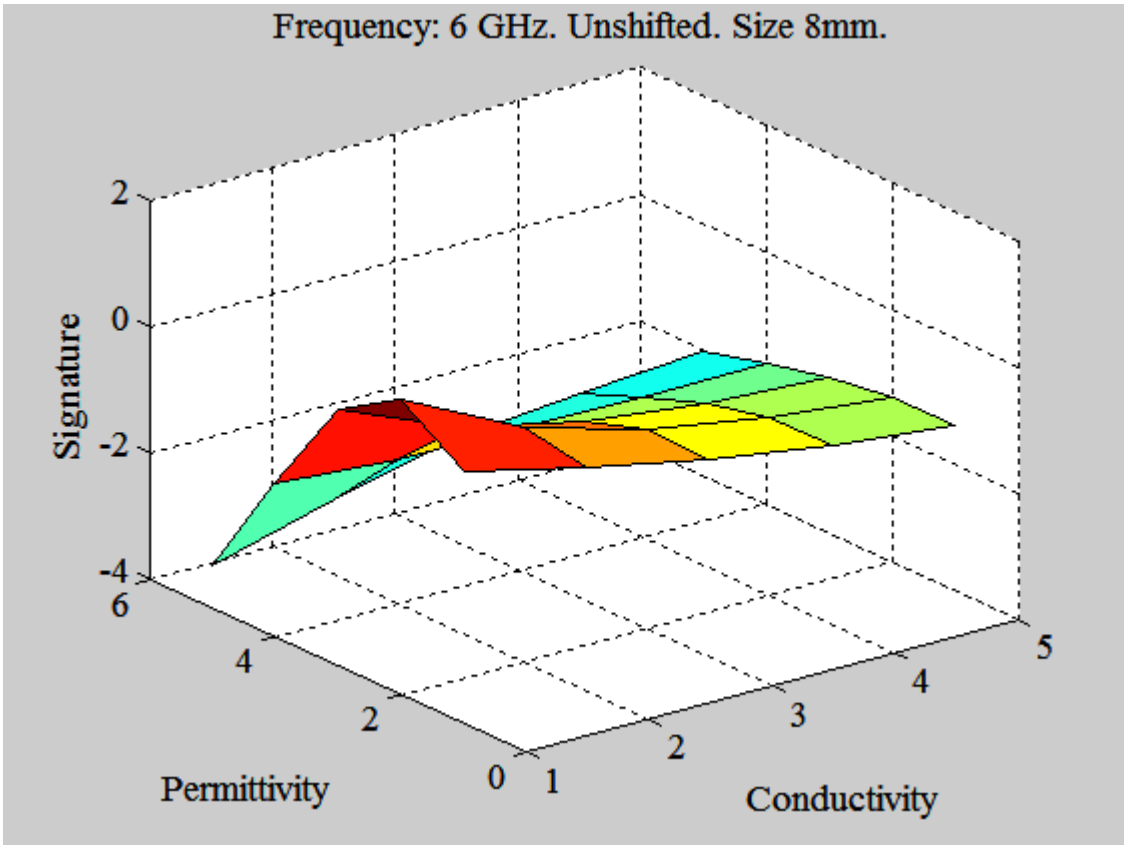

Figure 28: S21 signature as it appears in equation (3). The details of the plot are specified in the title. A "size" of 8mm indicates a side length of 8mm, i.e., a cuboid with dimensions 8mm by 8mm by 8mm.

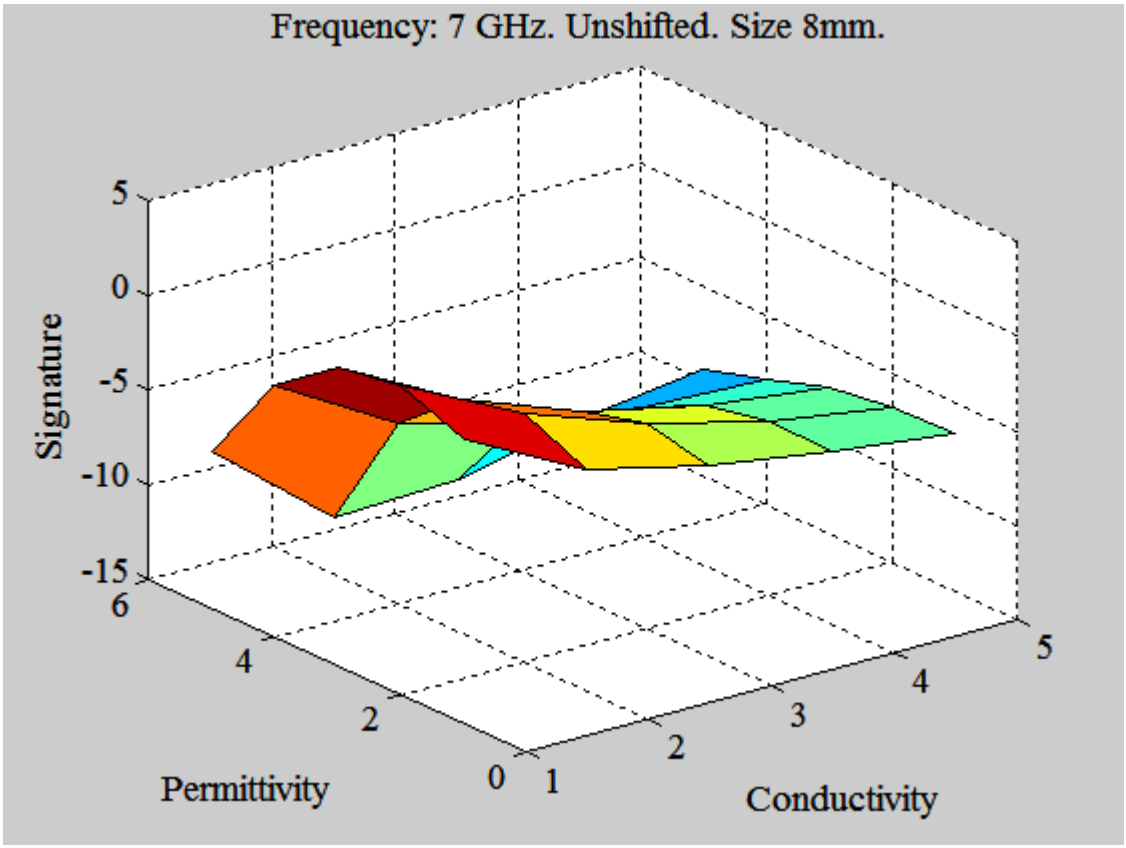

Figure 29: S21 signature as it appears in equation (3). The details of the plot are specified in the title. A "size" of 8mm indicates a side length of 8mm, i.e., a cuboid with dimensions 8mm by 8mm by 8mm.

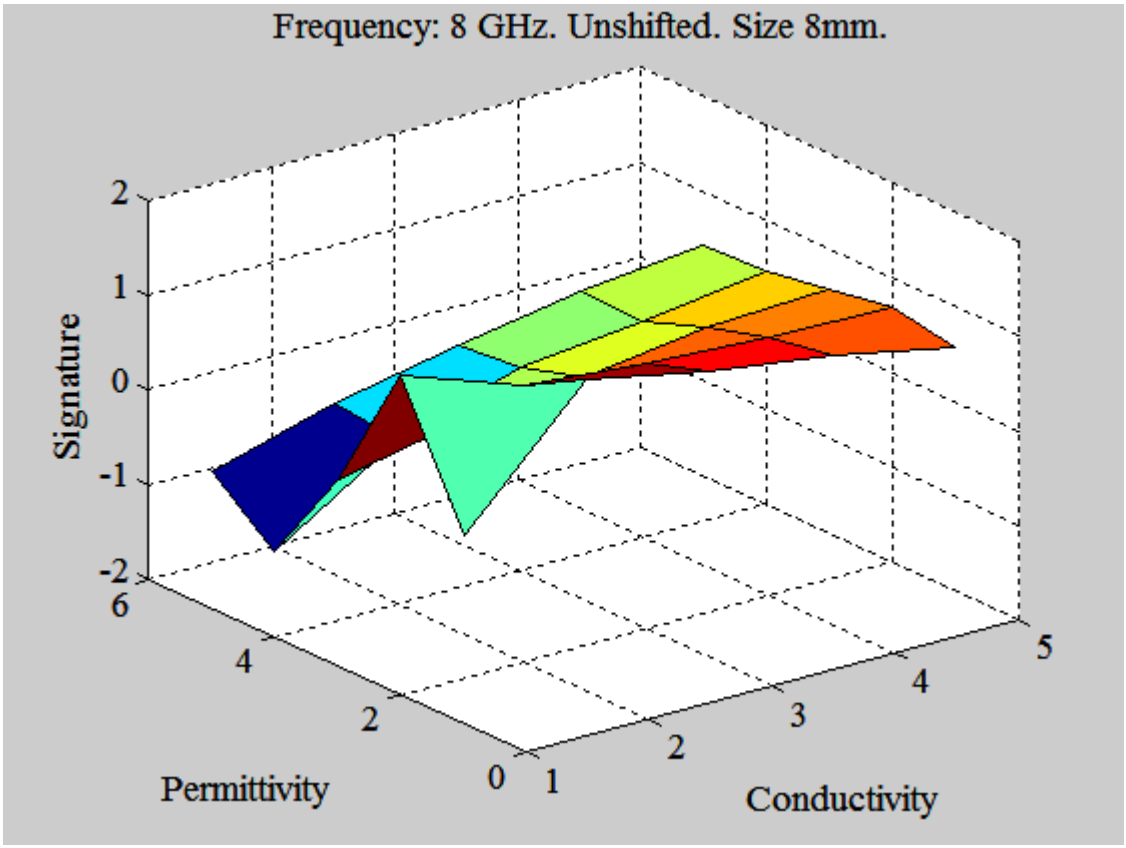

Figure 30: S21 signature as it appears in equation (3). The details of the plot are specified in the title. A "size" of 8mm indicates a side length of 8mm, i.e., a cuboid with dimensions 8mm by 8mm by 8mm.

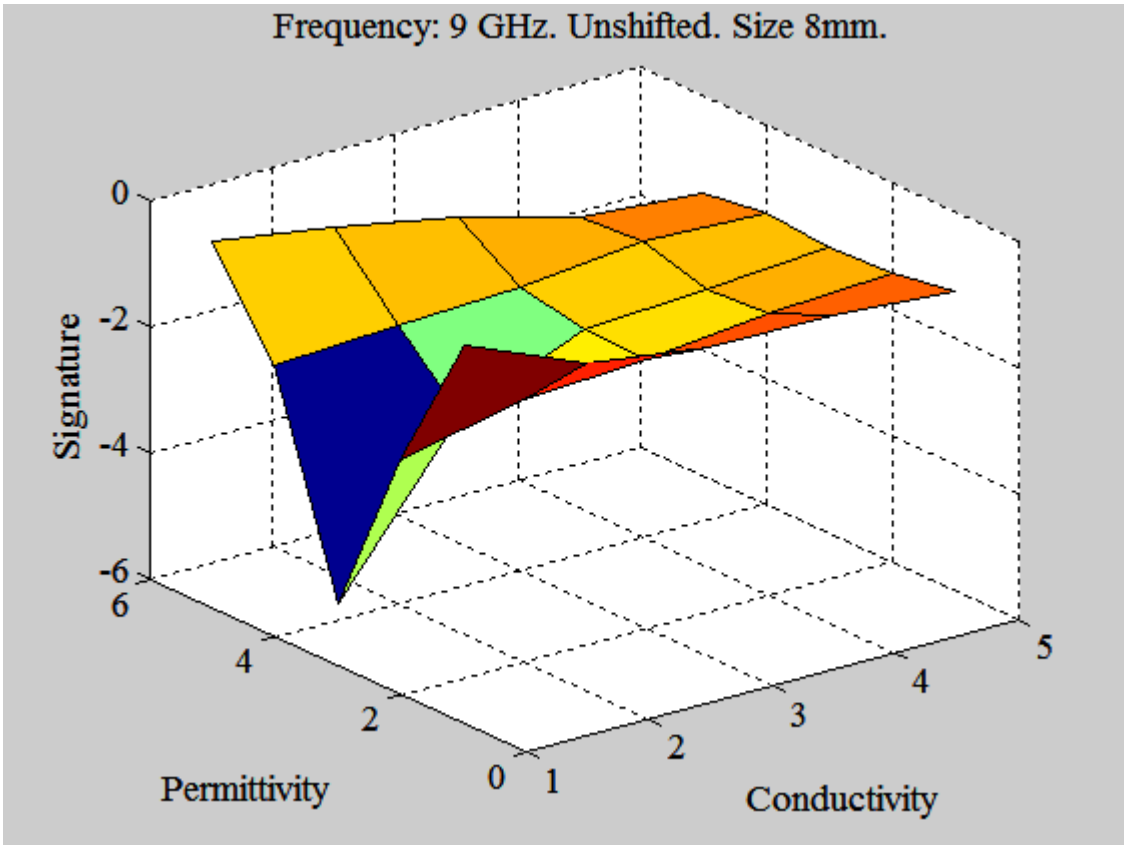

Figure 31: S21 signature as it appears in equation (3). The details of the plot are specified in the title. A "size" of 8mm indicates a side length of 8mm, i.e., a cuboid with dimensions 8mm by 8mm by 8mm.

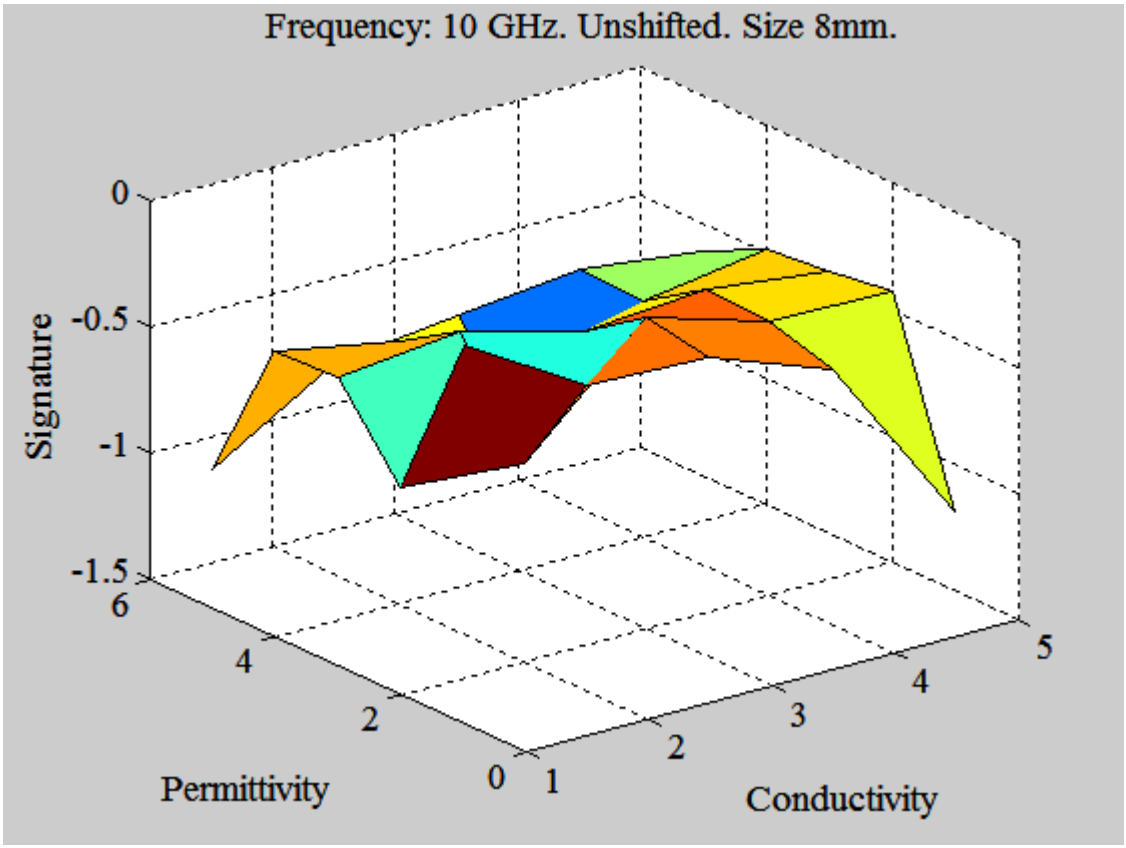

Figure 32: S21 signature as it appears in equation (3). The details of the plot are specified in the title. A "size" of 8mm indicates a side length of 8mm, i.e., a cuboid with dimensions 8mm by 8mm by 8mm.

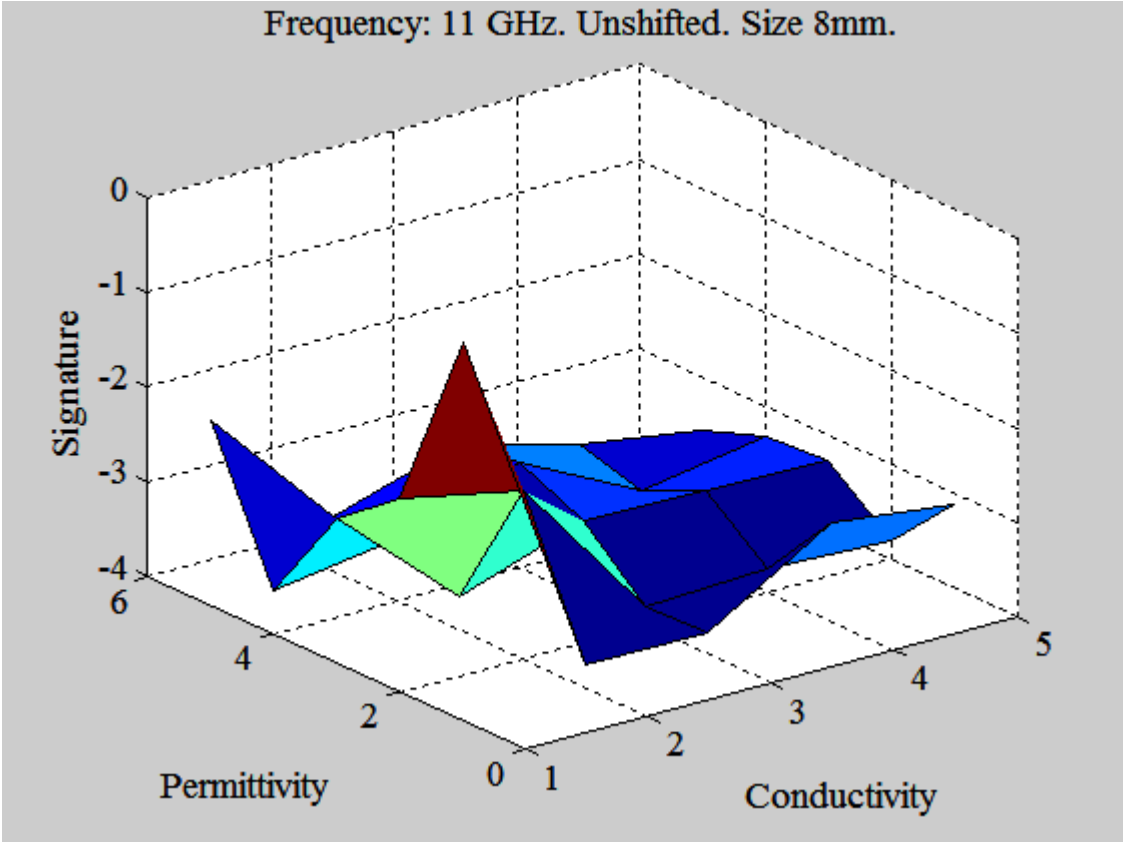

Figure 33: S21 signature as it appears in equation (3). The details of the plot are specified in the title. A "size" of 8mm indicates a side length of 8mm, i.e., a cuboid with dimensions 8mm by 8mm by 8mm.

In the graphs presented in Figure 25 to Figure 33, the signature is measured in dB. A lower value indicates that the tumour has attenuated the signal more than the tissue alone, and the larger this attenuation, the better the sensitivity of the antenna to the tumour. We can see that the optimal frequencies for detection appear around 4-6 GHz, where most of the contrasts have a larger than 1 dB difference. At around 7 GHz, our signal appears to jump to a contrast of almost 10 dB. This is merely due to the fact that the S21 parameters are shrinking to 0, and as such numerical noise is having a very powerful impact, due to the logarithmic nature of the graph. Comparing the S21 parameters at a frequency of 7 GHz, seen in the tables Table 10 and Table 11, we can see that the values for the tissue with the tumours hover around 0.00044, compared to the signature of no tumour, which has a value of 0.0000519. Though these differences may seem extreme on a logarithmic scale, due to the order of magnitude, or when normalized to the signature of the tumour, in reality they are quite small and corrupted readily by

numerical errors. This is also apparent when analyzing the data with the second signature, (4), as seen in the following figures.

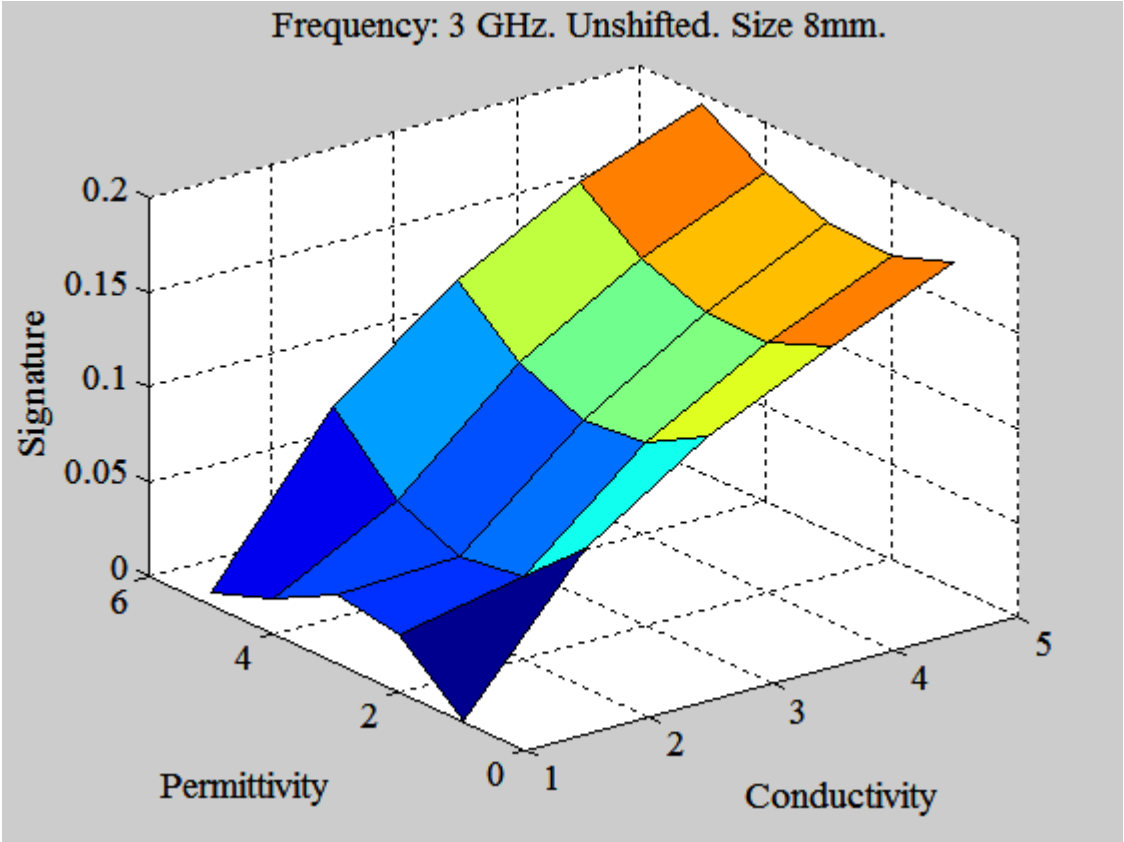

Figure 34: Signature as it appears in equation (4). Tumour details specified at top of plot. A "size" of 8mm indicates a side length of 8mm, i.e., a cuboid with dimensions 8mm by 8mm by 8mm.

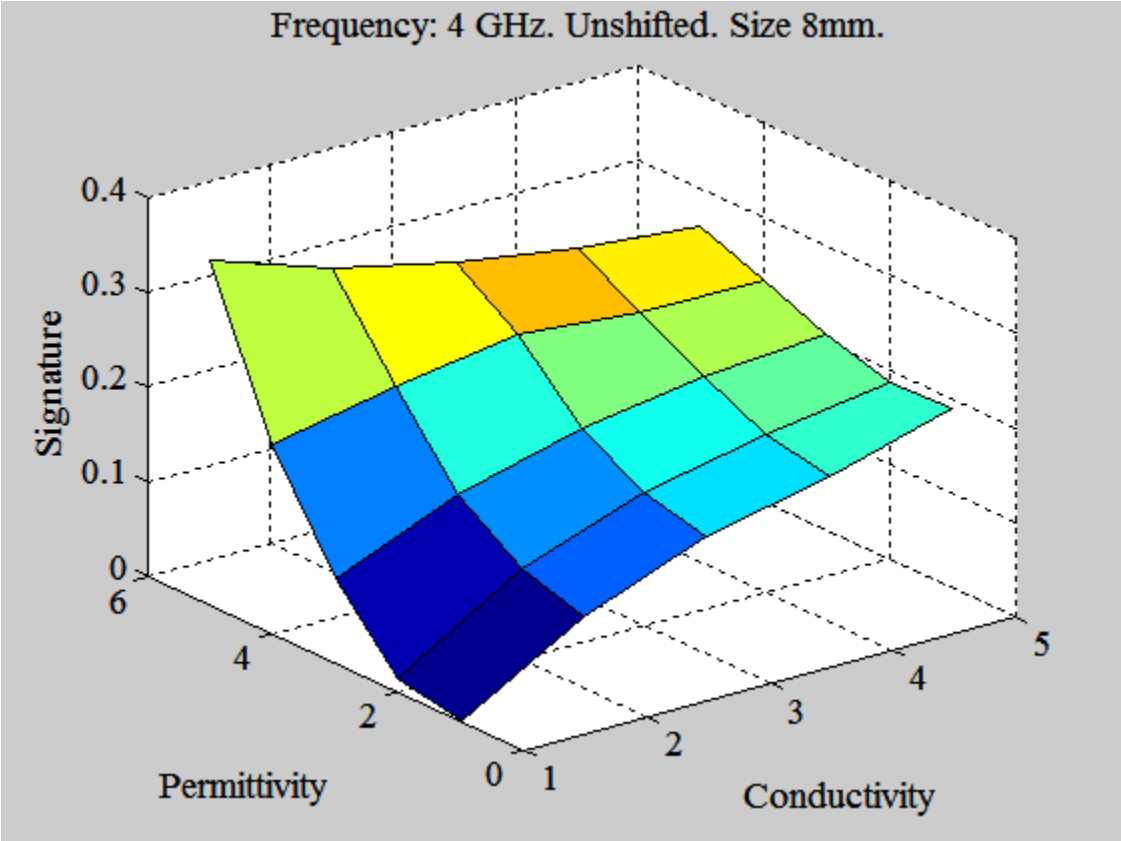

Figure 35: Signature as it appears in equation (4). Tumour details specified at top of plot. A "size" of 8mm indicates a side length of 8mm, i.e., a cuboid with dimensions 8mm by 8mm by 8mm.

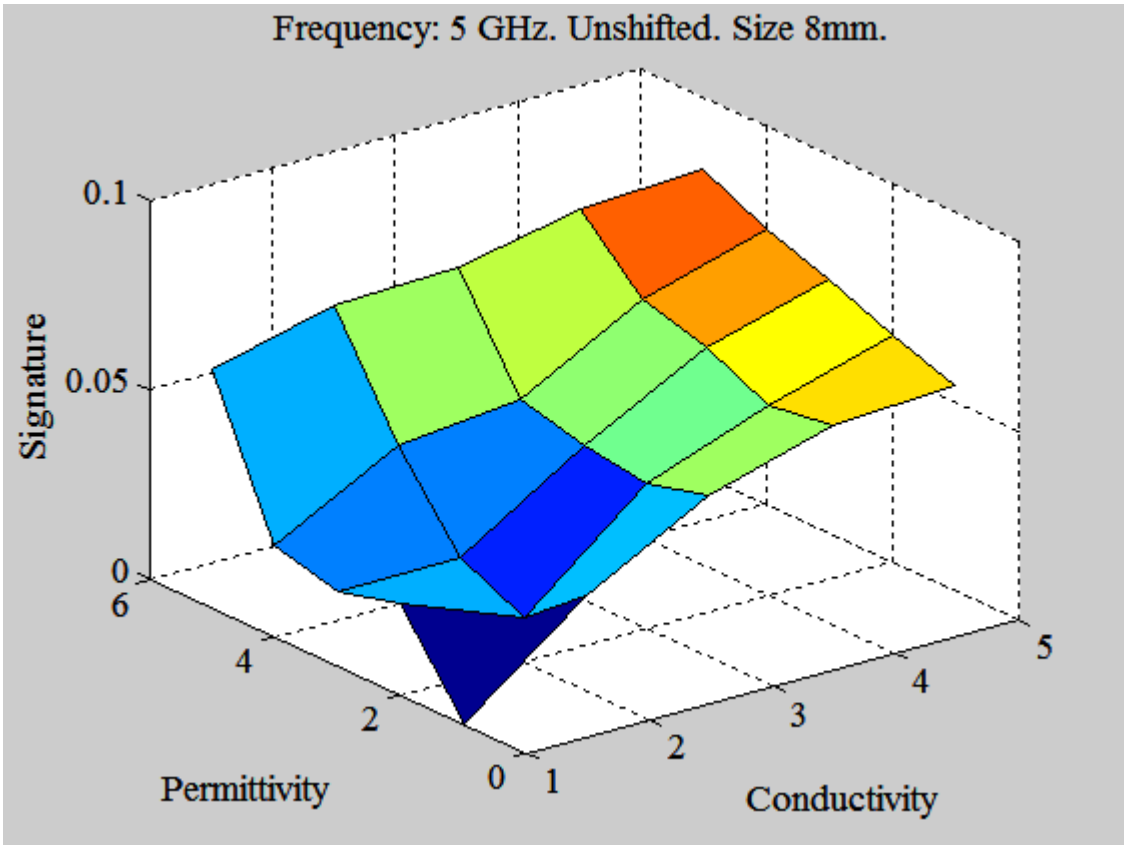

Figure 36: Signature as it appears in equation (4). Tumour details specified at top of plot. A "size" of 8mm indicates a side length of 8mm, i.e., a cuboid with dimensions 8mm by 8mm by 8mm.

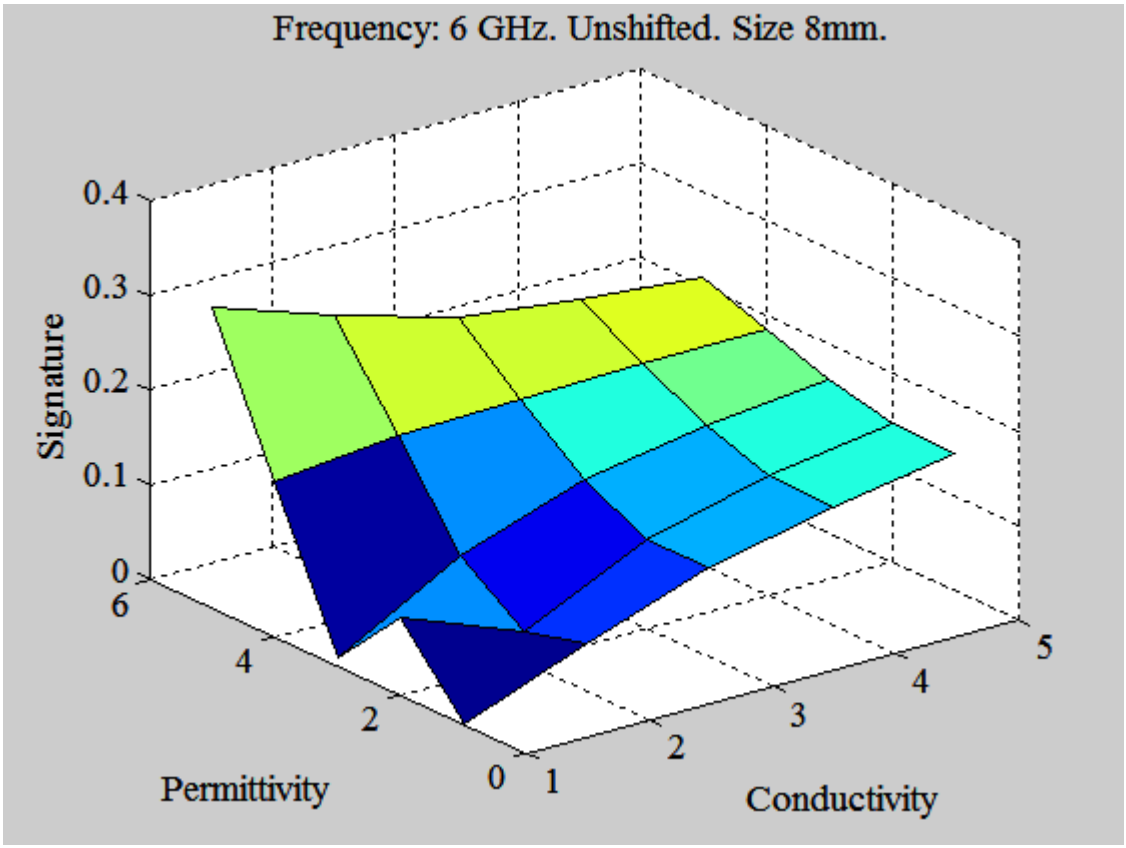

Figure 37: Signature as it appears in equation (4). Tumour details specified at top of plot. A "size" of 8mm indicates a side length of 8mm, i.e., a cuboid with dimensions 8mm by 8mm by 8mm.

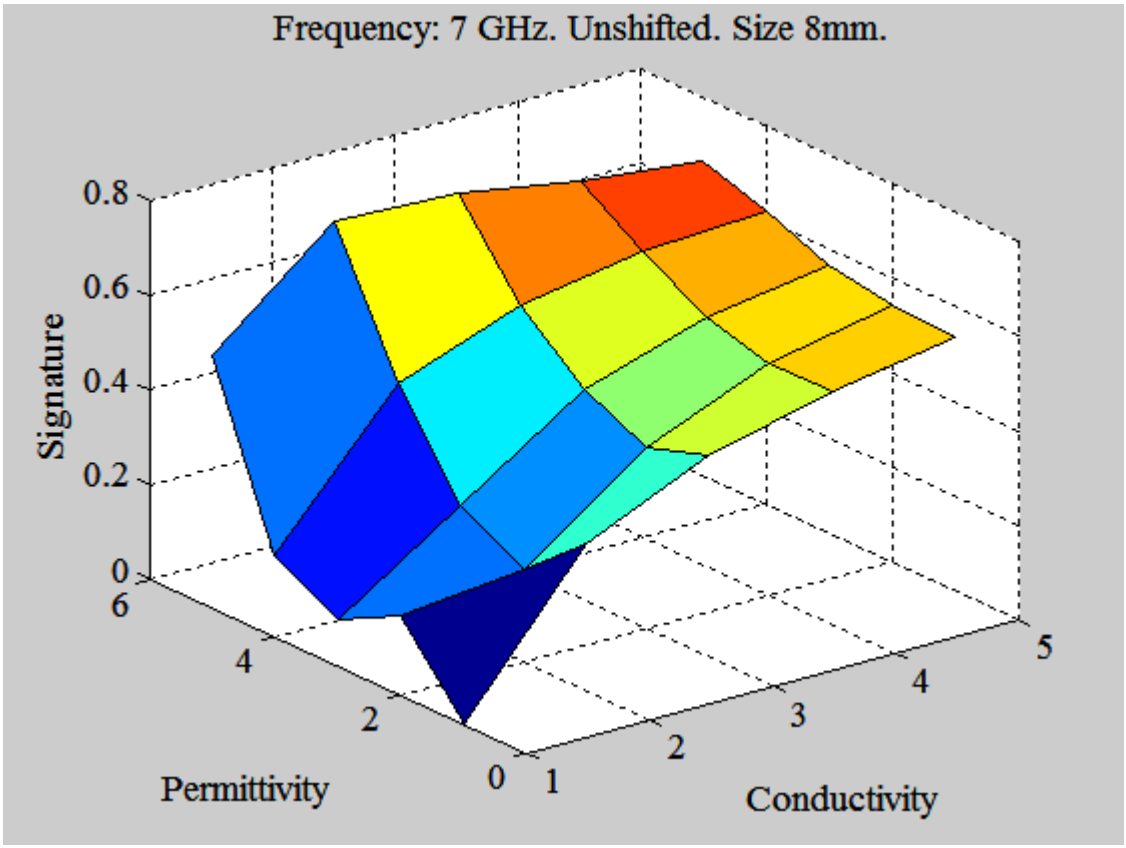

Figure 38: Signature as it appears in equation (4). Tumour details specified at top of plot. A "size" of 8mm indicates a side length of 8mm, i.e., a cuboid with dimensions 8mm by 8mm by 8mm.

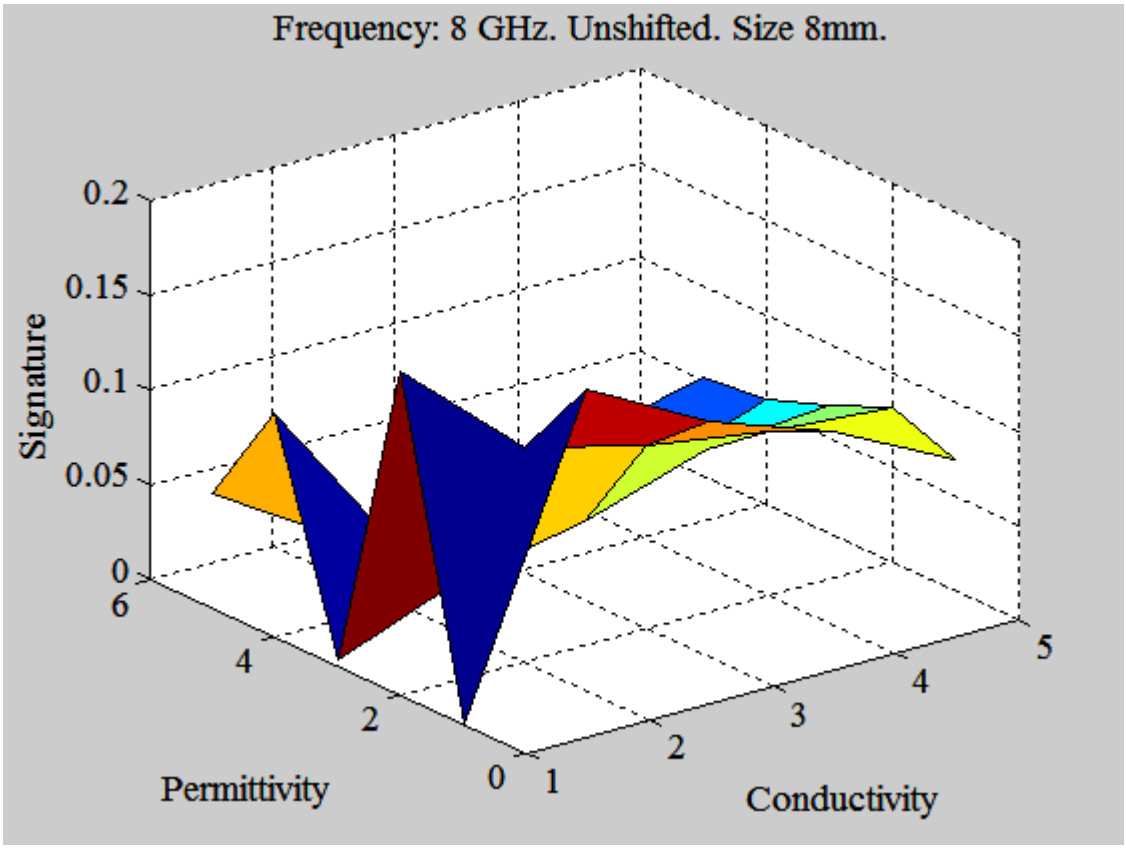

Figure 39: Signature as it appears in equation (4). Tumour details specified at top of plot. A "size" of 8mm indicates a side length of 8mm, i.e., a cuboid with dimensions 8mm by 8mm by 8mm.

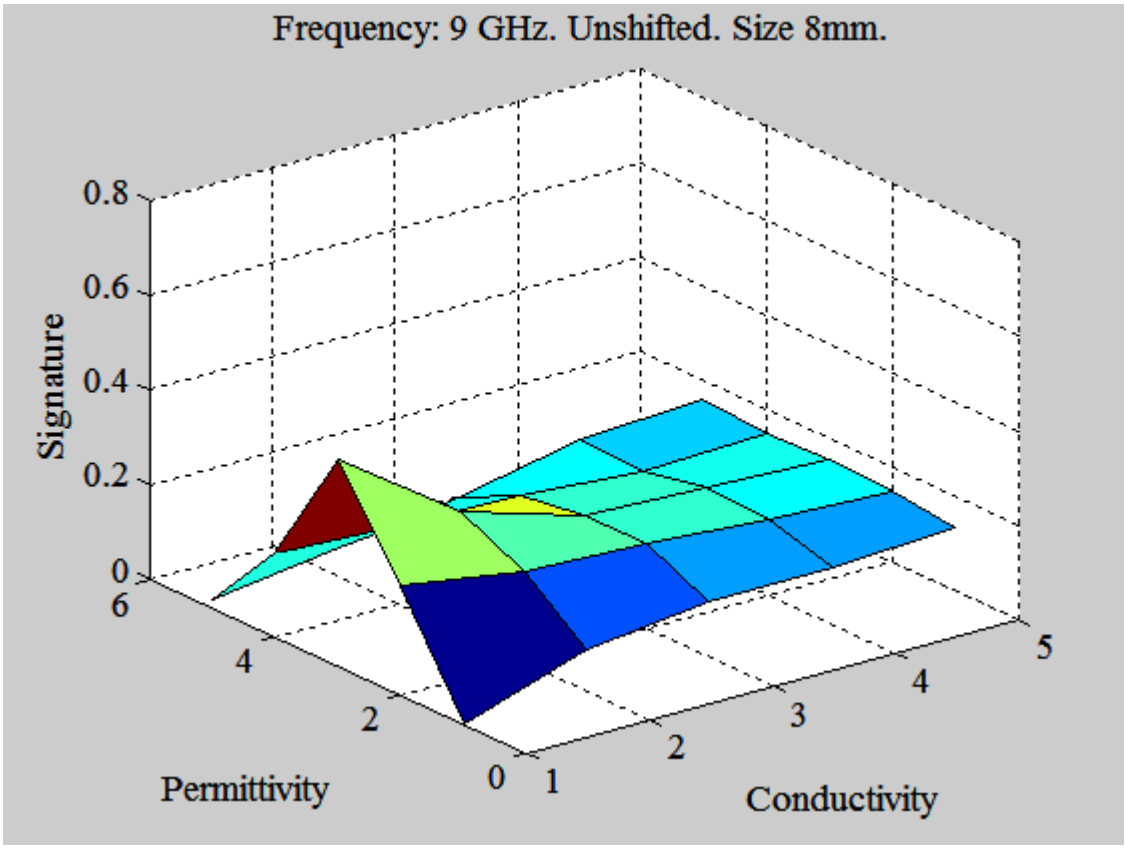

Figure 40: Signature as it appears in equation (4). Tumour details specified at top of plot. A "size" of 8mm indicates a side length of 8mm, i.e., a cuboid with dimensions 8mm by 8mm by 8mm.

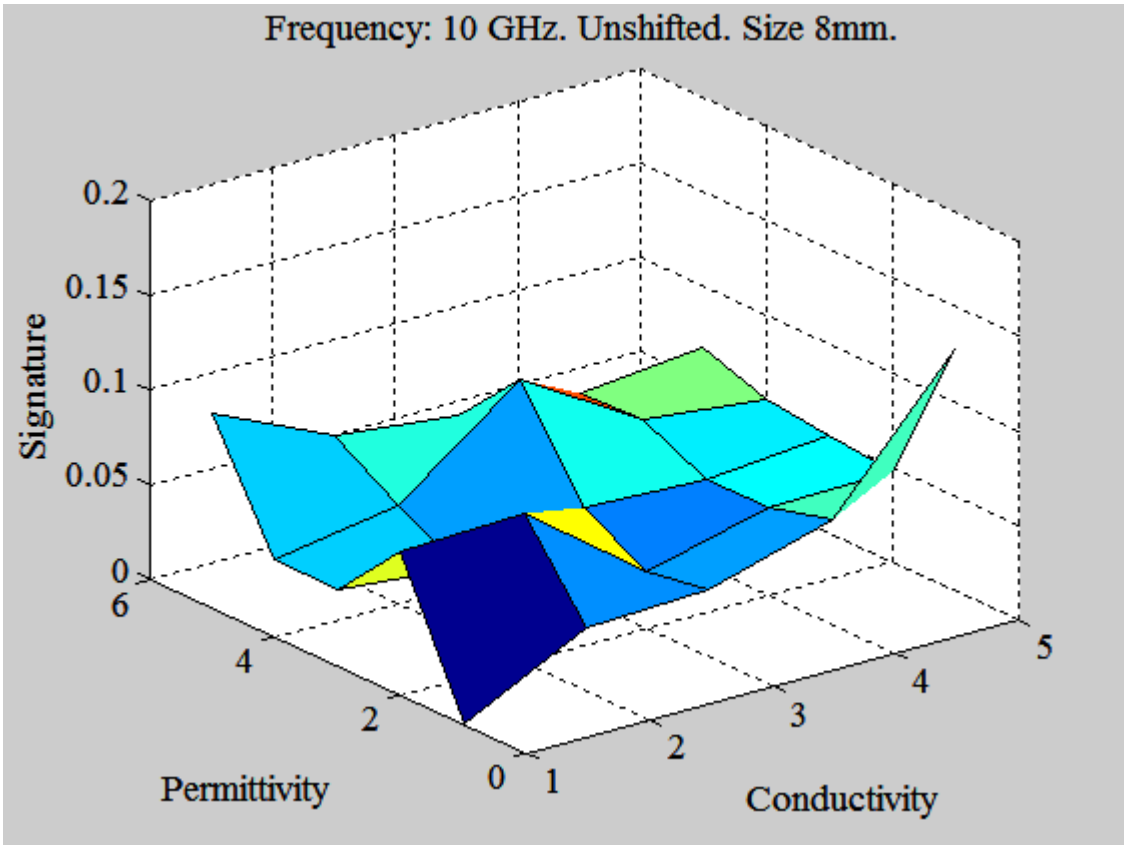

Figure 41: Signature as it appears in equation (4). Tumour details specified at top of plot. A "size" of 8mm indicates a side length of 8mm, i.e., a cuboid with dimensions 8mm by 8mm by 8mm.

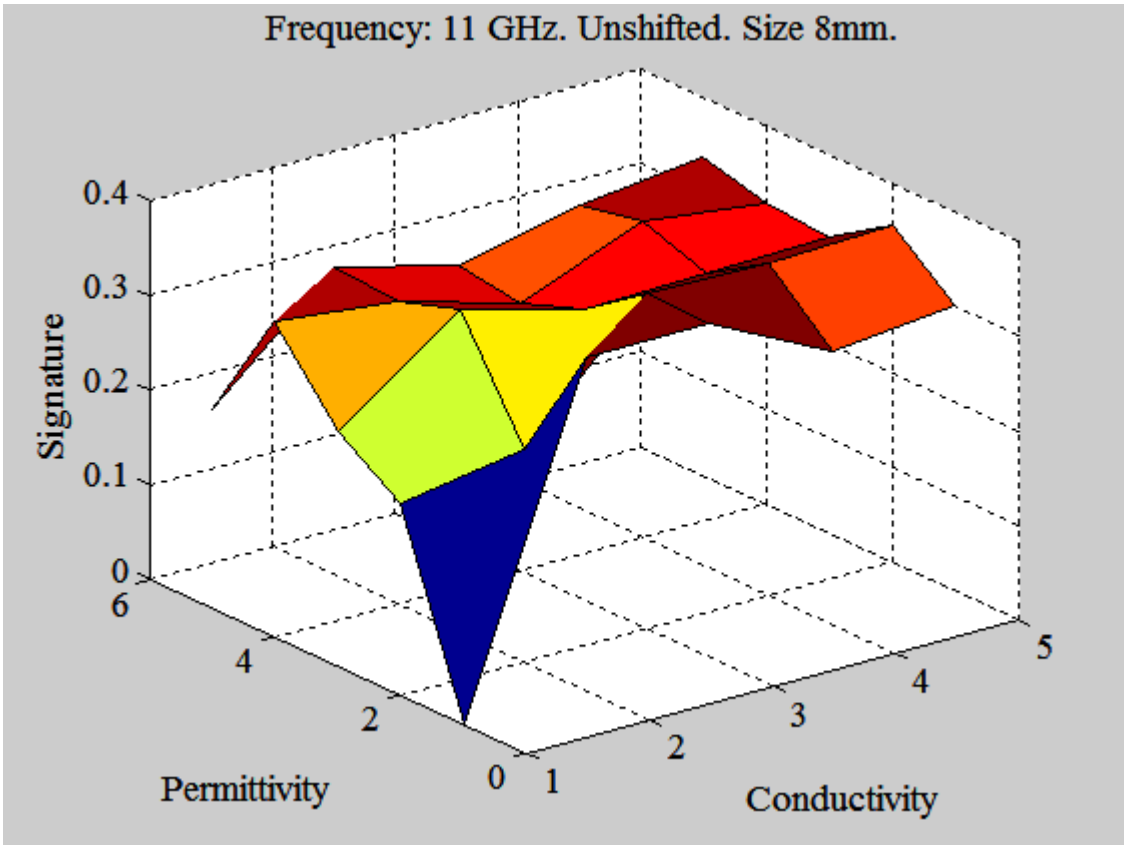

Figure 42: Signature as it appears in equation (4). Tumour details specified at top of plot. A "size" of 8mm indicates a side length of 8mm, i.e., a cuboid with dimensions 8mm by 8mm by 8mm.

Again, as we can see, the signals have become relatively noisy at 7 GHz and beyond, and a signature of almost 0.4 at a frequency of 11 GHz is clearly flawed. We again see the best sensitivity in the frequency range of 4-6 GHz. An interesting note is the lack of sensitivity at 3 GHz to permittivity, and yet the strong sensitivity at the same frequency to conductivity. As well, it is worthwhile to note that at the frequencies of 4-6 GHz, the antenna system seems very sensitive to permittivity, but as the conductivity increases, this sensitivity decreases. This hints at an antagonistic effect that the two dielectric parameters have on each other. As of yet there is no theory as to the cause of such an effect, however, its consequences must be considered in the future designs of this system.

Size

The side length is varied from 2 to 6 mm, and the permittivity is varied from a contrast of 2 to 4, as mentioned previously.

The signature present in equation (3) will now be analyzed.

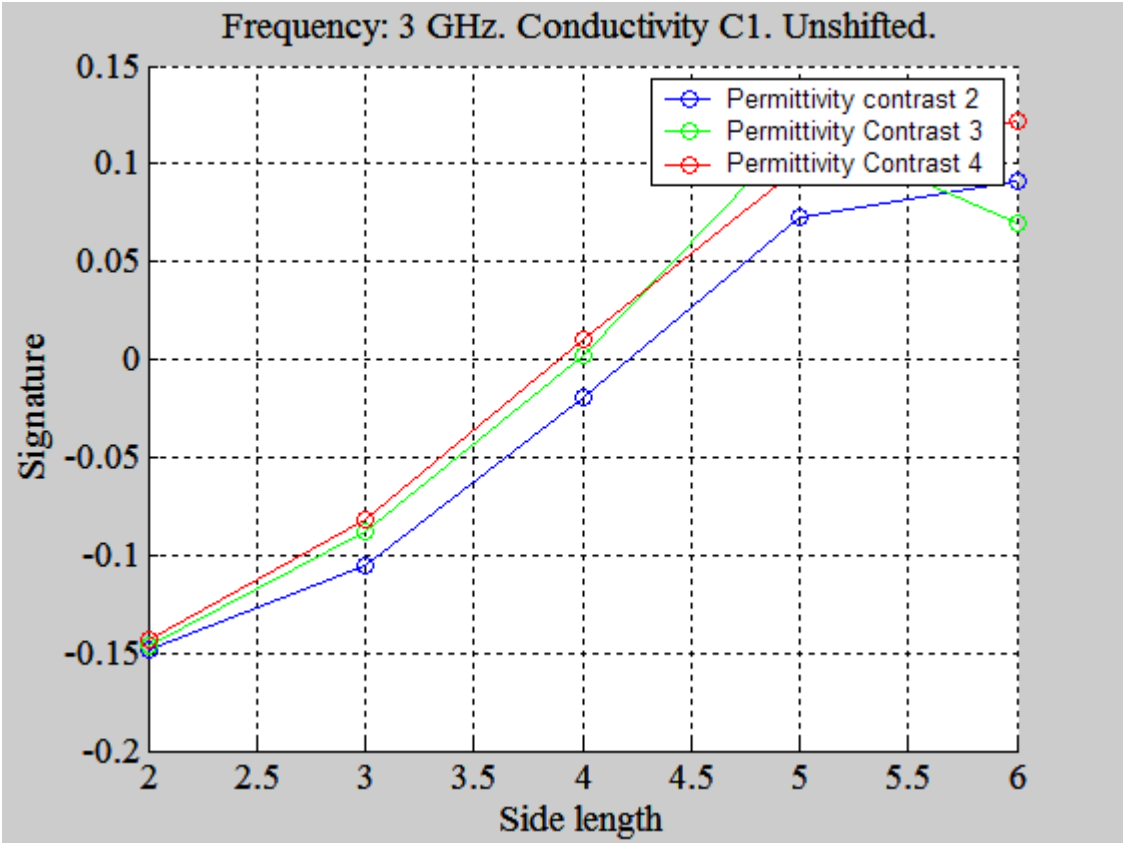

Figure 43: The signature in equation (3). Specific information regarding the set up stated in the plot title.

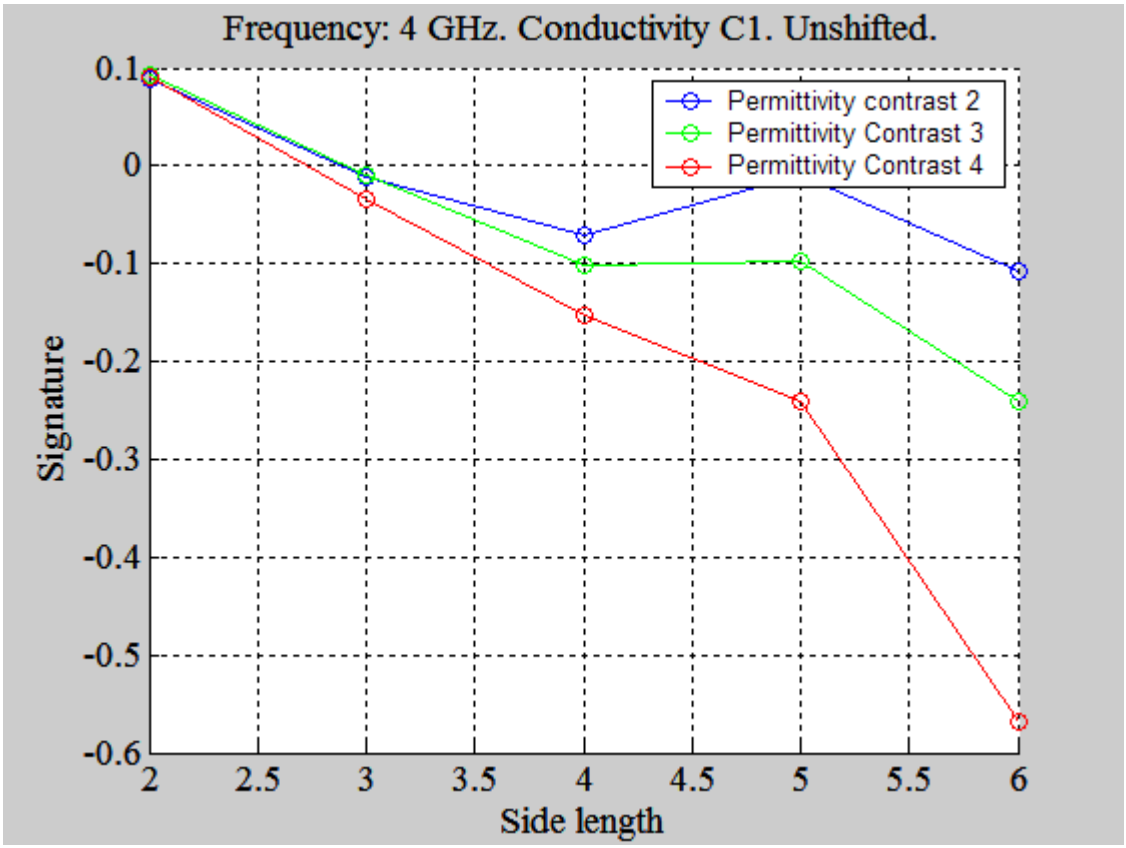

Figure 44: The signature in equation (3). Specific information regarding the set up stated in the plot title.

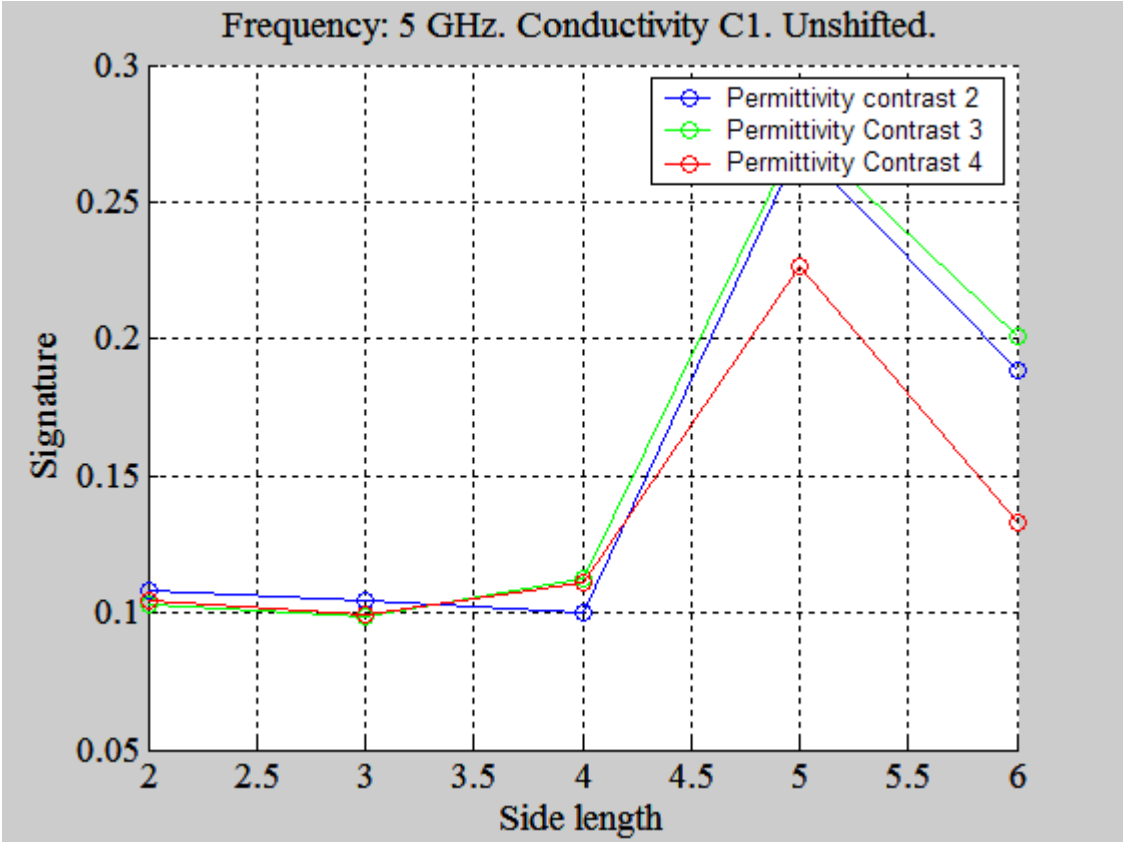

Figure 45: The signature in equation (3). Specific information regarding the set up stated in the plot title.

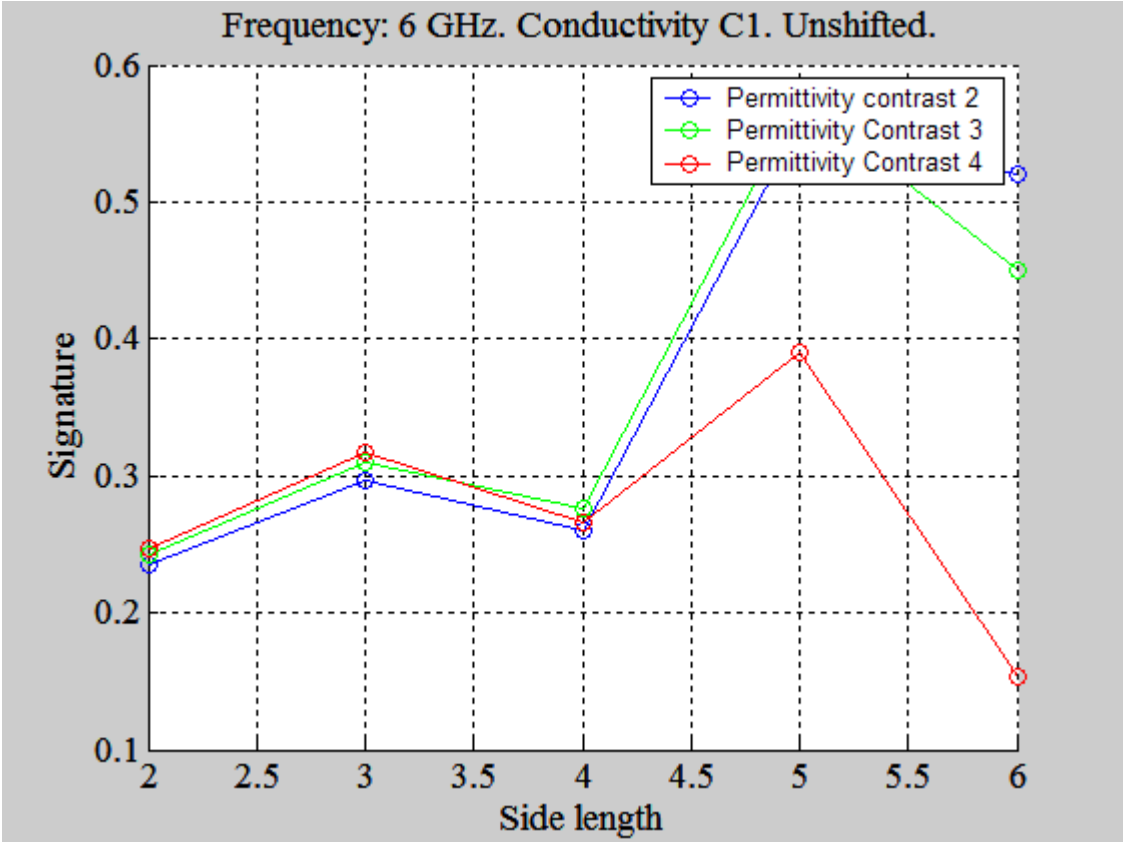

Figure 46: The signature in equation (3). Specific information regarding the set up stated in the plot title.

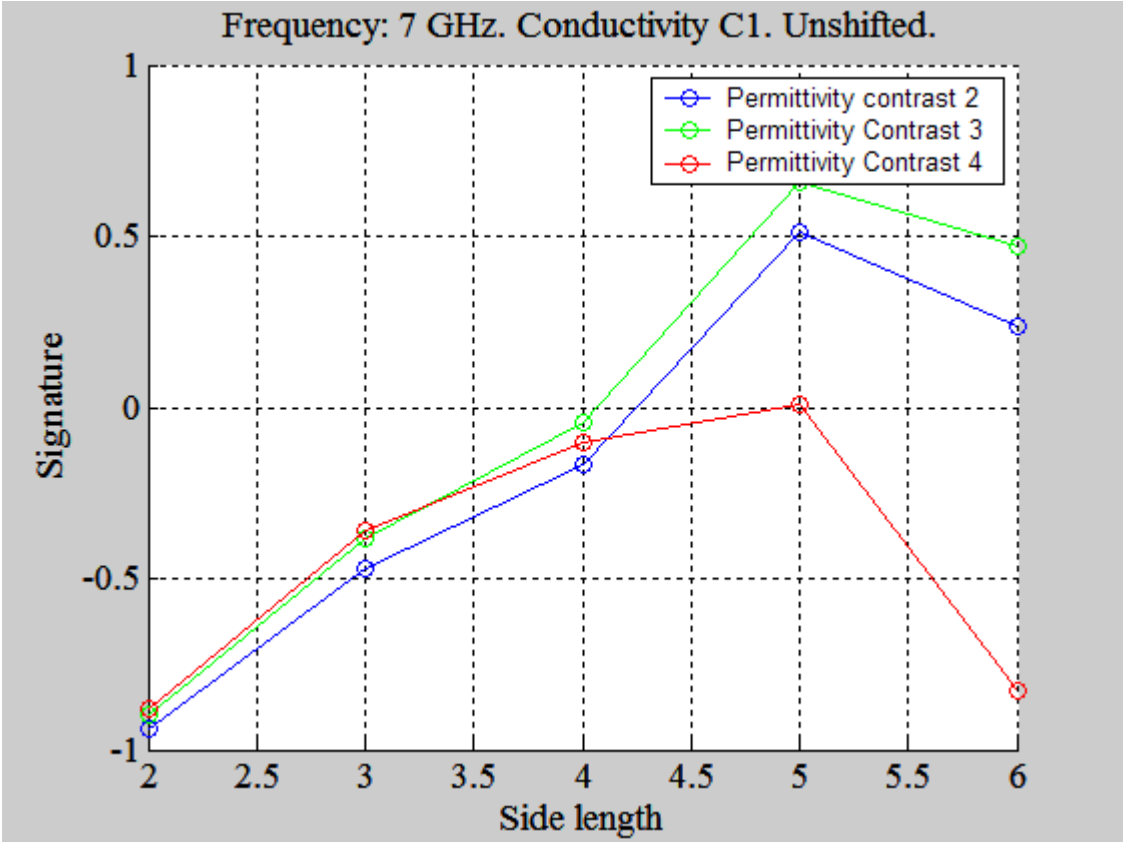

Figure 47: The signature in equation (3). Specific information regarding the set up stated in the plot title.

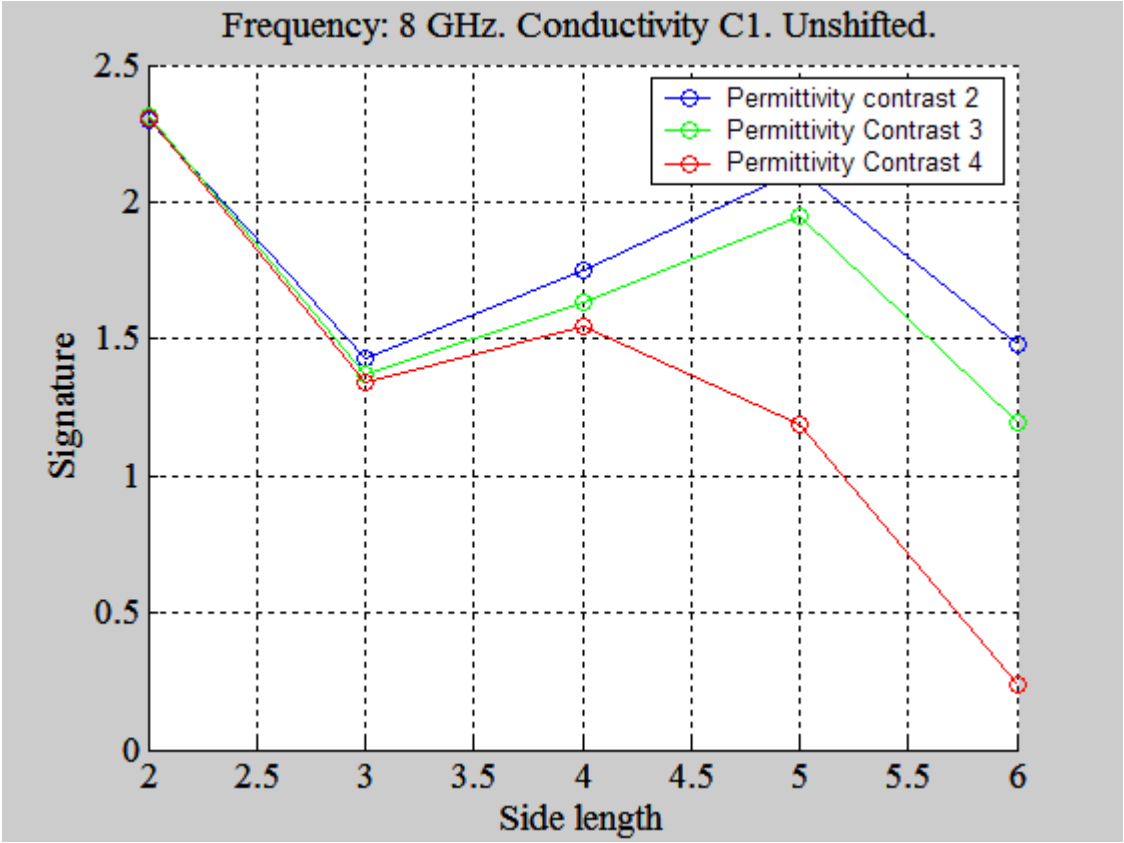

Figure 48: The signature in equation (3). Specific information regarding the set up stated in the plot title.

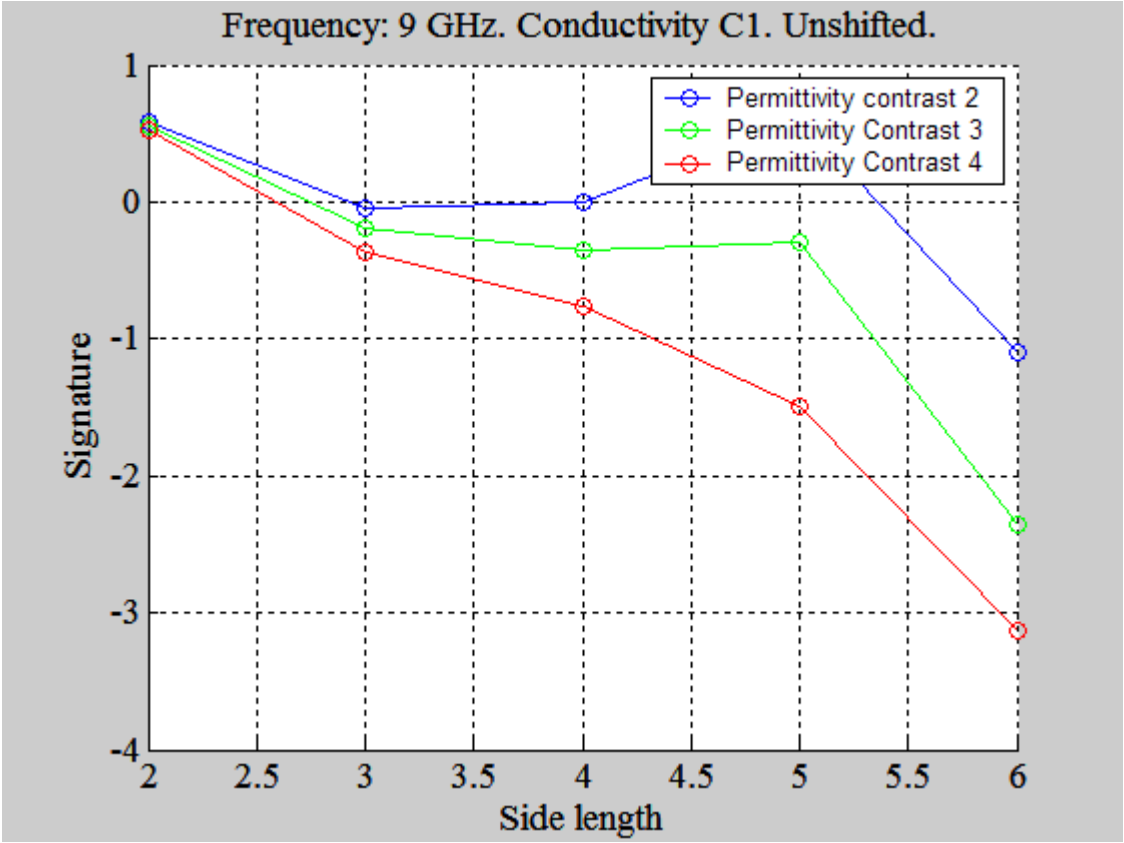

Figure 49: The signature in equation (3). Specific information regarding the set up stated in the plot title.

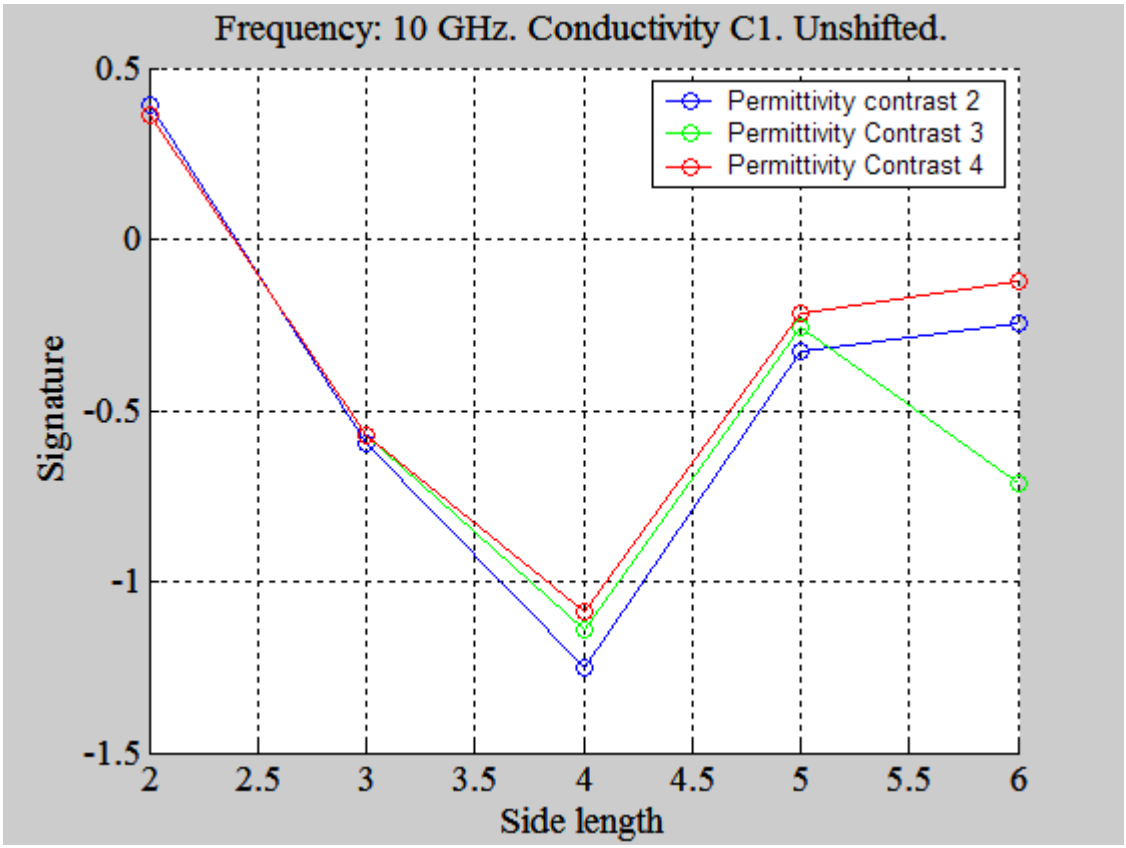

Figure 50: The signature in equation (3). Specific information regarding the set up stated in the plot title.

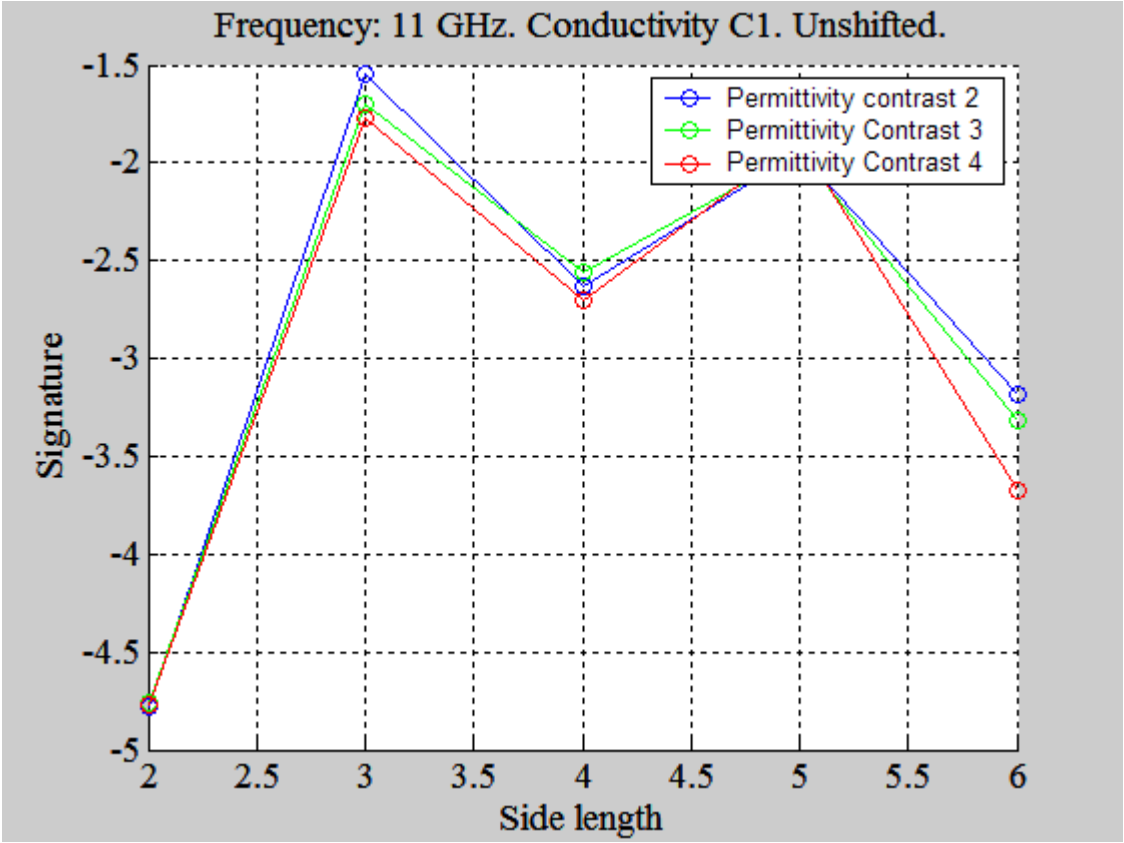

Figure 51: The signature in equation (3). Specific information regarding the set up stated in the plot title.

Aside from the final figure, Figure 51, there exists no difference greater than 1 dB in any of the cases. Since at 11 GHz a large amount of numerical noise is present, we are forced to conclude that using the signature present in equation (3) results in absolutely no sensitivity of the antenna to tumours with a volume of less than 216 mm^3.

The following figures relate to the signature of equation (4).

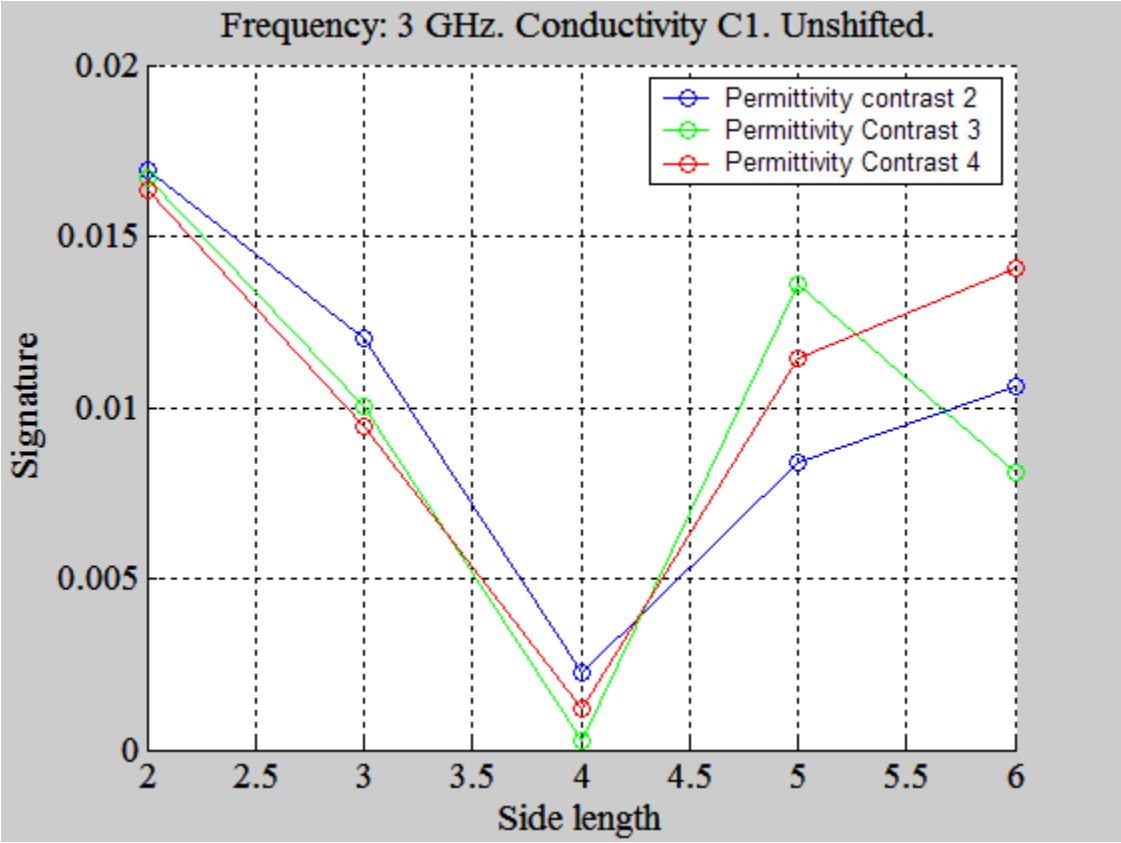

Figure 52: Size varied with a signature according to equation (4). Sizes used are 2,3,4,5, and 6 mm, with linear interpolation between. Permittivity is also varied. Other details specified in title of plot.

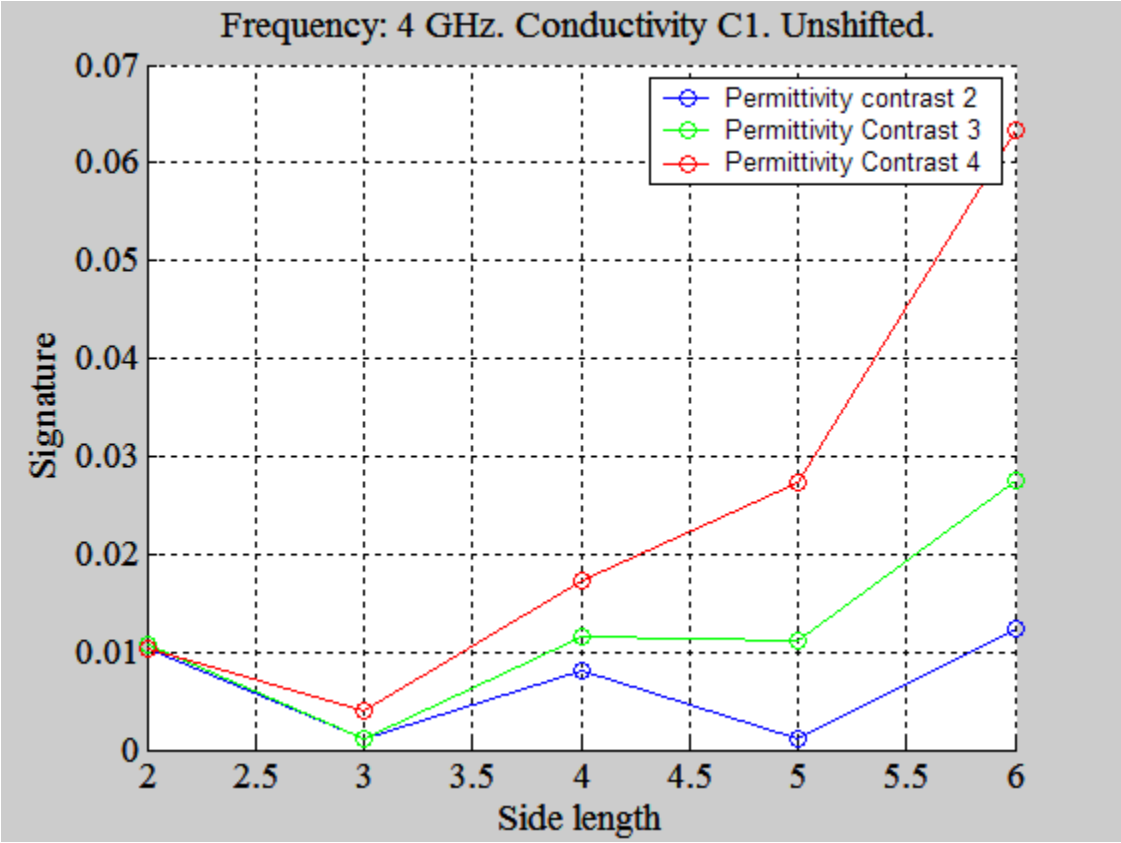

Figure 53: Size varied with a signature according to equation (4). Sizes used are 2,3,4,5, and 6 mm, with linear interpolation between. Permittivity is also varied. Other details specified in title of plot.

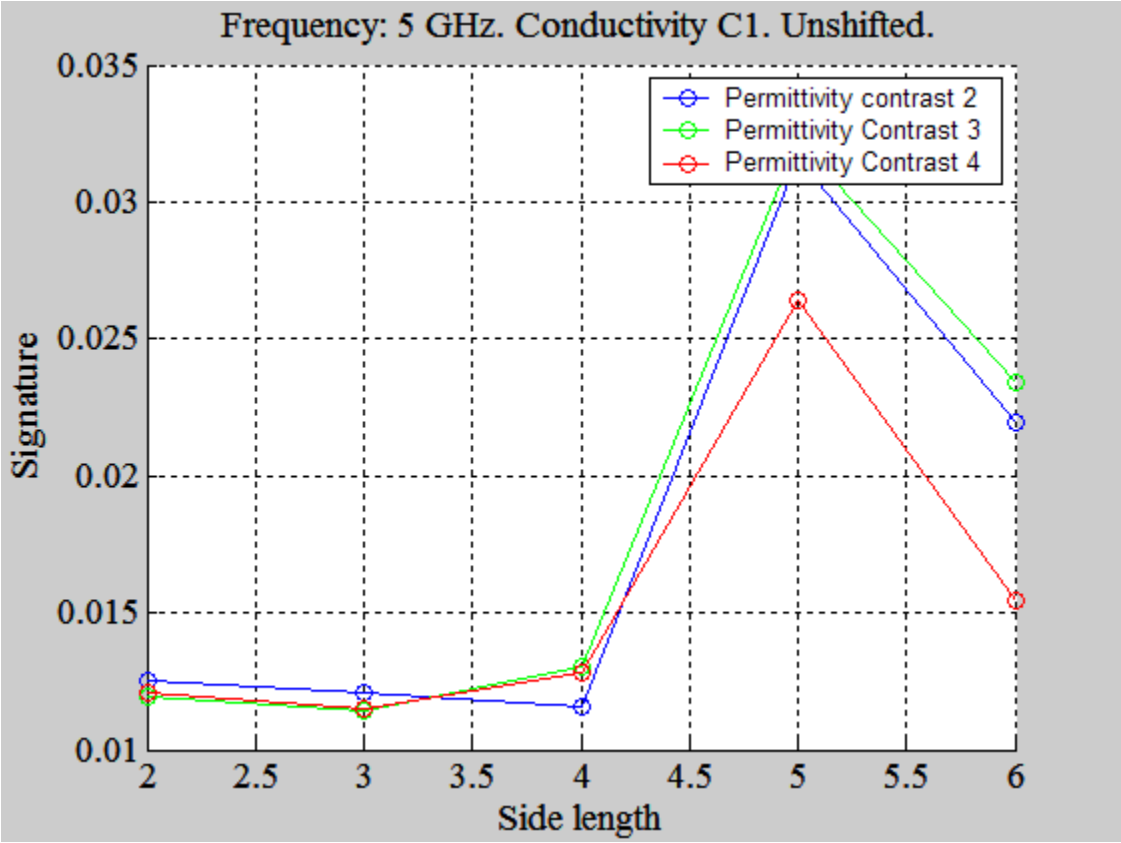

Figure 54: Size varied with a signature according to equation (4). Sizes used are 2,3,4,5, and 6 mm, with linear interpolation between. Permittivity is also varied. Other details specified in title of plot.

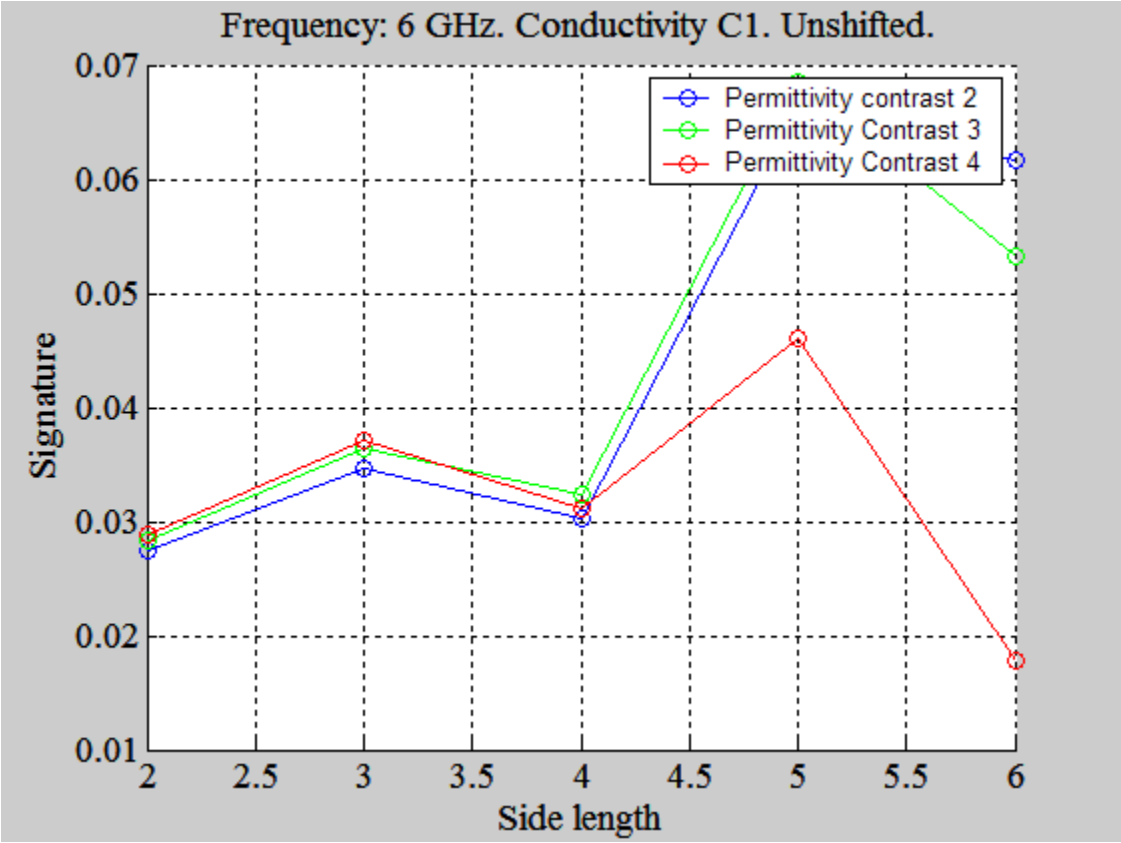

Figure 55: Size varied with a signature according to equation (4). Sizes used are 2,3,4,5, and 6 mm, with linear interpolation between. Permittivity is also varied. Other details specified in title of plot.

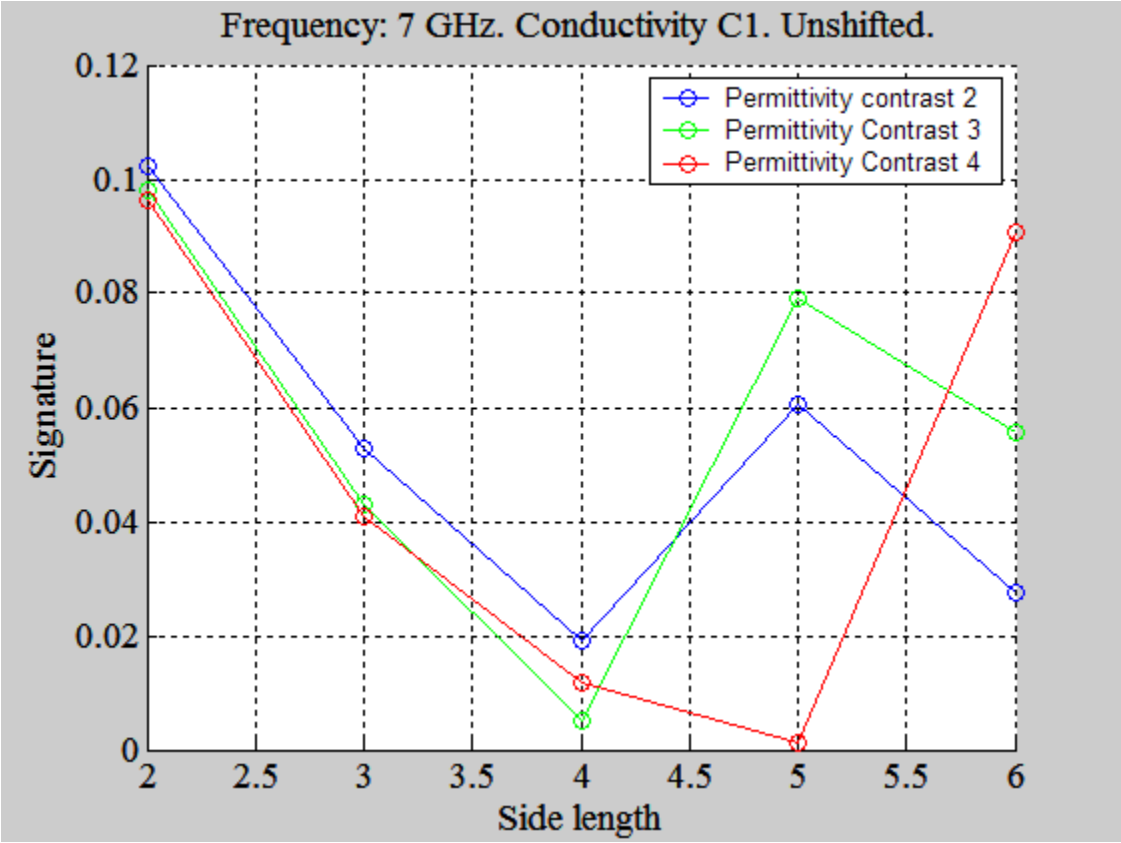

Figure 56: Size varied with a signature according to equation (4). Sizes used are 2,3,4,5, and 6 mm, with linear interpolation between. Permittivity is also varied. Other details specified in title of plot.

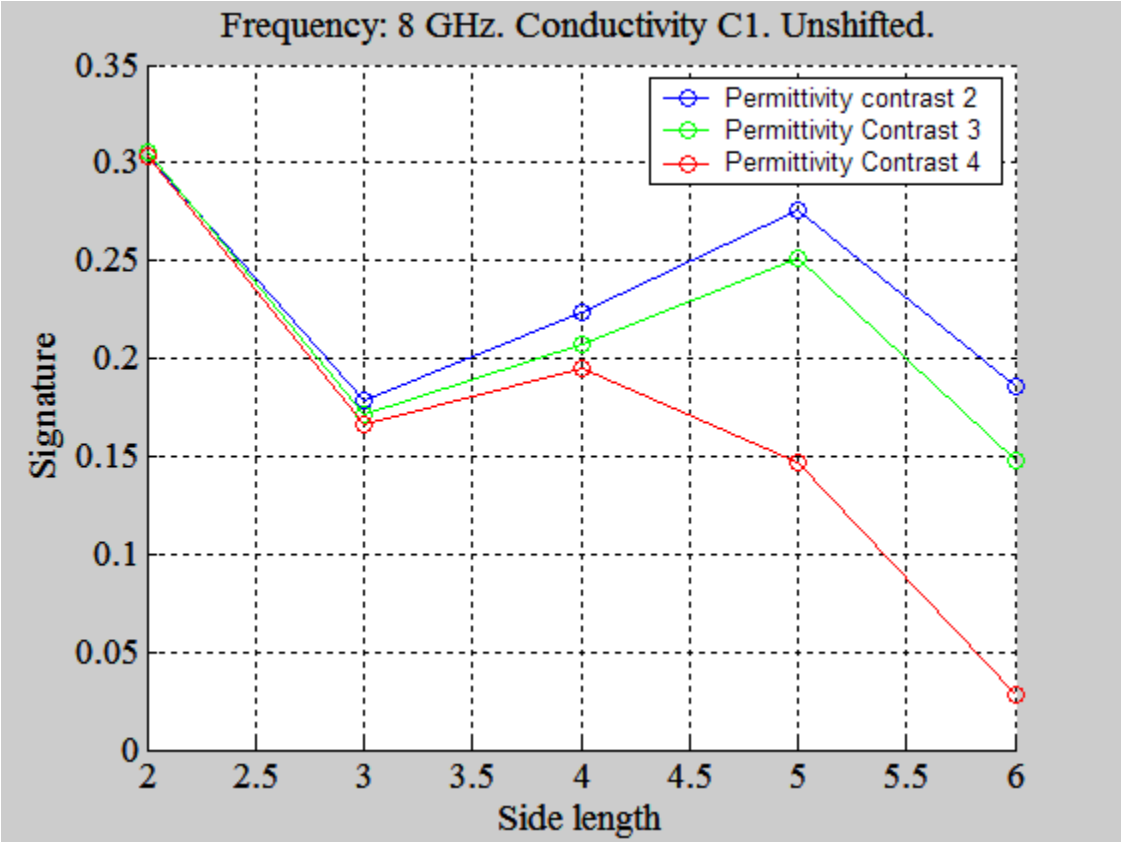

Figure 57: Size varied with a signature according to equation (4). Sizes used are 2,3,4,5, and 6 mm, with linear interpolation between. Permittivity is also varied. Other details specified in title of plot.

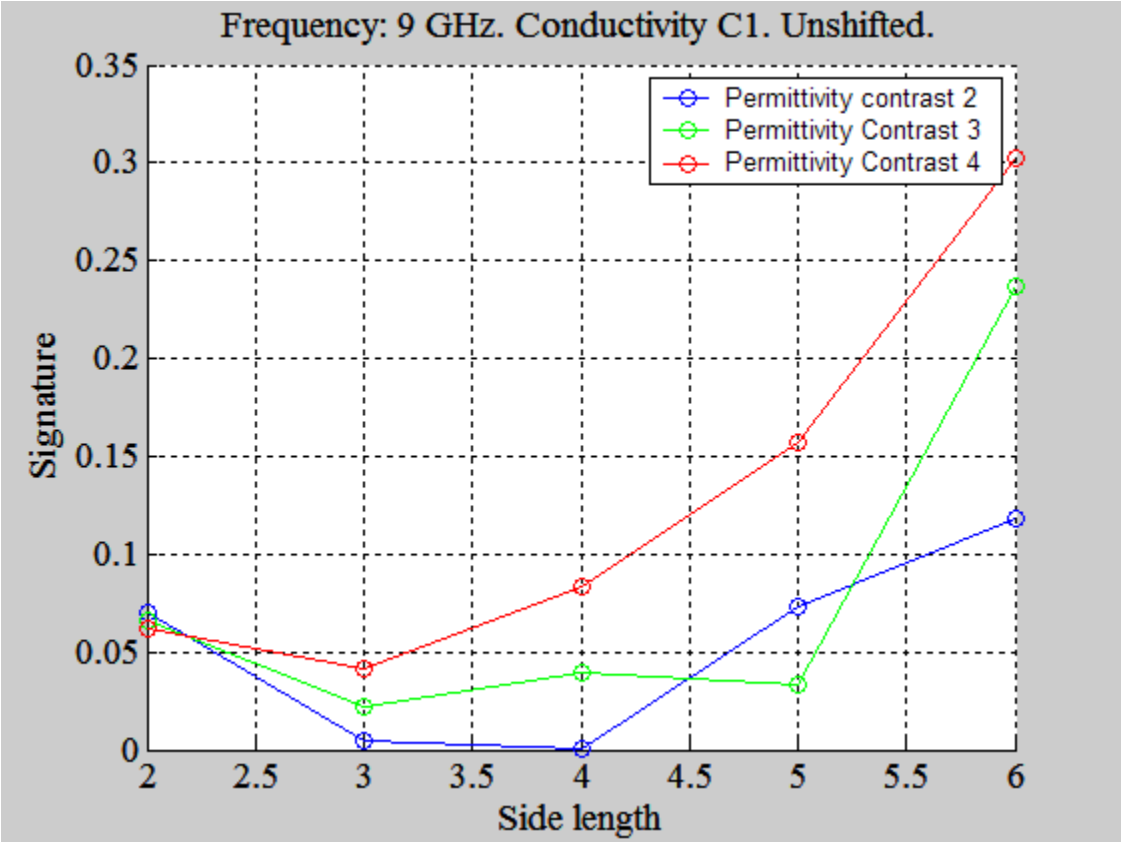

Figure 58: Size varied with a signature according to equation (4). Sizes used are 2,3,4,5, and 6 mm, with linear interpolation between. Permittivity is also varied. Other details specified in title of plot.

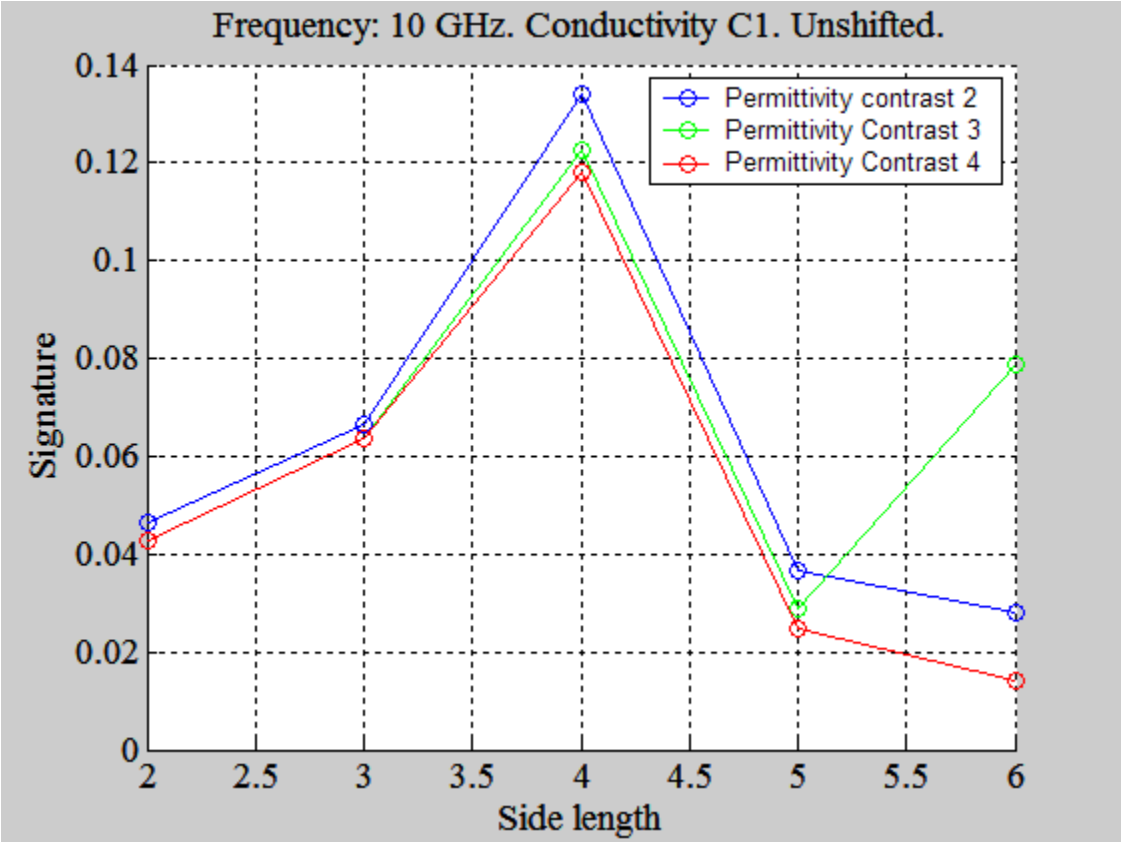

Figure 59: Size varied with a signature according to equation (4). Sizes used are 2,3,4,5, and 6 mm, with linear interpolation between. Permittivity is also varied. Other details specified in title of plot.

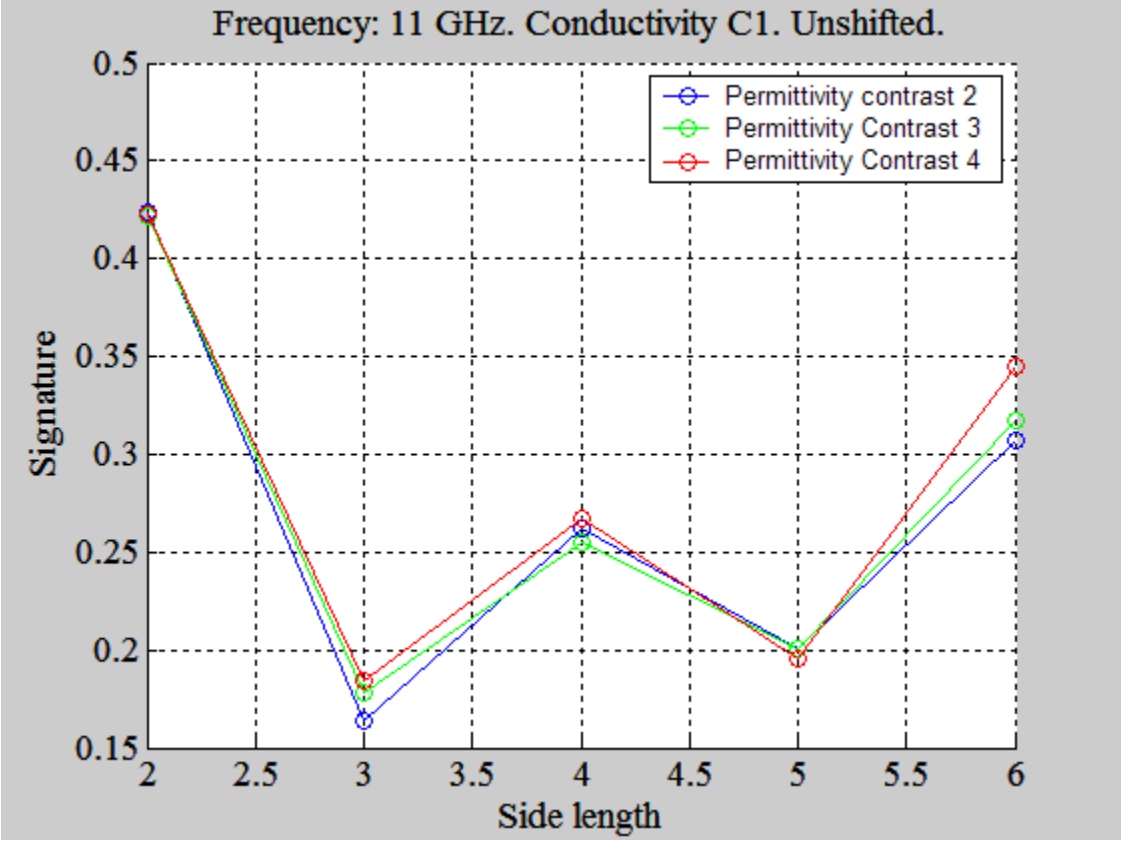

Figure 60: Size varied with a signature according to equation (4). Sizes used are 2,3,4,5, and 6 mm, with linear interpolation between. Permittivity is also varied. Other details specified in title of plot.

We can see that the behaviour of the signature with respect to size is very irregular and erratic. As expected, for the most part a higher permittivity results in a higher signature. However, at 3 GHz, the signature lowers from 2mm to 4mm and then rises from 4mm to 6mm. At 5 and 6 GHz, the signal spontaneously lowers at a side length of 6 mm. Again, 4 GHz is our most sensitive frequency, with data that intuitively makes sense. However, one is not able to dismiss this data immediately. Due to the wavelength size of the microwaves used, it is conceivable some unforeseen scattering occurs with particular tumour sizes at particular frequencies, which may reduce the signature. Since the wavelength is dependent on the frequency, there may be situation where at one frequency, the signature is reduced for a certain size, but at another frequency, the signature is reduced for an all together different size. Theoretically, as the tumour size decreases, this reduction in signature would be apparent at a higher frequency, where the wavelength will again match the tumour size. This may help explain the 3 GHz phenomenon. Since the frequency is so low, the wavelength matches

up with a larger tumour size, in this case approximately 4mm by 4mm by 4mm, causing a strange reduction in signature. This effect will have to be taken into account in future applications.

Location

The location of the tumour will be investigated with regard to the three axes available, x, y, and z. They will be investigated in that order in this section of the report.

The first axis, the x direction, was the first to be investigated and was originally simulated using a tumour with constant relative permittivity of 50 across all frequencies and constant effective conductivity of 4 S/m across all frequencies. The following graph displays the result across the frequency band using the signature in equation (3).

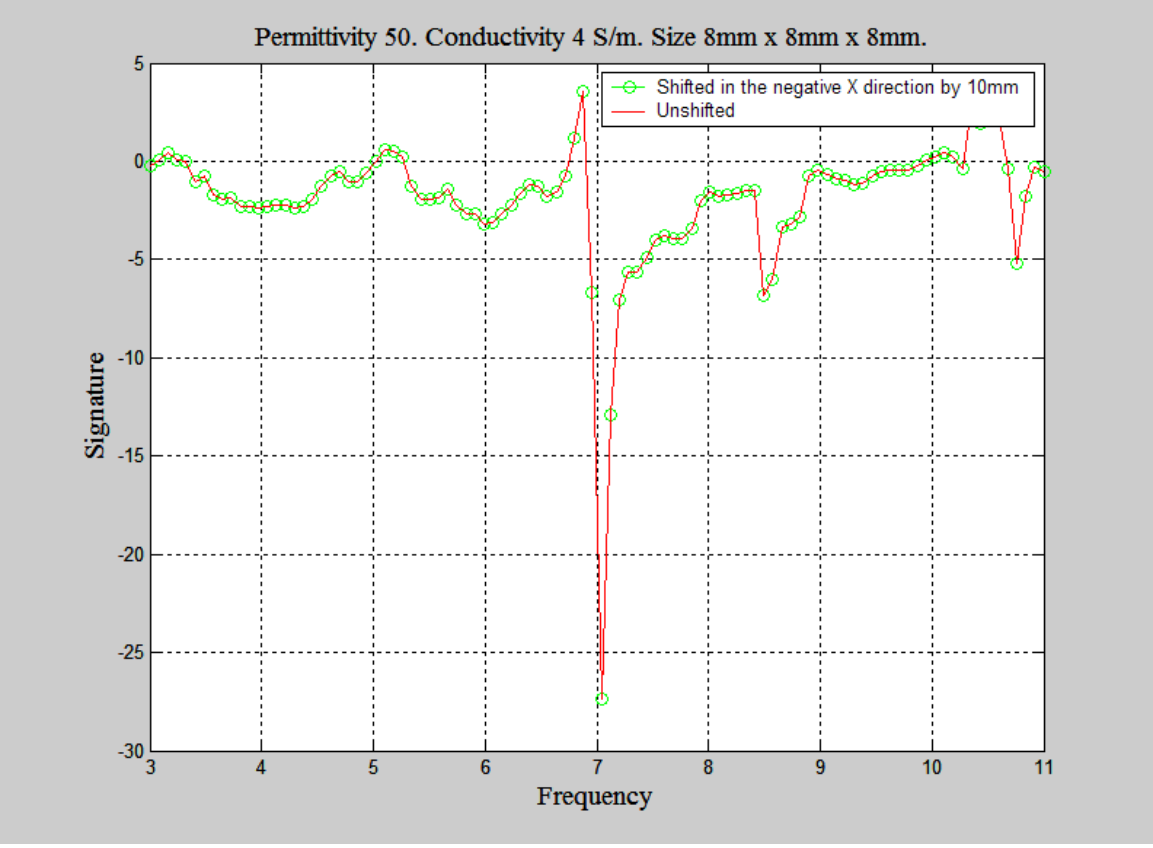

Figure 61: X direction shift compared to no X direction shift using the signature specified in equation (3). Relevant details regarding the tumour are stated in the plot title.

As we can see from Figure 61, there is absolutely no change with regard to a shift in the X direction. This will be advantageous in the experimental stages, as there will be no need to frustratingly perfect the X location of the tumour, as it has no effect on the signature provided by the tumour.

The y direction was varied using a conductivity contrast of 3. The results are displayed in the following figures, using signature equation (3).

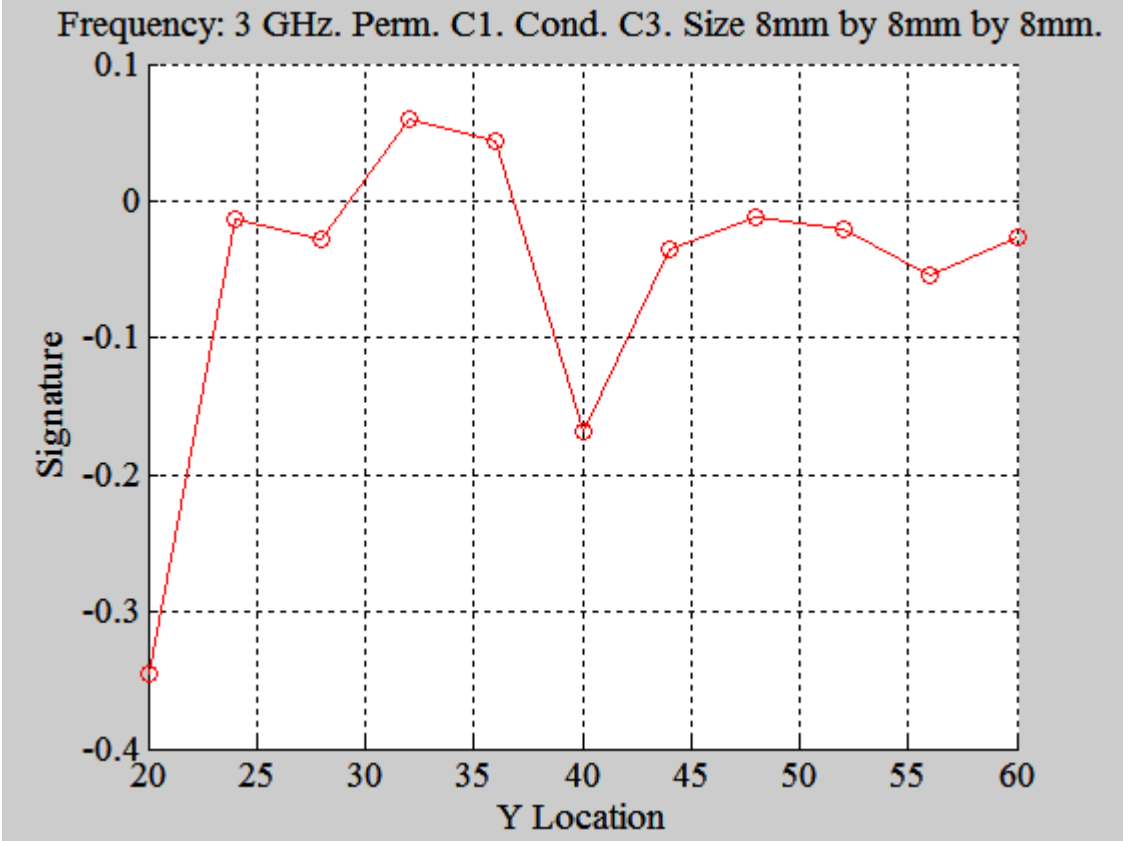

Figure 62: Y location changing at 3 GHz using signature equation (3). Other relevant details in plot title.

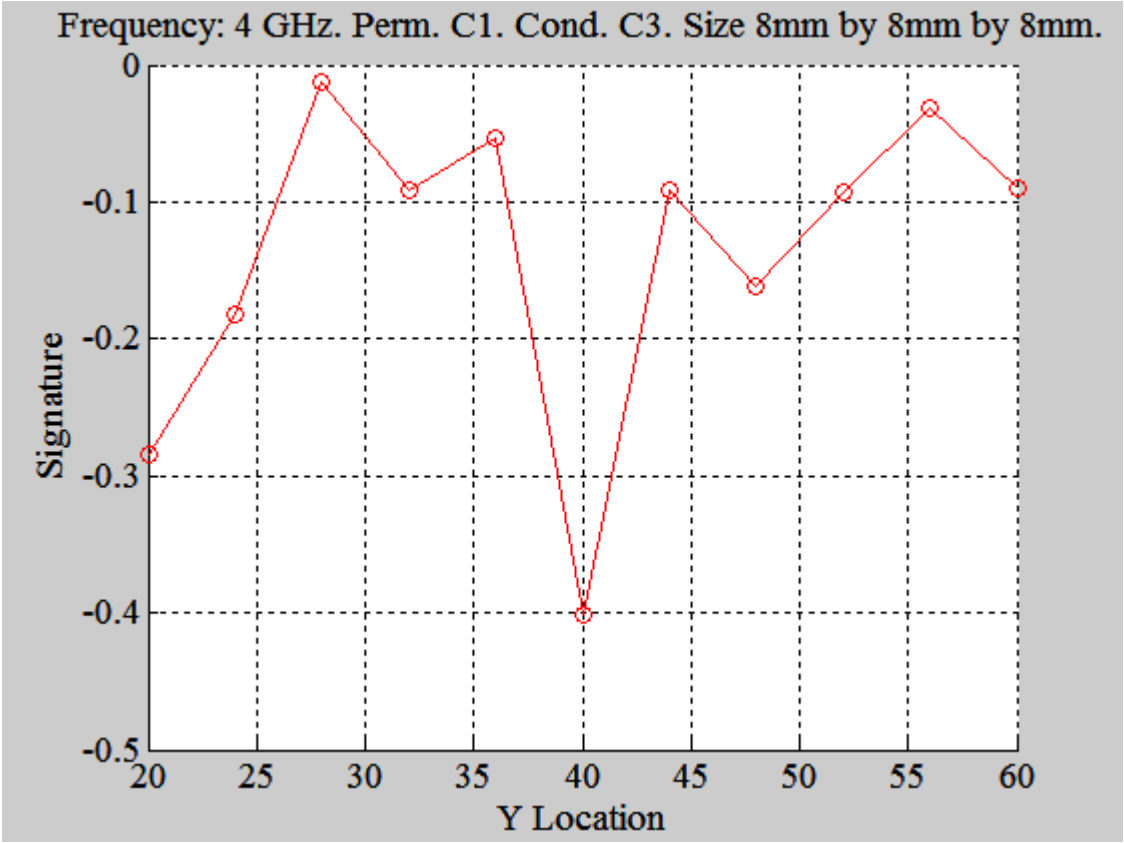

Figure 63: Y location changing at 4 GHz using signature equation (3). Other relevant details in plot title.

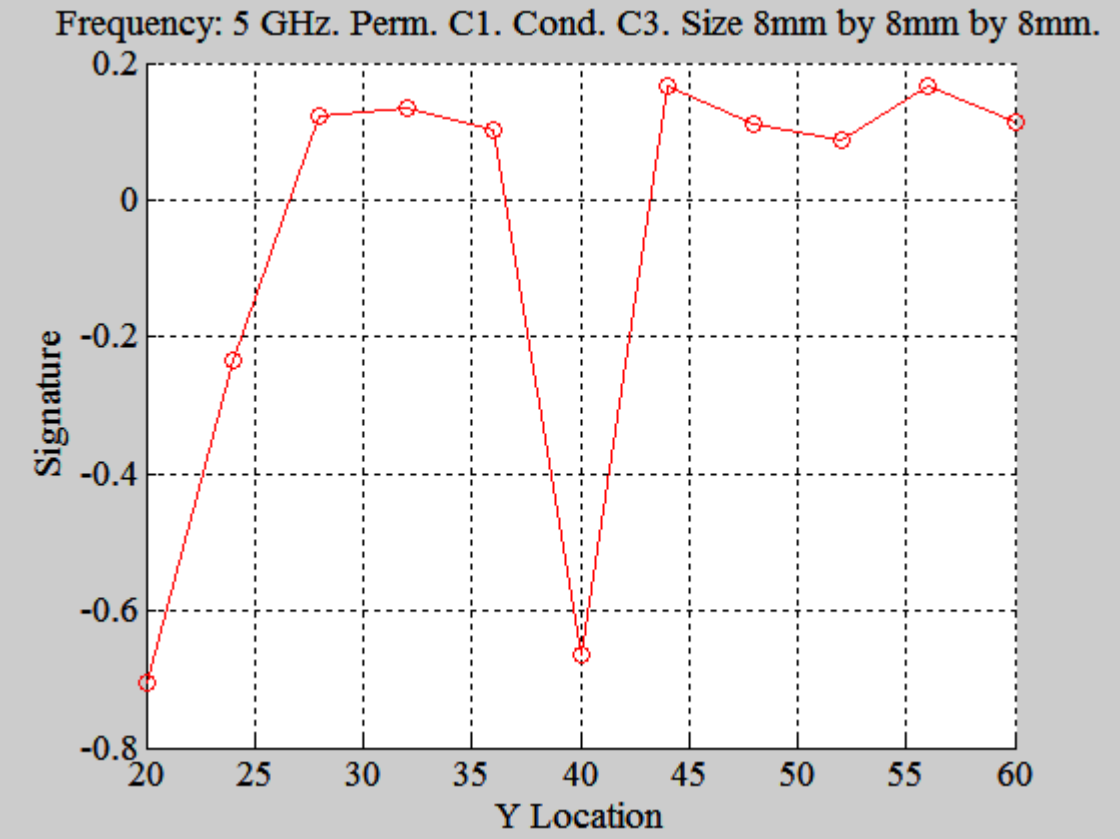

Figure 64: Y location changing at 5 GHz using signature equation (3). Other relevant details in plot title.

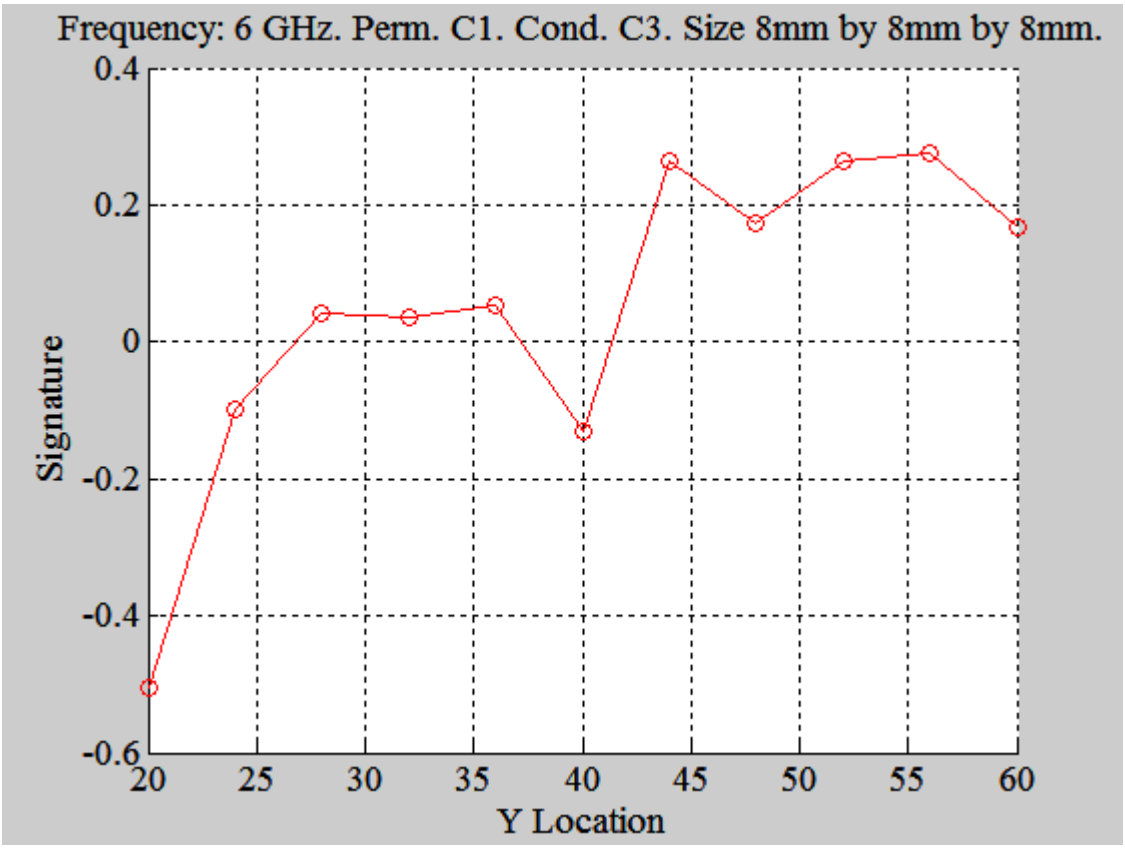

Figure 65: Y location changing at 6 GHz using signature equation (3). Other relevant details in plot title.

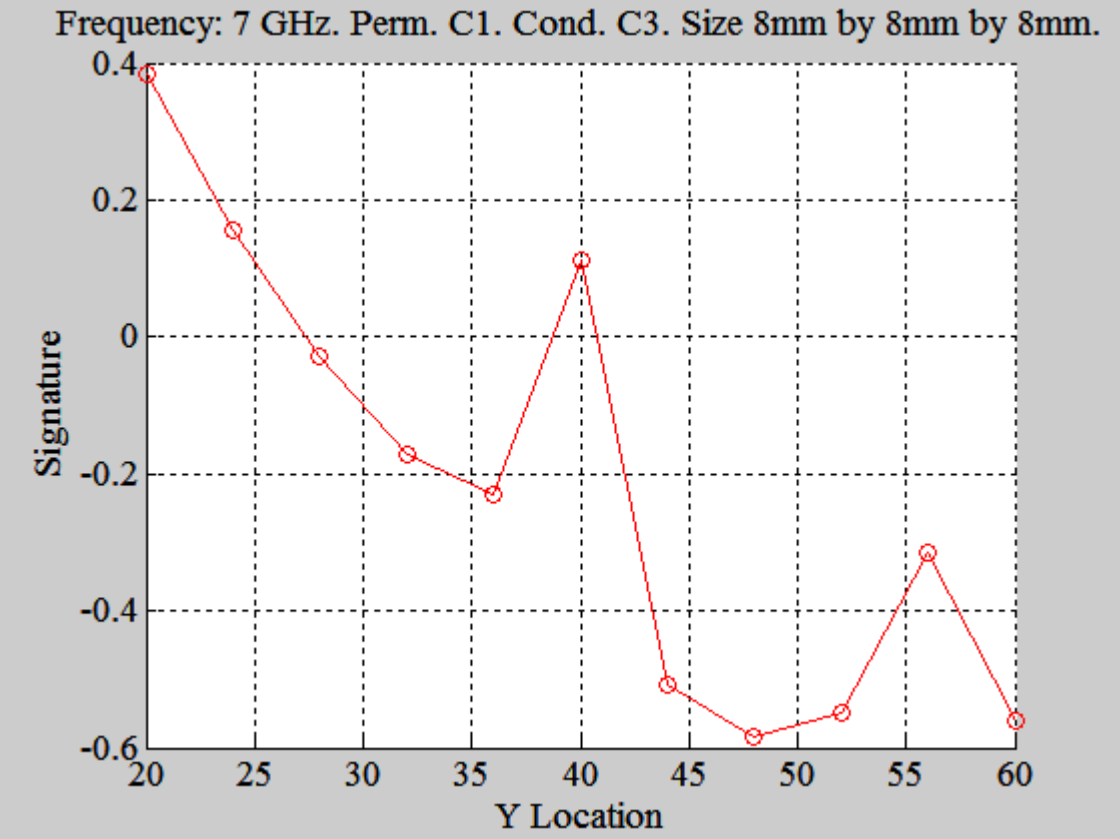

Figure 66: Y location changing at 7 GHz using signature equation (3). Other relevant details in plot title.

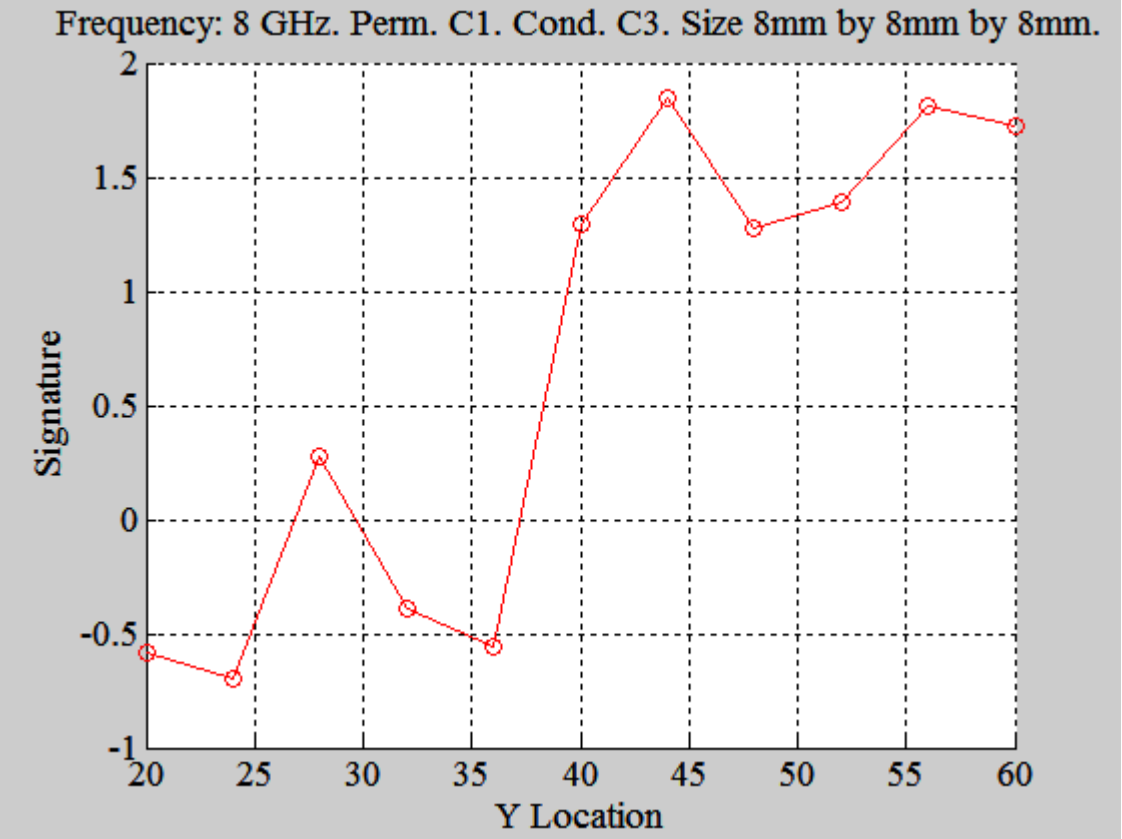

Figure 67: Y location changing at 8 GHz using signature equation (3). Other relevant details in plot title.

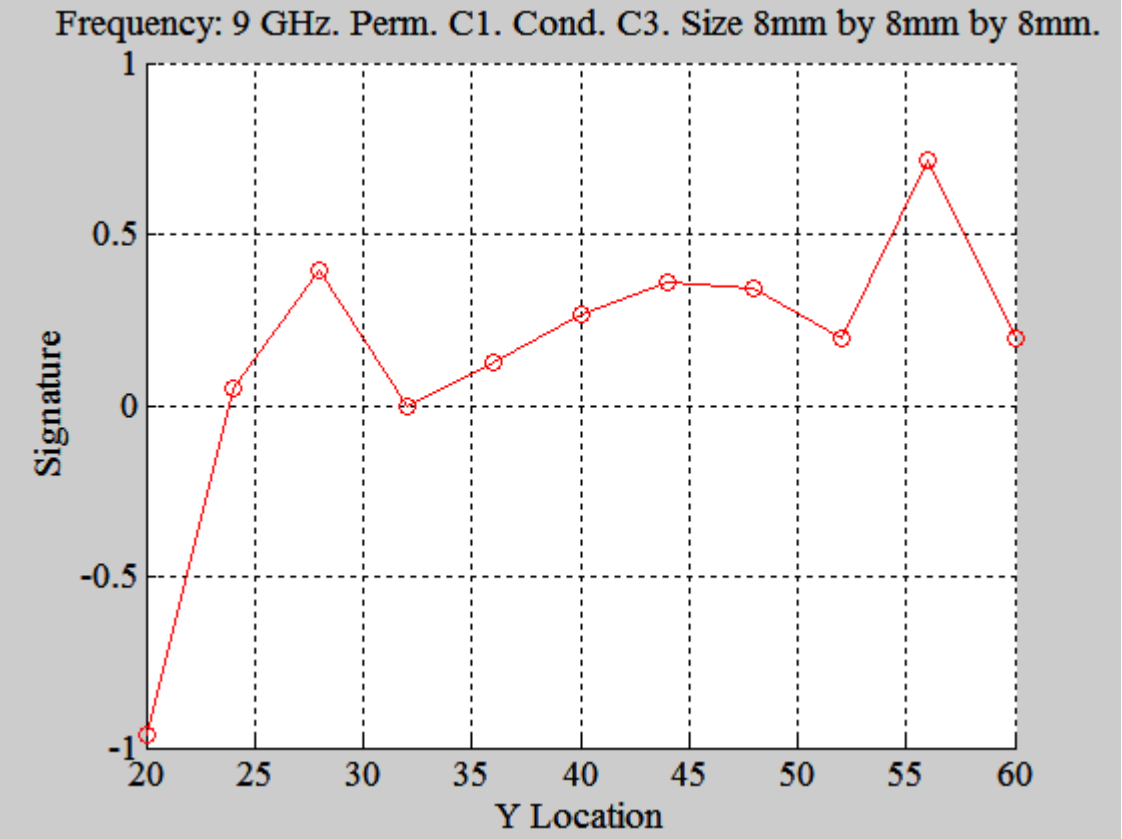

Figure 68: Y location changing at 9 GHz using signature equation (3). Other relevant details in plot title.

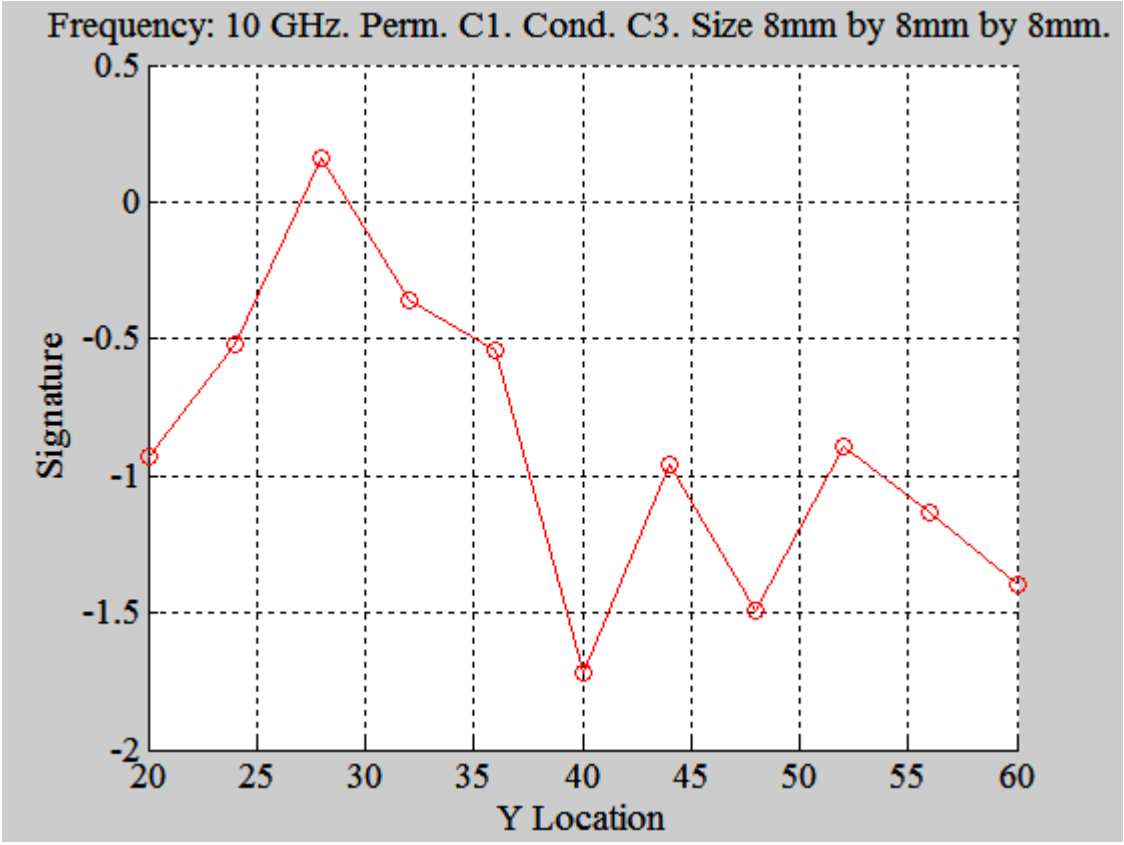

Figure 69: Y location changing at 10 GHz using signature equation (3). Other relevant details in plot title.

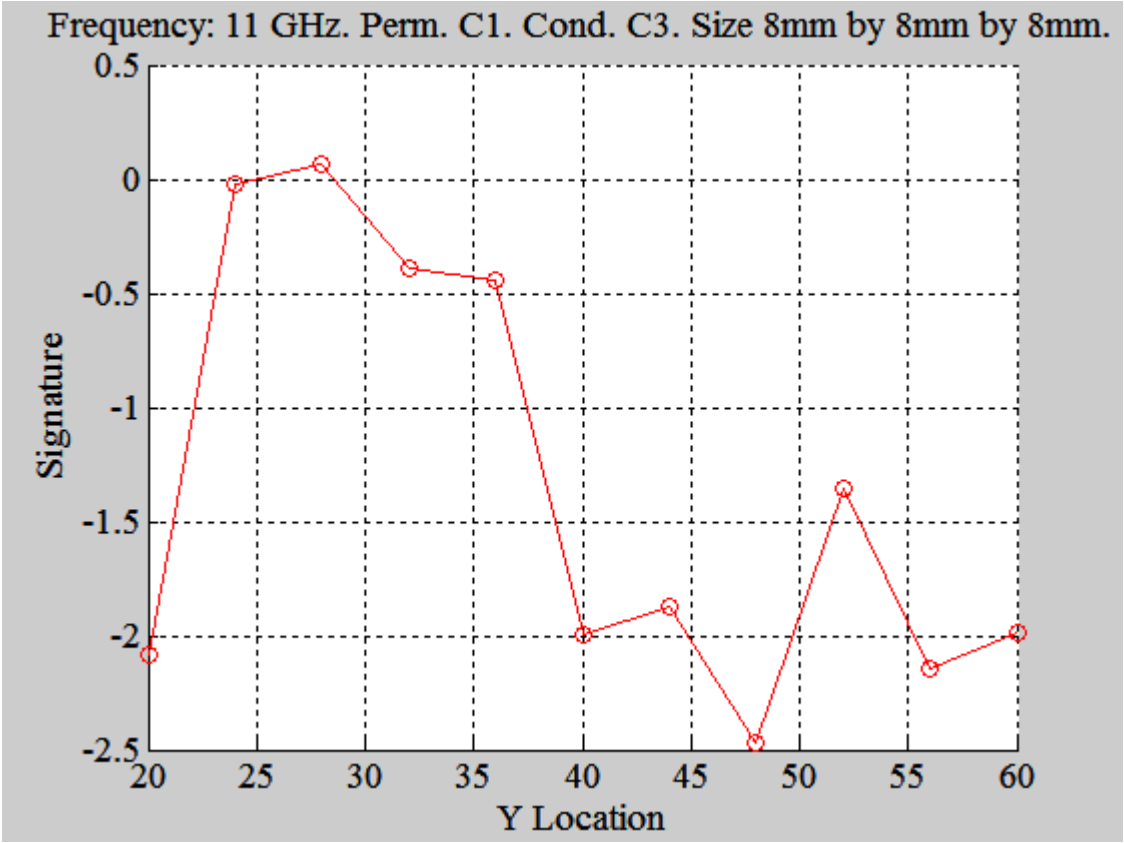

Figure 70: Y location changing at 11 GHz using signature equation (3). Other relevant details in plot title.

Observing this data, we can see that there is no reasonable sensitivity at any frequencies at any of the Y locations. Note the Y location shift starts at 20 mm. The same analysis is repeated using signature equation (4) to confirm these results.

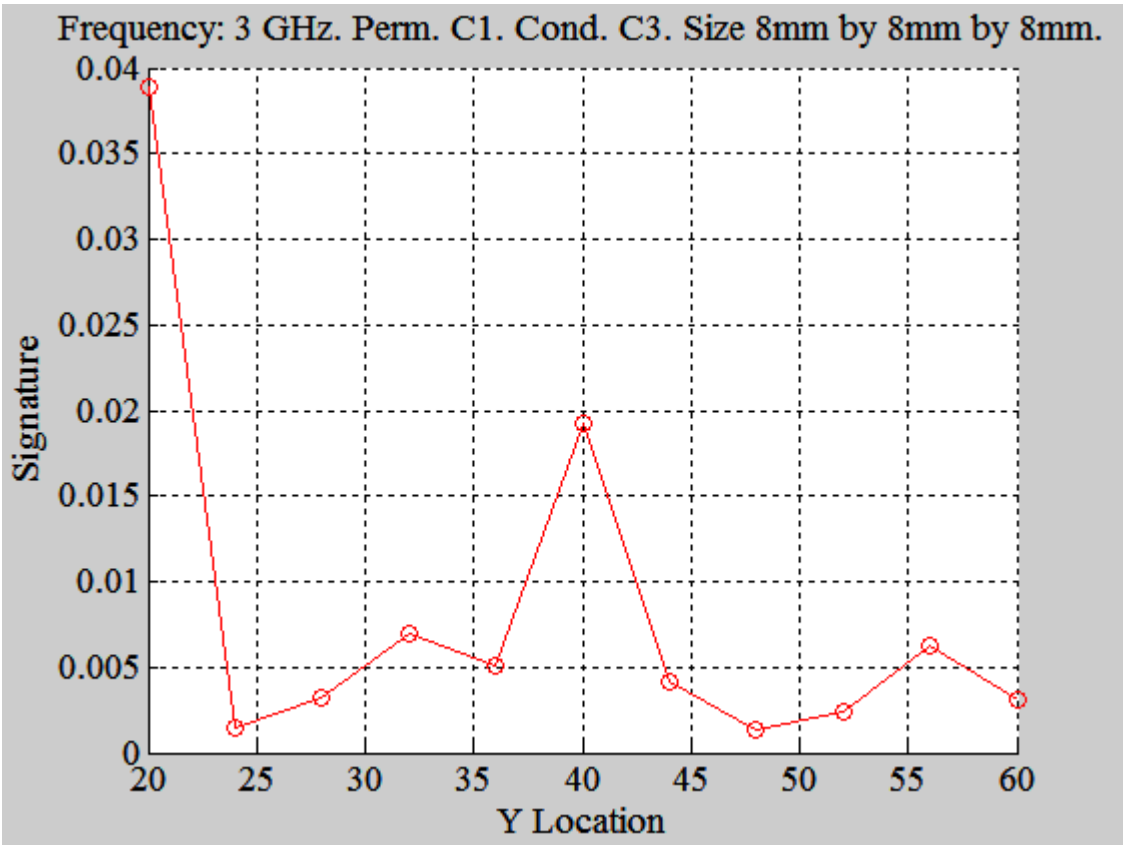

Figure 71: Y direction shift using signature equation (4) at a frequency of 3 GHz. Other relevant details specified in plot title.

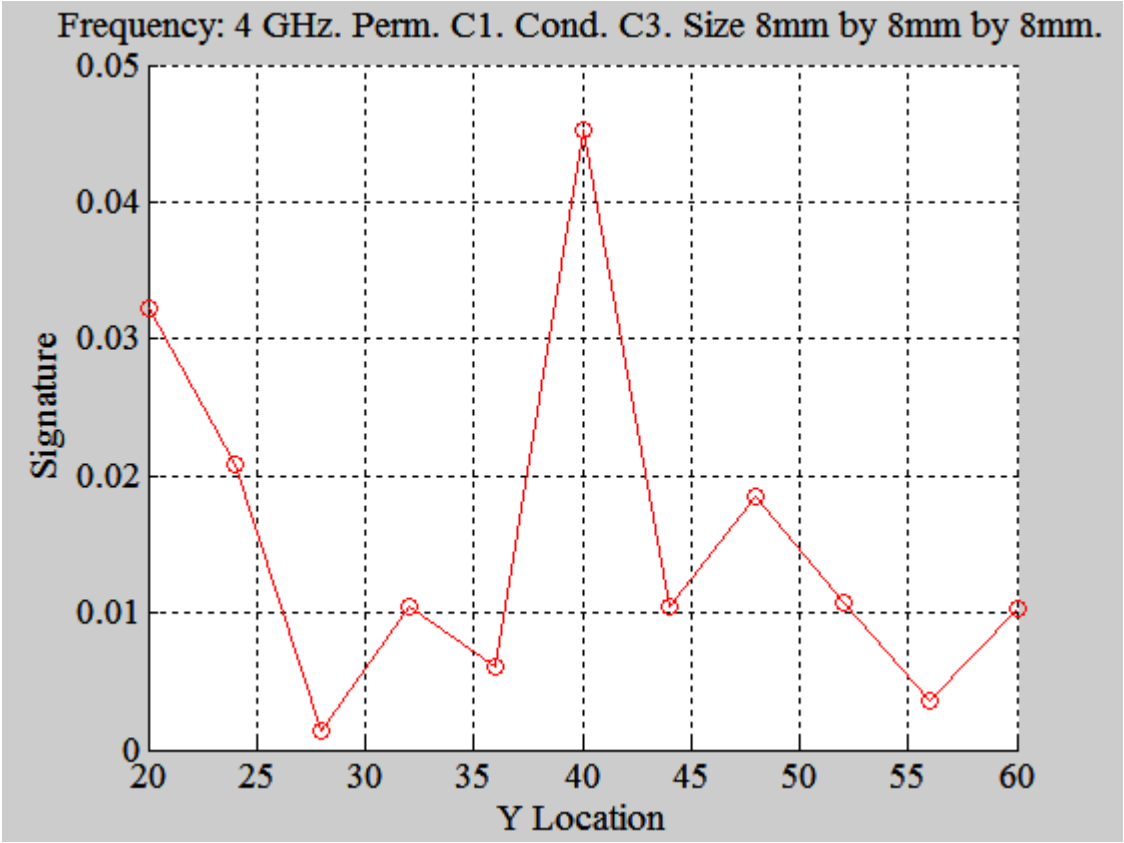

Figure 72: Y direction shift using signature equation (4) at a frequency of 4 GHz. Other relevant details specified in plot title.

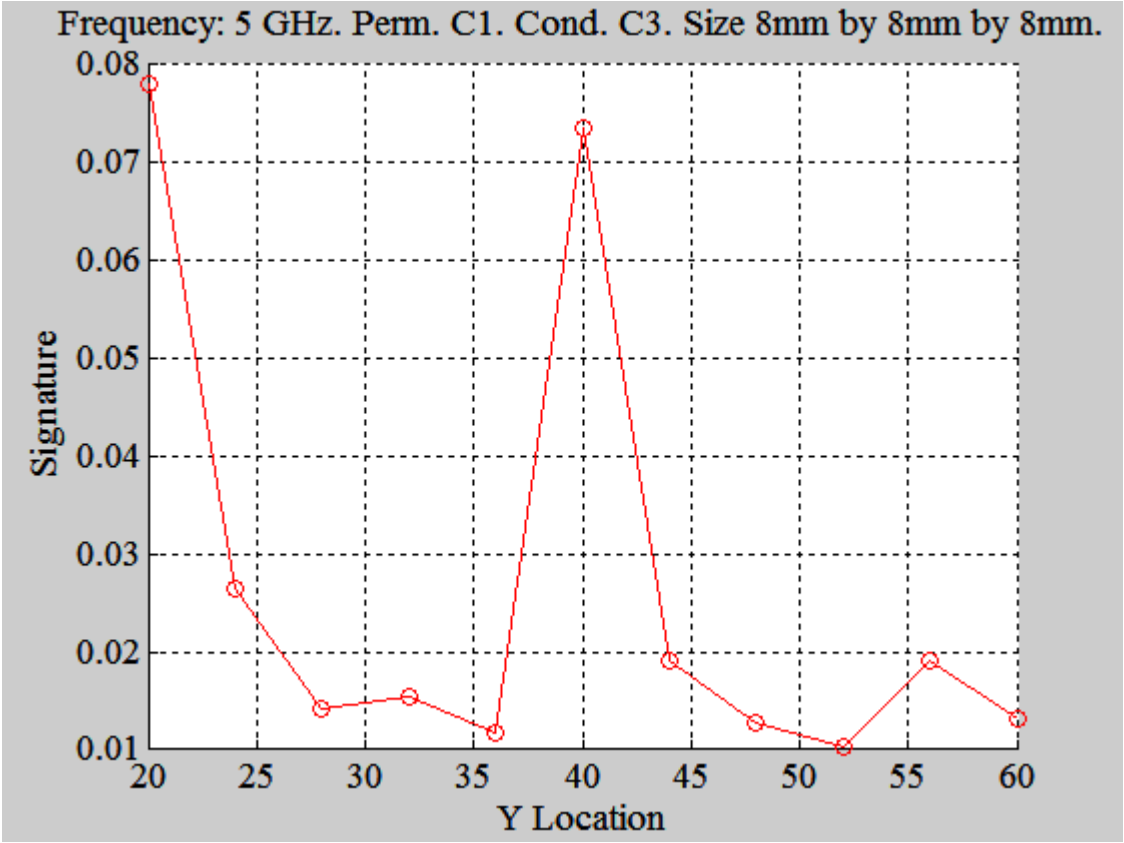

Figure 73: Y direction shift using signature equation (4) at a frequency of 5 GHz. Other relevant details specified in plot title.

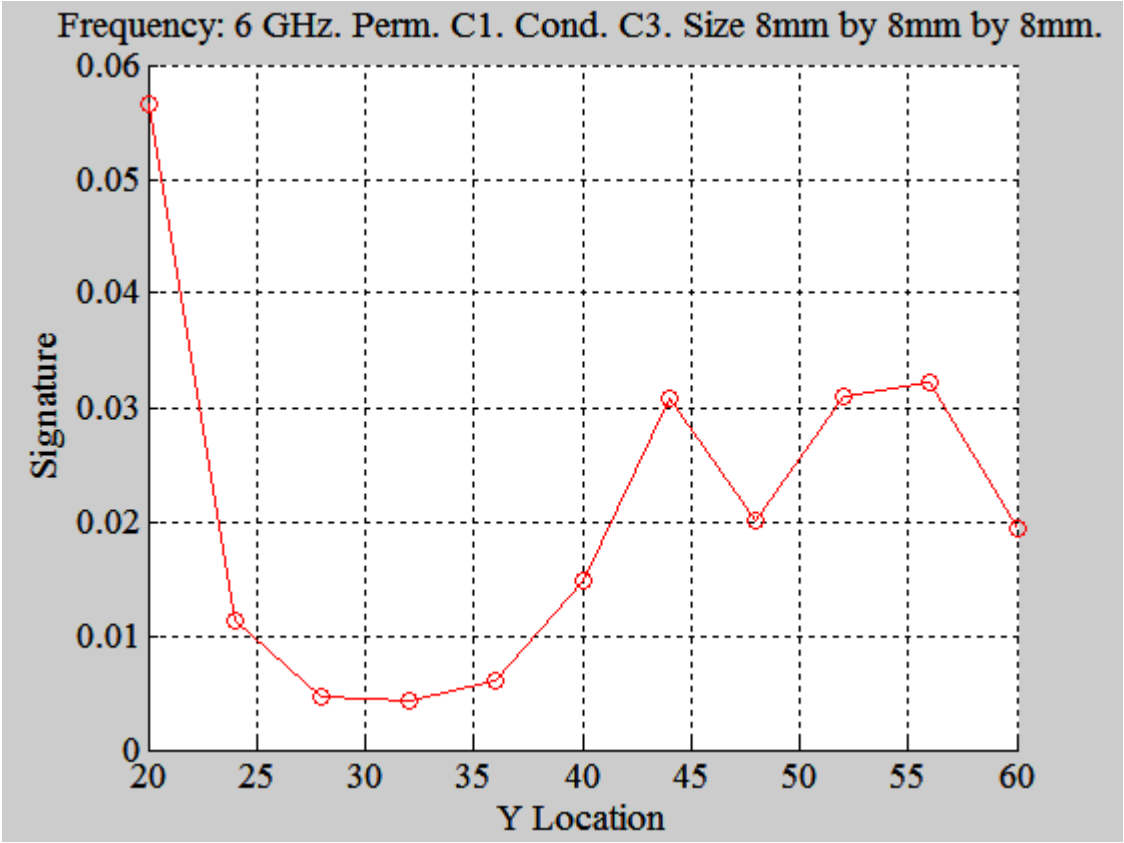

Figure 74: Y direction shift using signature equation (4) at a frequency of 6 GHz. Other relevant details specified in plot title.

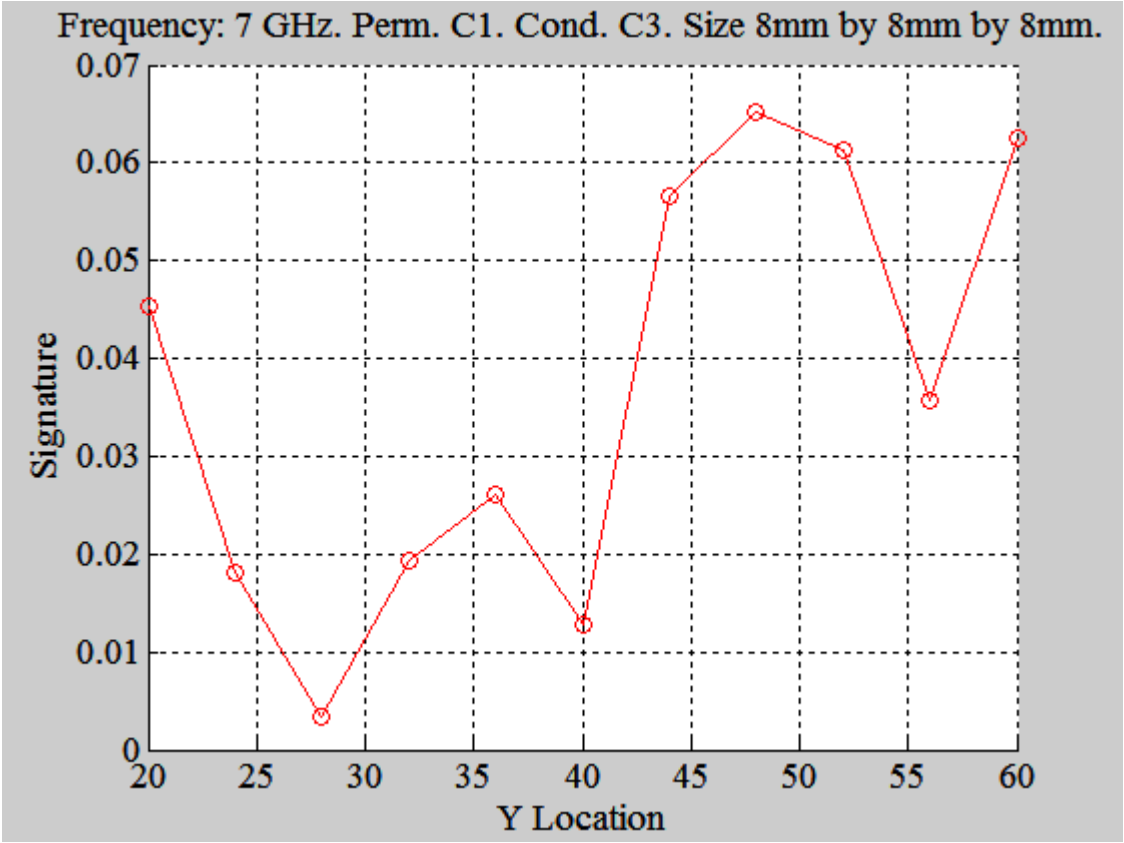

Figure 75: Y direction shift using signature equation (4) at a frequency of 7 GHz. Other relevant details specified in plot title.

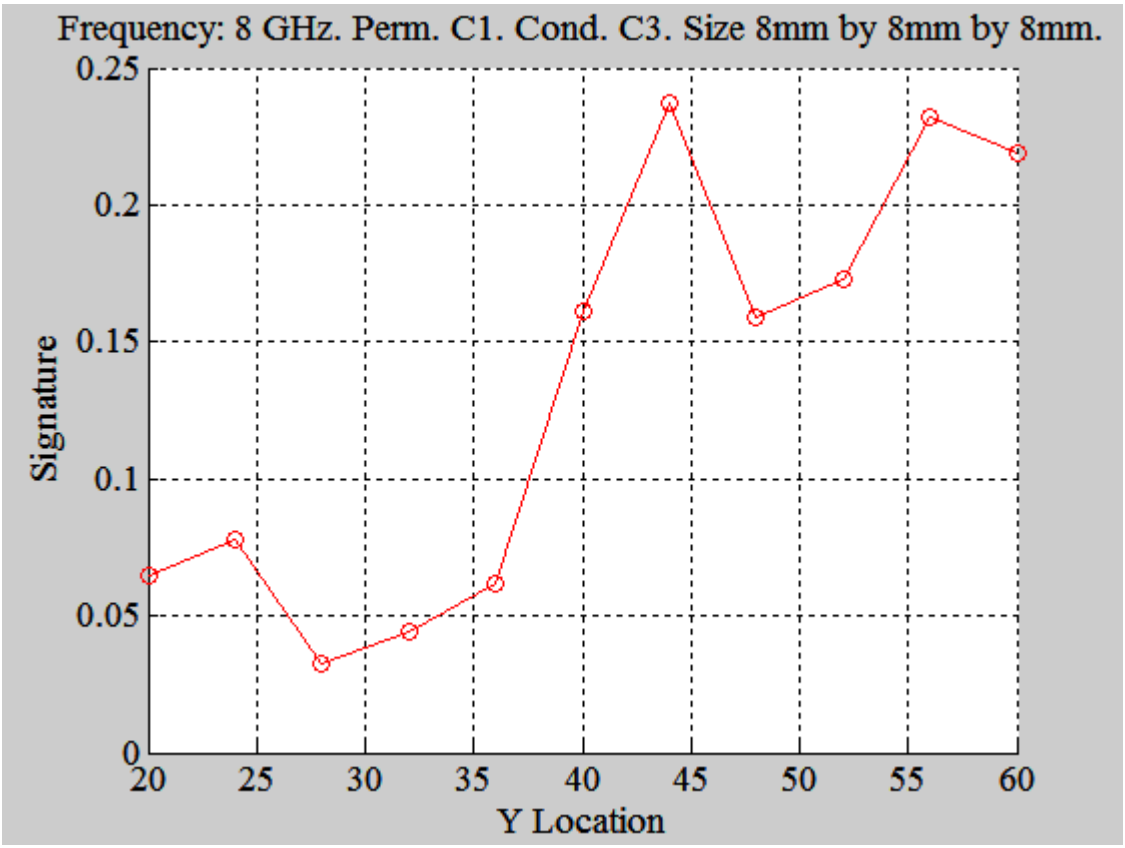

Figure 76: Y direction shift using signature equation (4) at a frequency of 8 GHz. Other relevant details specified in plot title.

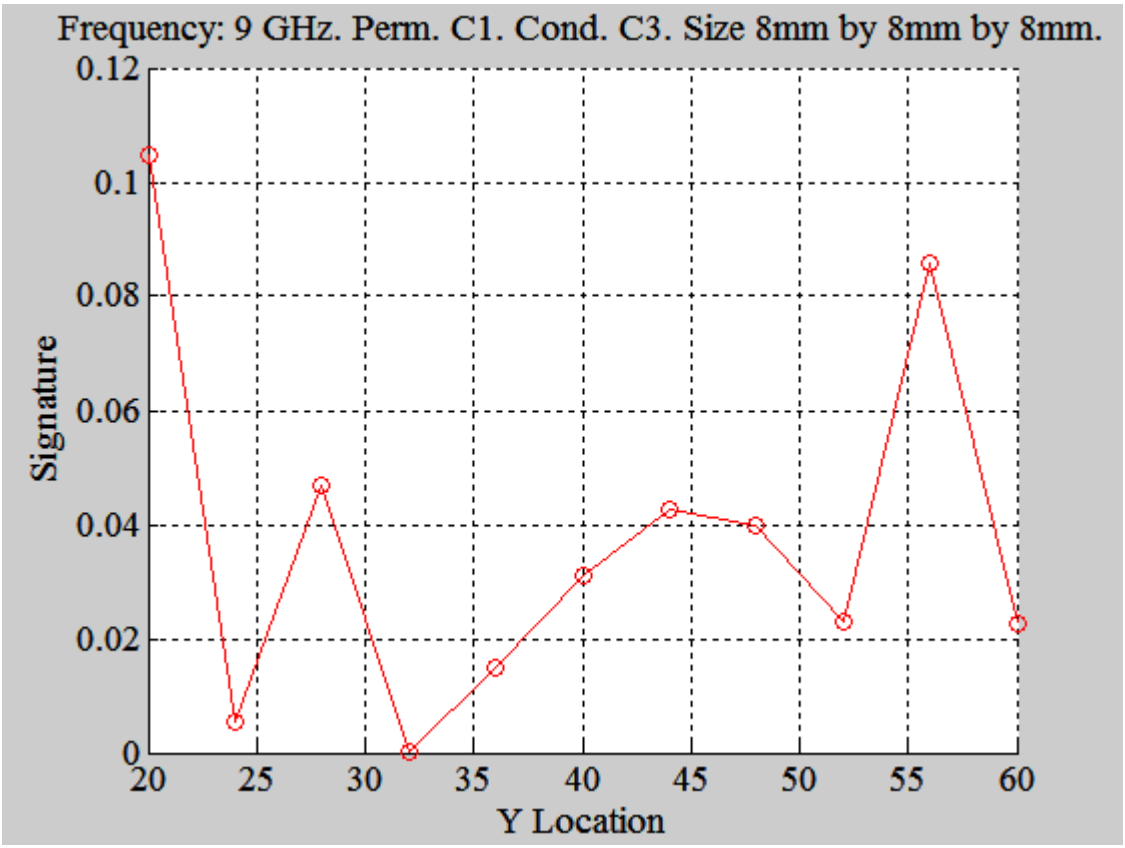

Figure 77: Y direction shift using signature equation (4) at a frequency of 9 GHz. Other relevant details specified in plot title.

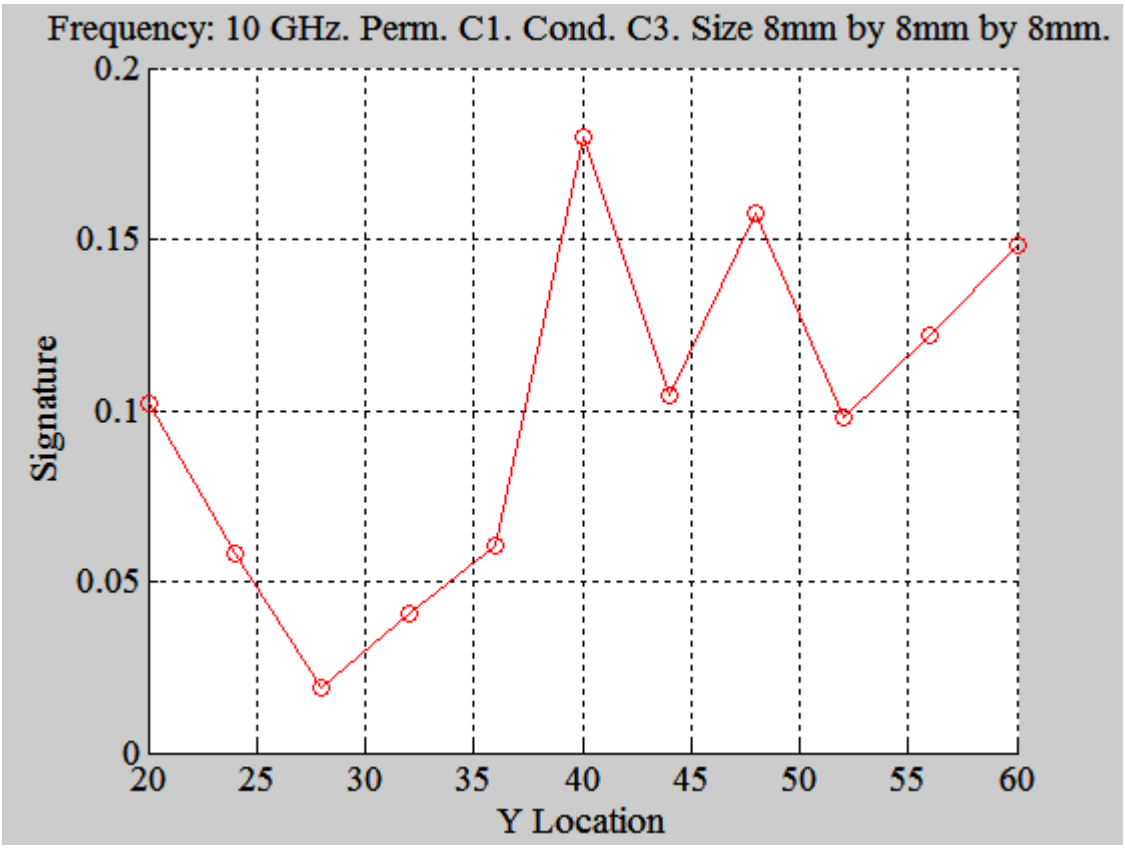

Figure 78: Y direction shift using signature equation (4) at a frequency of 10 GHz. Other relevant details specified in plot title.

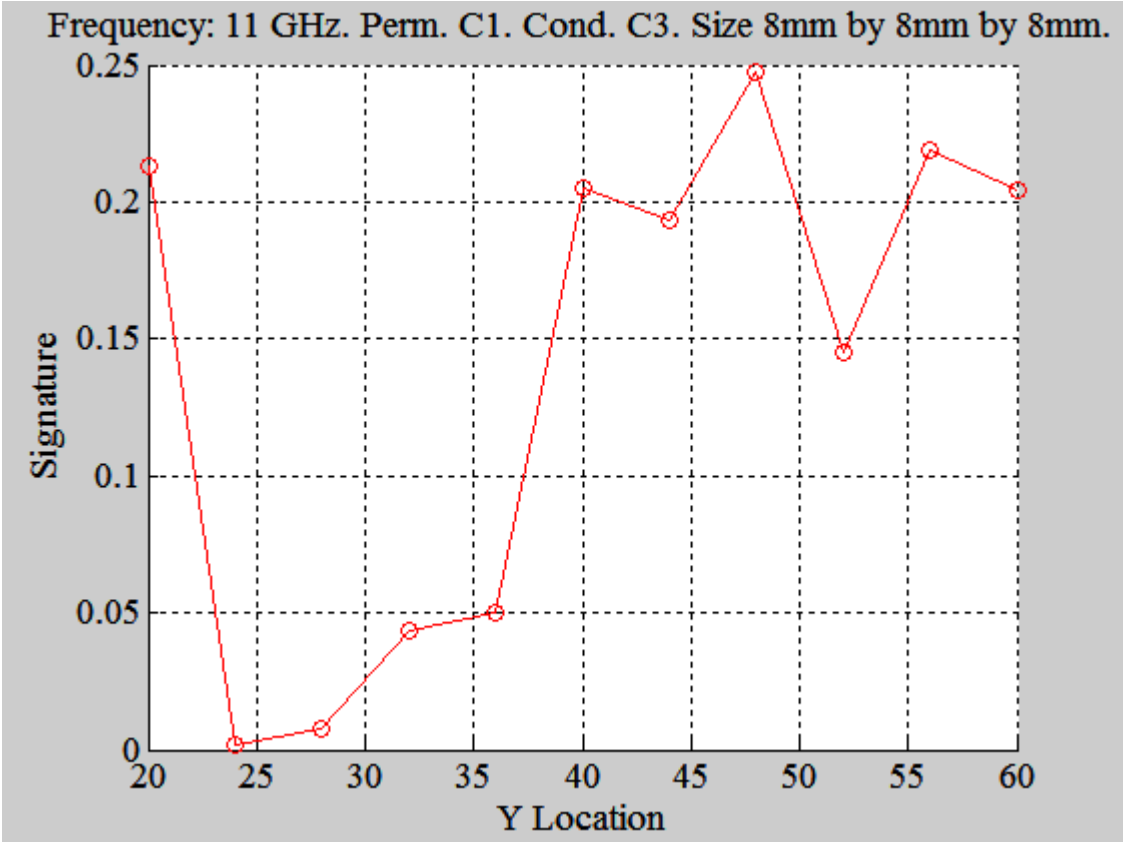

Figure 79: Y direction shift using signature equation (4) at a frequency of 11 GHz. Other relevant details specified in plot title.

Again, we can see that there is little to no signature present in a Y direction shift greater than 20mm.

For the Z direction shift, it was found that upon further analysis of the data with a solely a permittivity contrast of 3 compared with the data provided by varying the Z location with solely a conductivity contrast of 3, it was decided that for the sake of simplification and succinctness, only the data on conductivity will be presented. The appendix contains a table with the values for the permittivity contrast of 3. If the reader is interested, see **Error! Reference source not found.**. The following data uses signature equation (3).

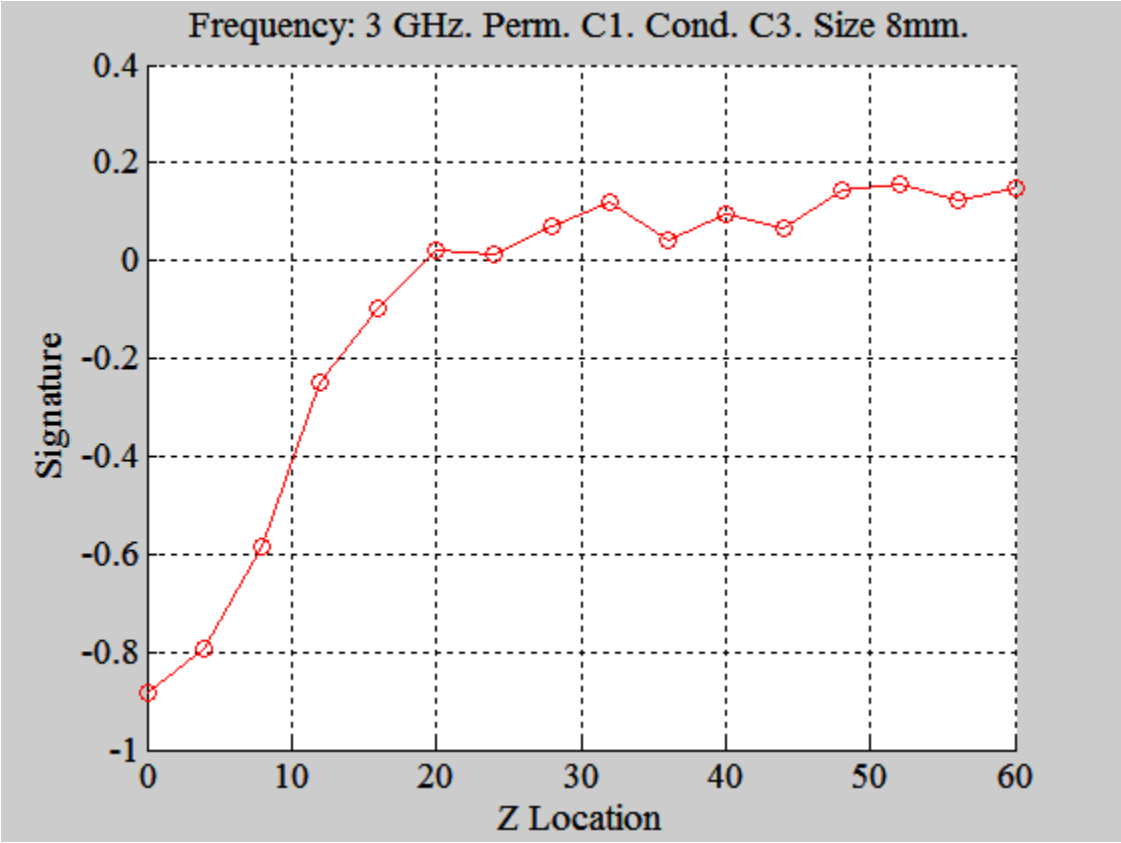

Figure 80: Signature using equation (3). The details of the plot are specified in the plot title.

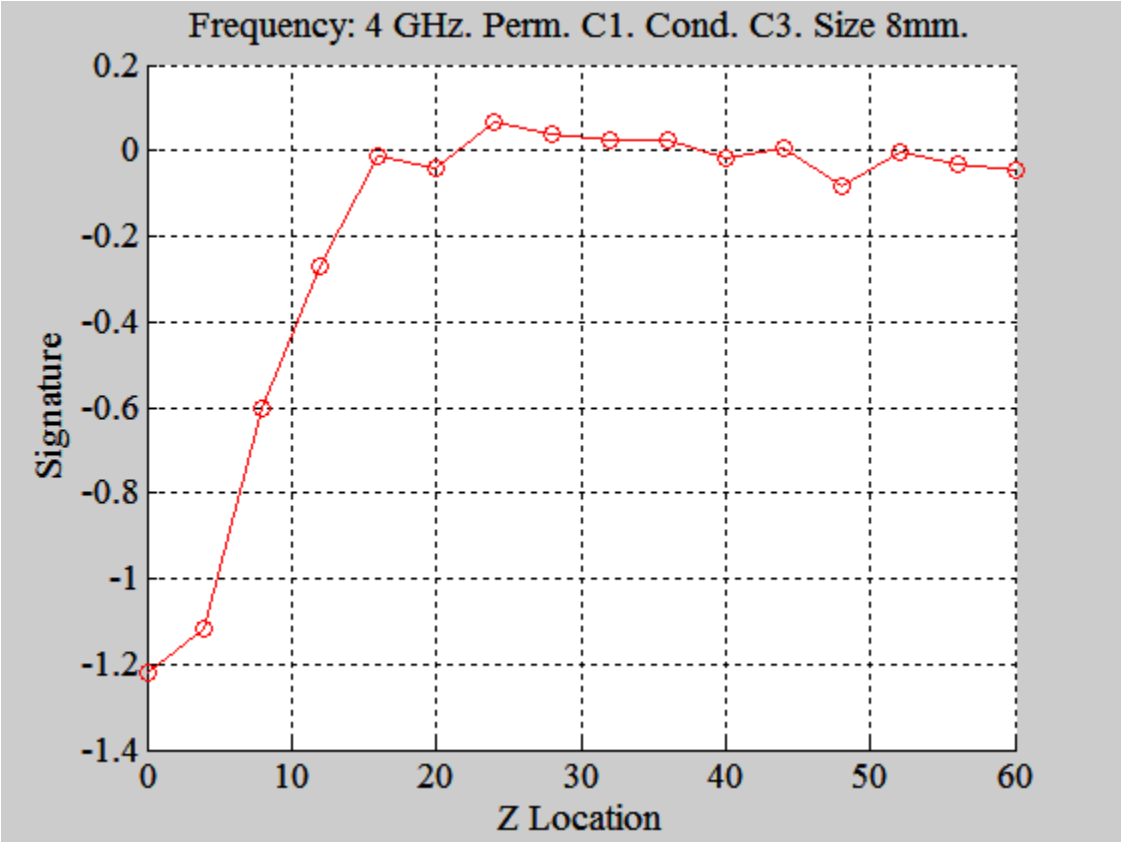

Figure 81: Signature using equation (3). The details of the plot are specified in the plot title.

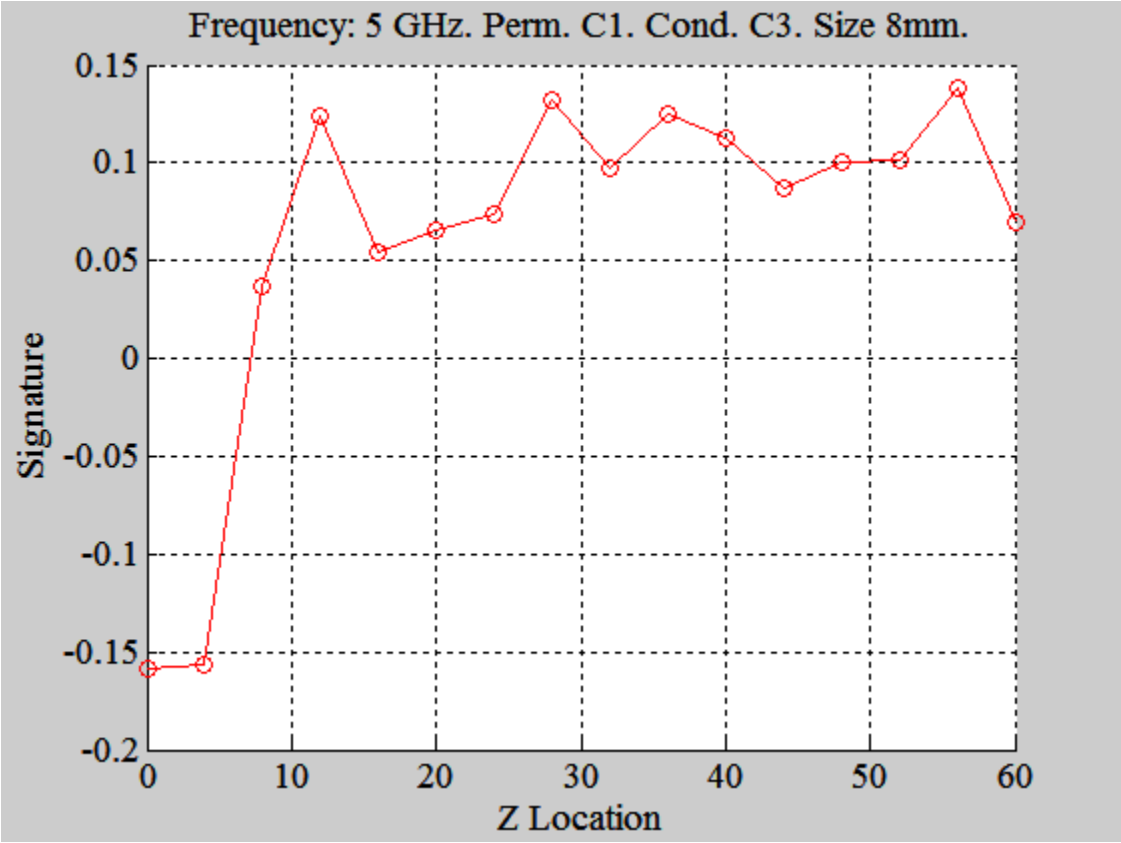

Figure 82: Signature using equation (3). The details of the plot are specified in the plot title.

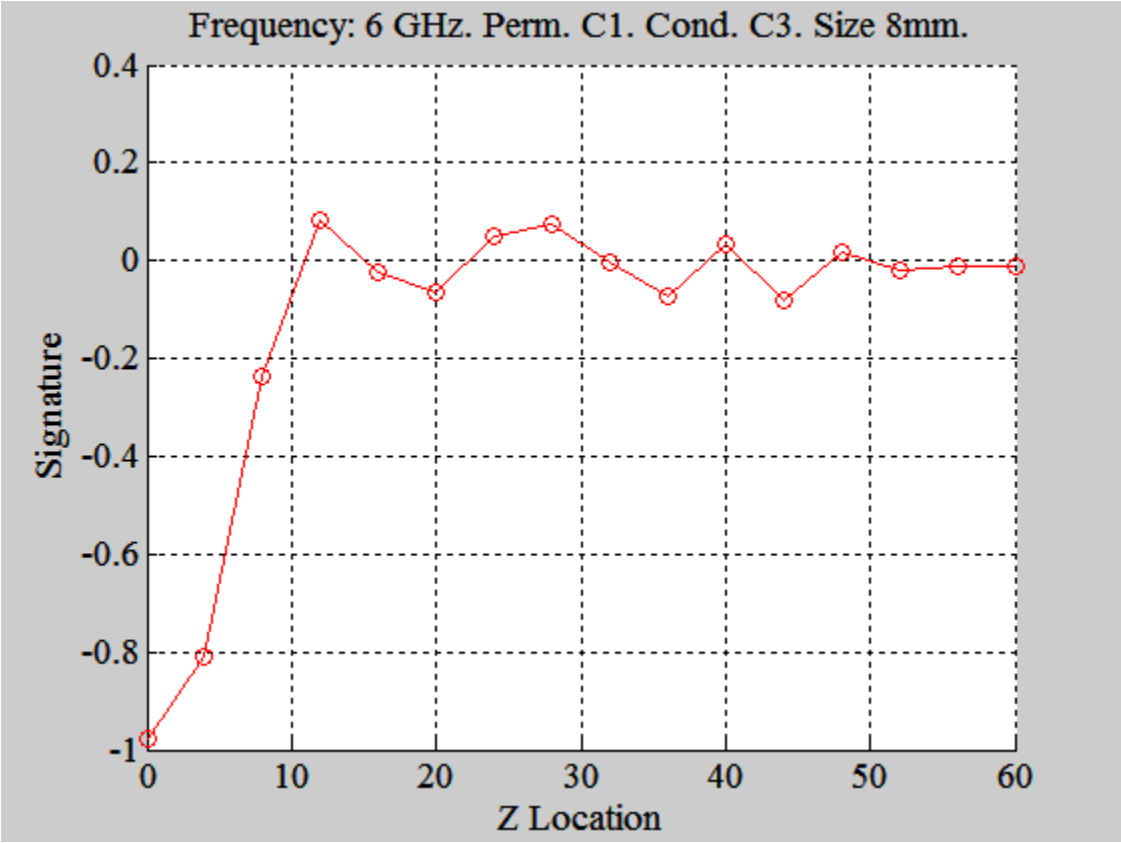

Figure 83: Signature using equation (3). The details of the plot are specified in the plot title.

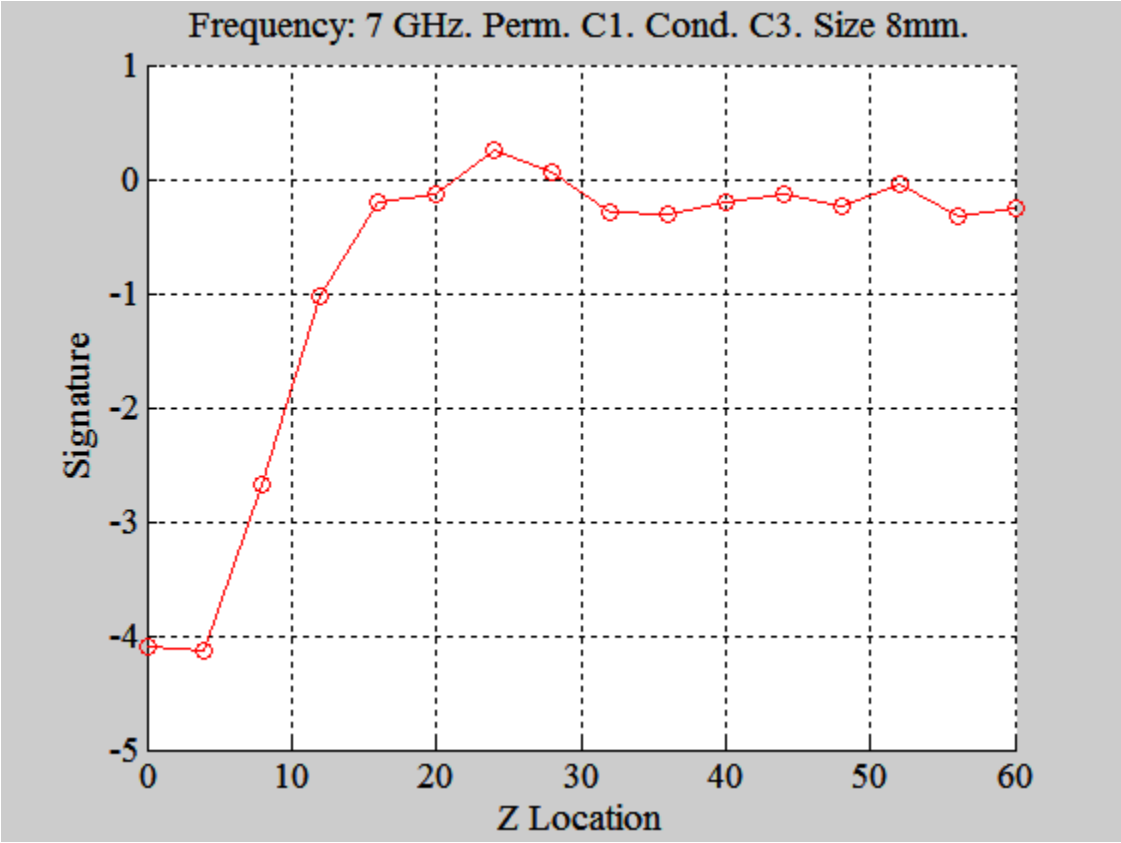

Figure 84: Signature using equation (3). The details of the plot are specified in the plot title.

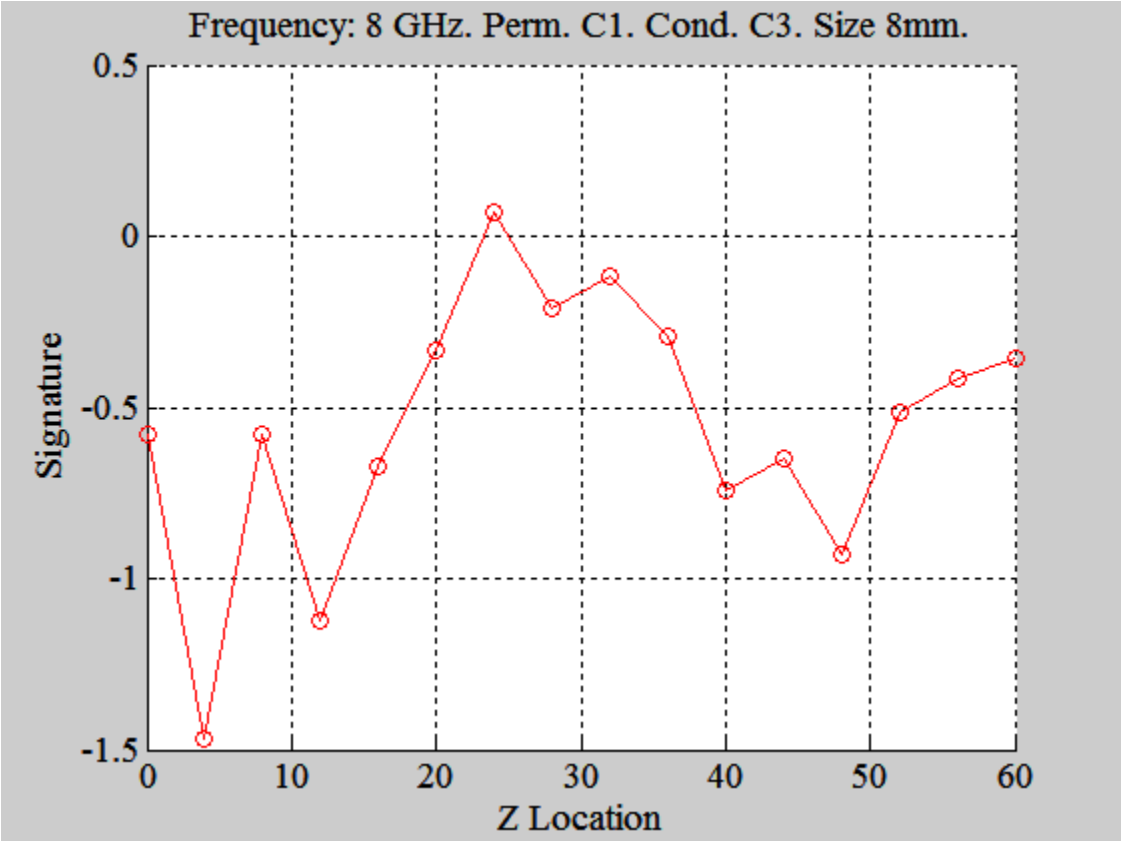

Figure 85: Signature using equation (3). The details of the plot are specified in the plot title.

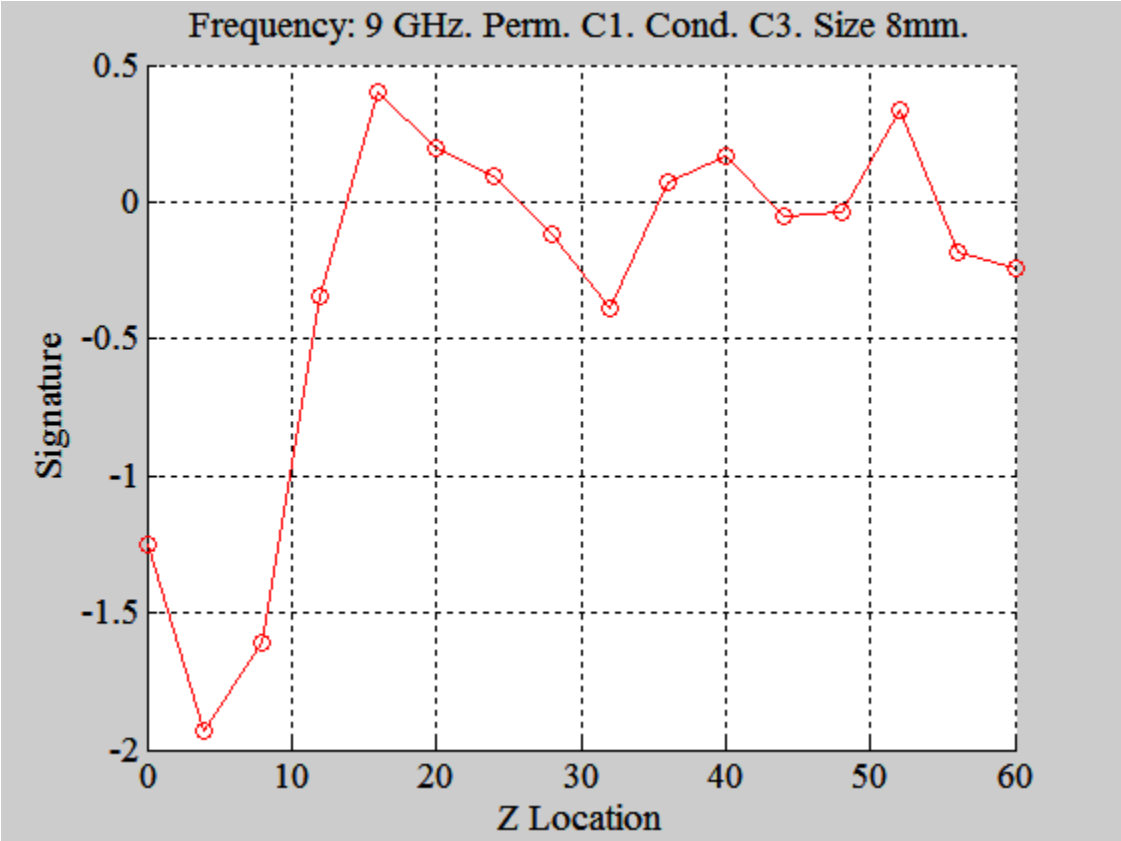

Figure 86: Signature using equation (3). The details of the plot are specified in the plot title.

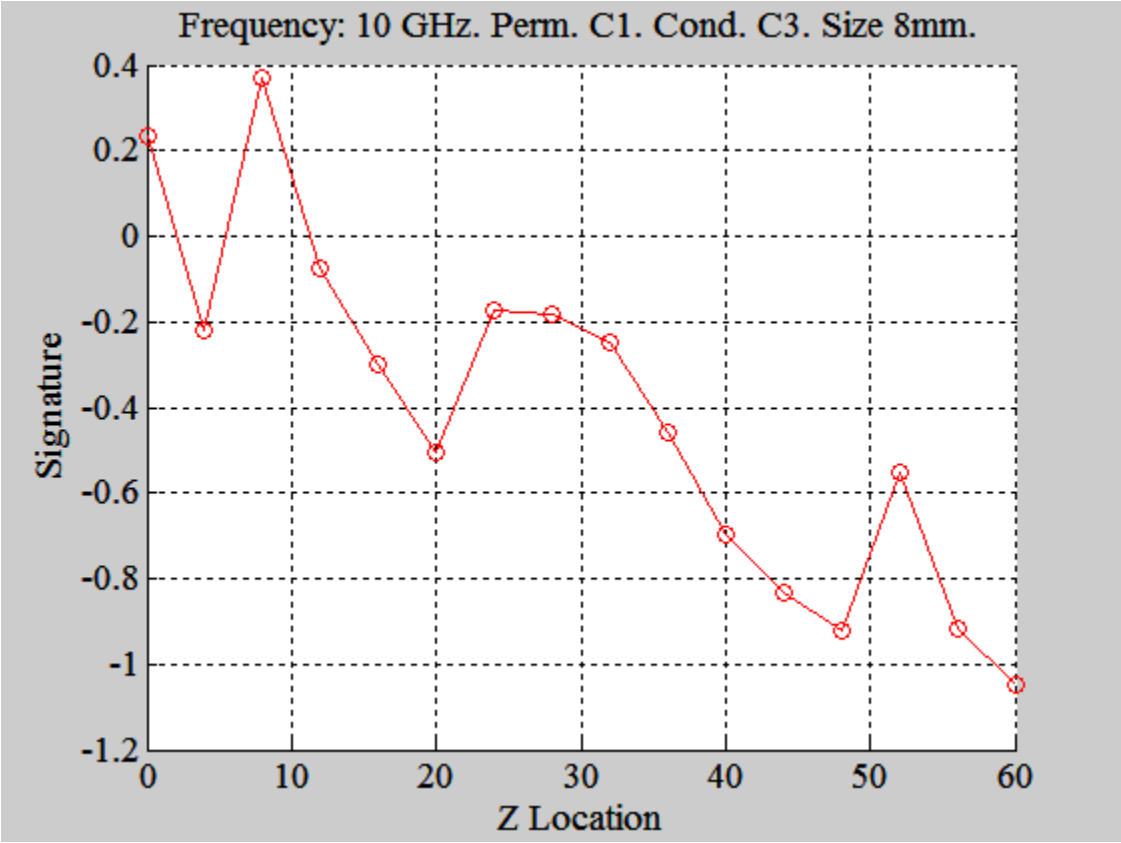

Figure 87: Signature using equation (3). The details of the plot are specified in the plot title.

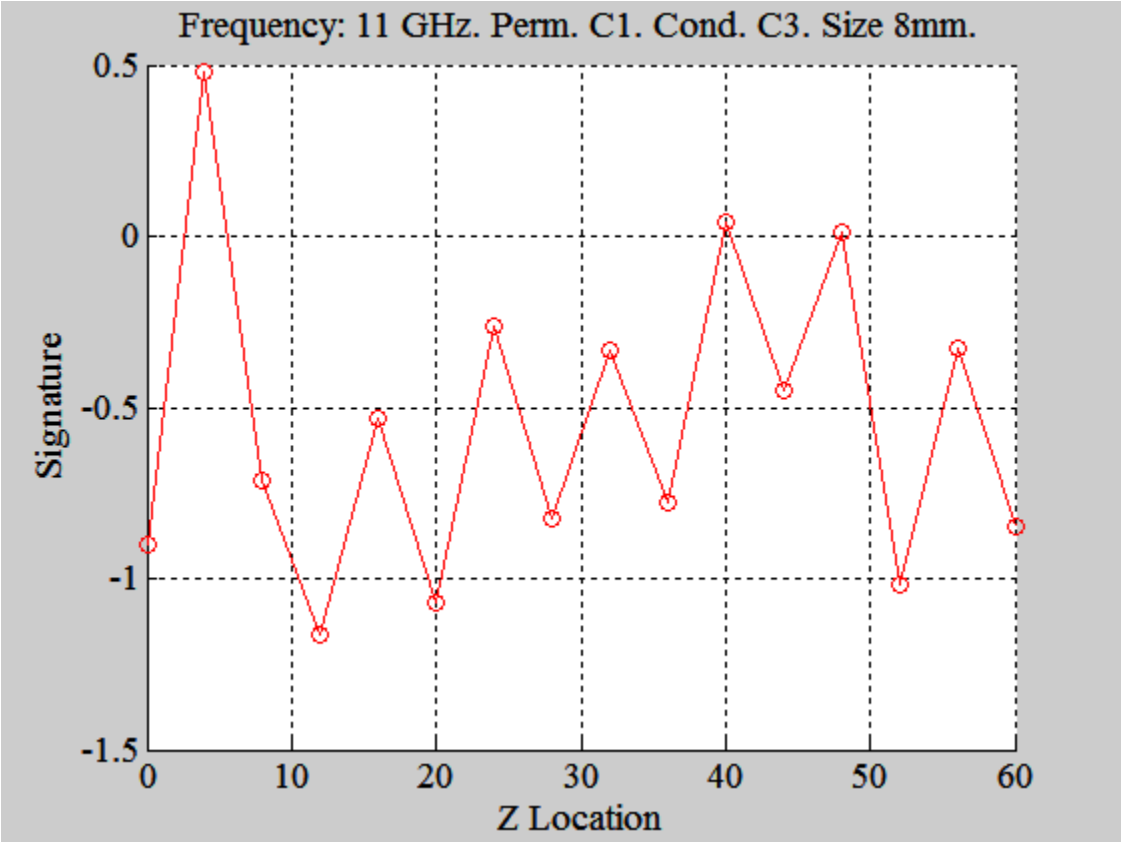

Figure 88: Signature using equation (3). The details of the plot are specified in the plot title.

Analyzing the data, we can see that it is fairly accurate up to 6 GHz, and it is only around 7 GHz where numerical noise begins to corrupt our data, as seen by the unusually large -4 dB attenuation at a z location of 0mm (i.e., the tumour is centered in the tissue). This is especially visible in Figure 88. We can see that initially we have a fairly good sensitivity to the tumour when it is centered, and this sharply rolls off, in the longest case when the tumour has been shifted by 20mm, and in the quickest case when the tumour has been shifted by a mere 8mm.

The following data use the signature in equation (4).

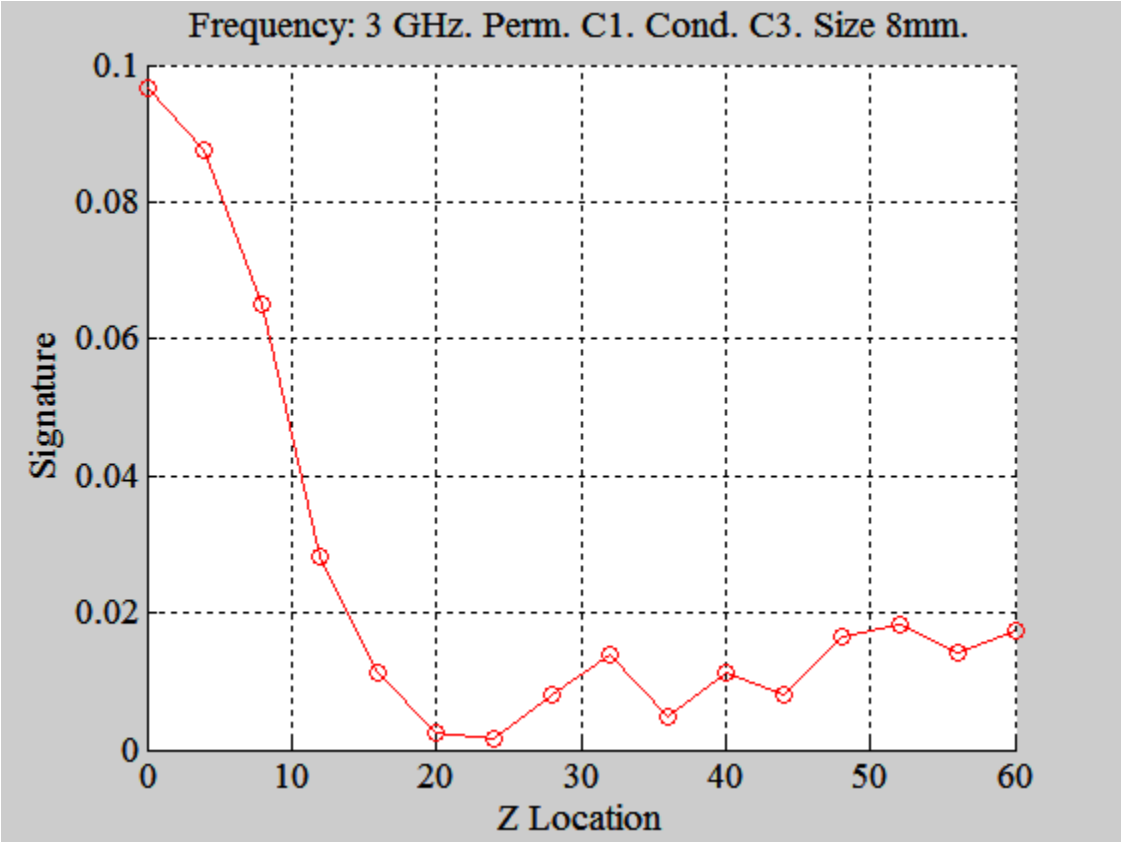

Figure 89: The signature present in equation (4) for a shift in the z location of the tumour. Relevant details are included in the plot title.

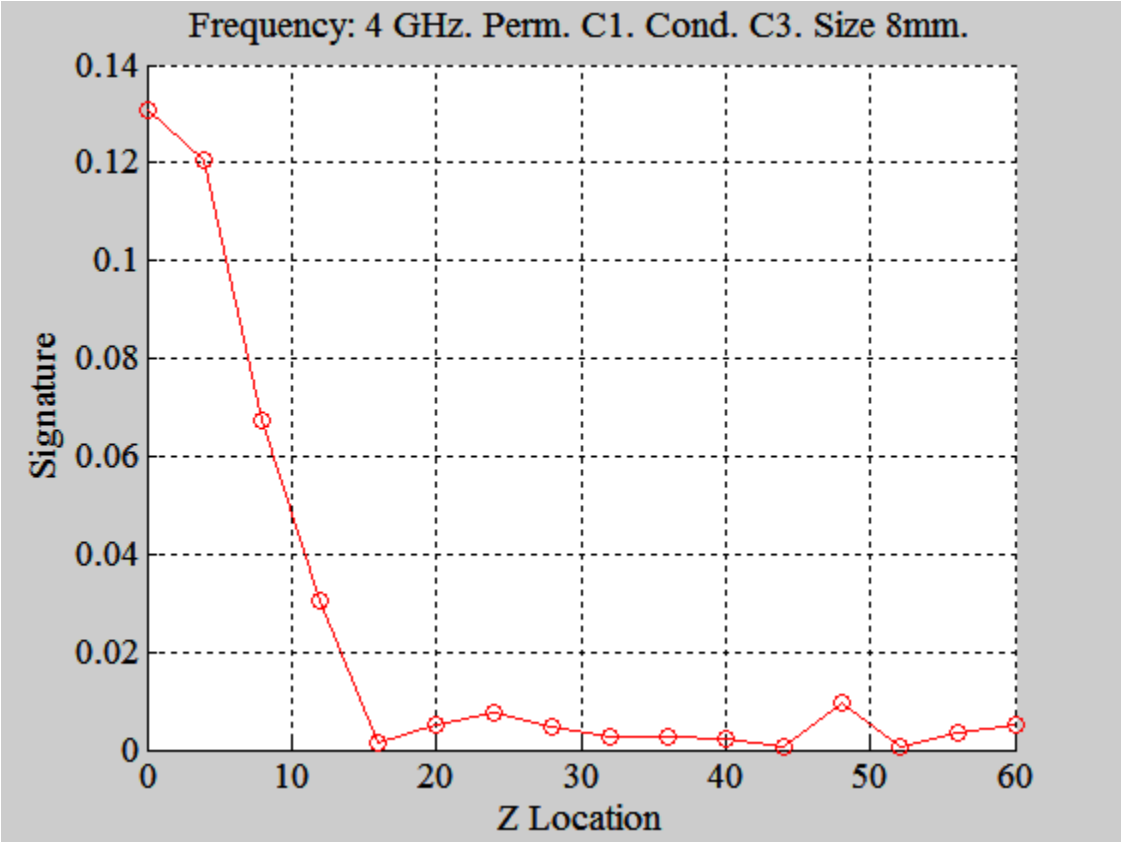

Figure 90: The signature present in equation (4) for a shift in the z location of the tumour. Relevant details are included in the plot title.

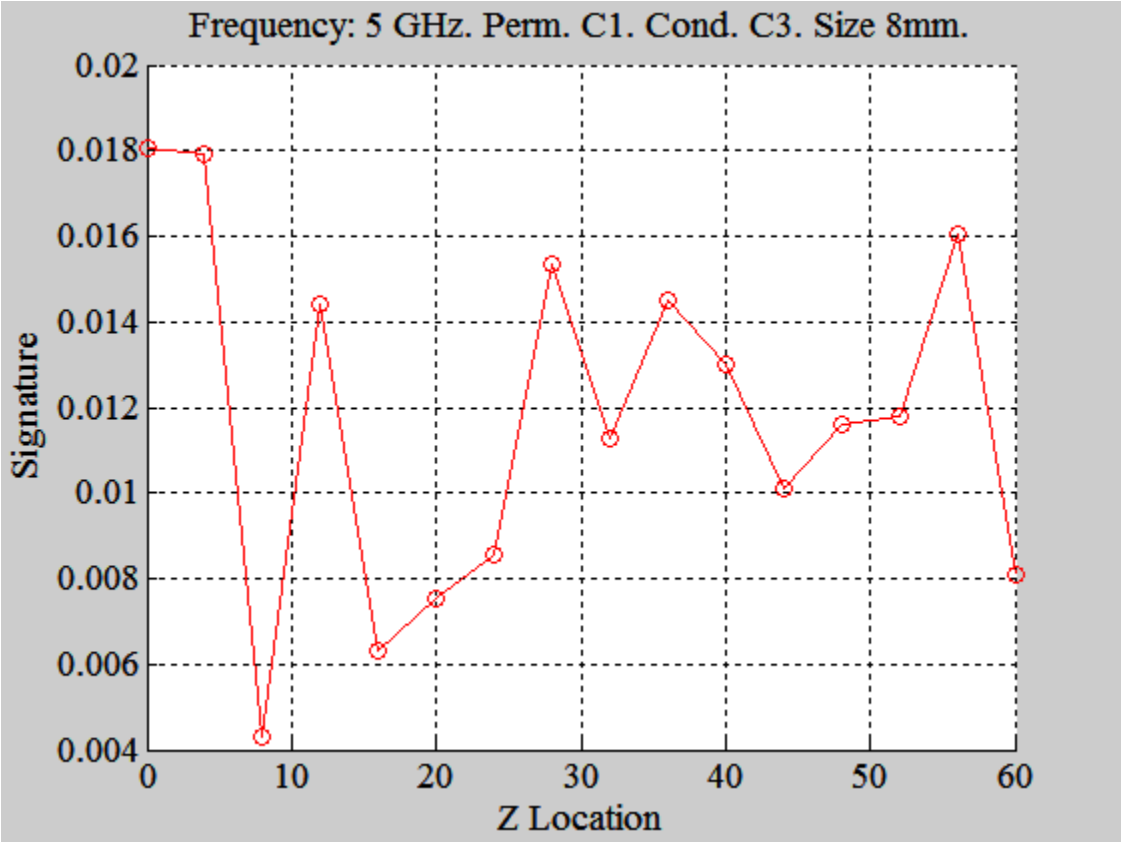

Figure 91: The signature present in equation (4) for a shift in the z location of the tumour. Relevant details are included in the plot title.

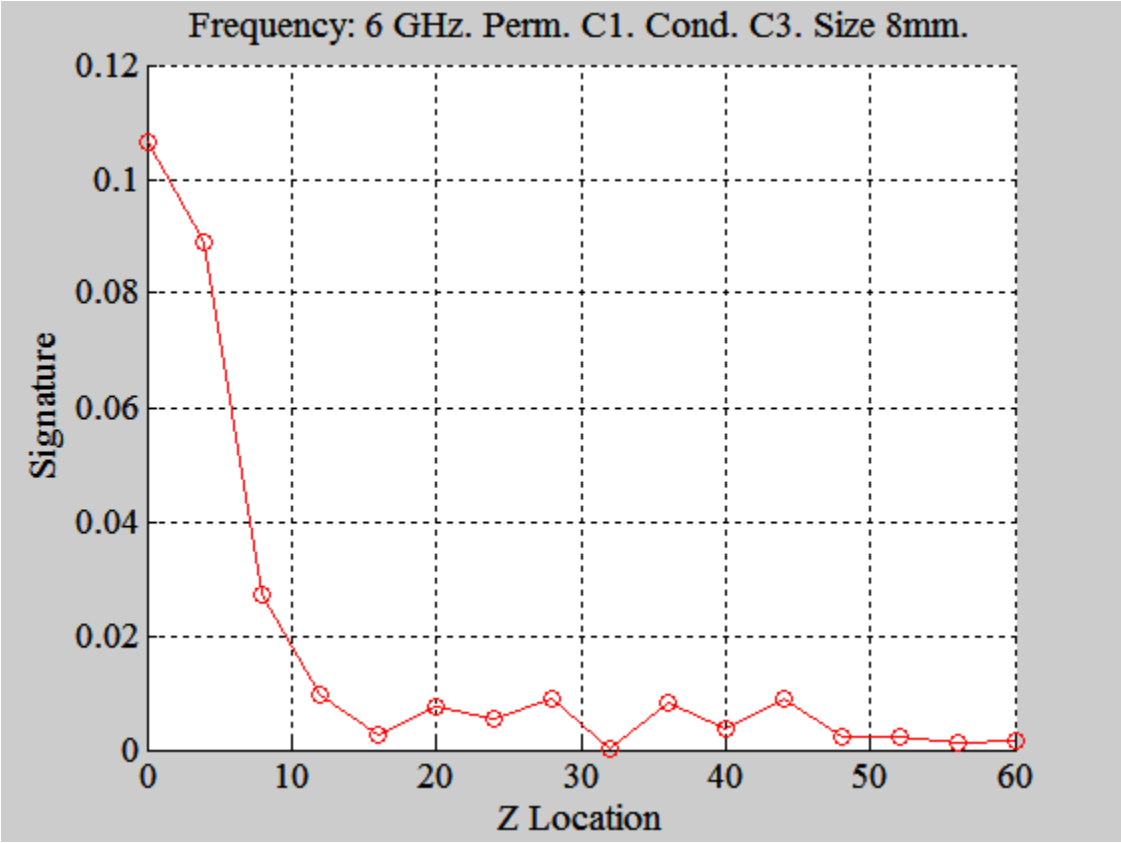

Figure 92: The signature present in equation (4) for a shift in the z location of the tumour. Relevant details are included in the plot title.

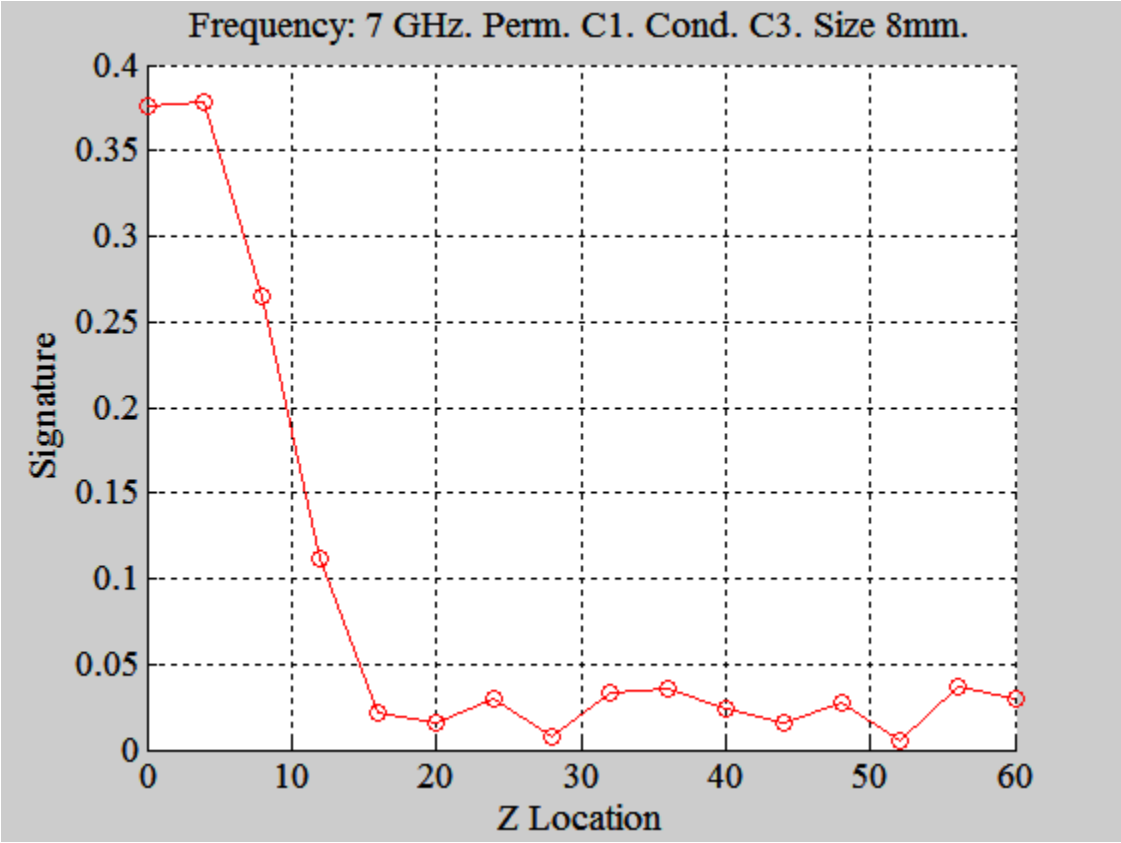

Figure 93: The signature present in equation (4) for a shift in the z location of the tumour. Relevant details are included in the plot title.

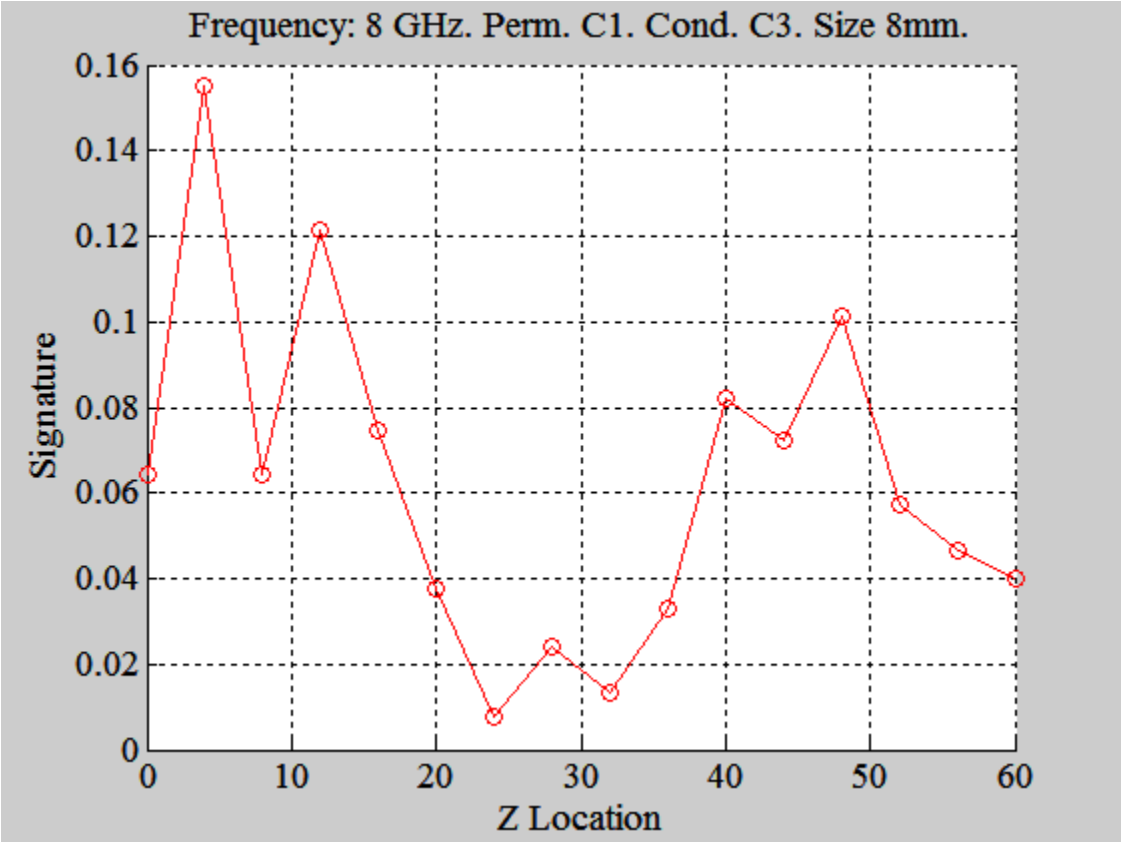

Figure 94: The signature present in equation (4) for a shift in the z location of the tumour. Relevant details are included in the plot title.

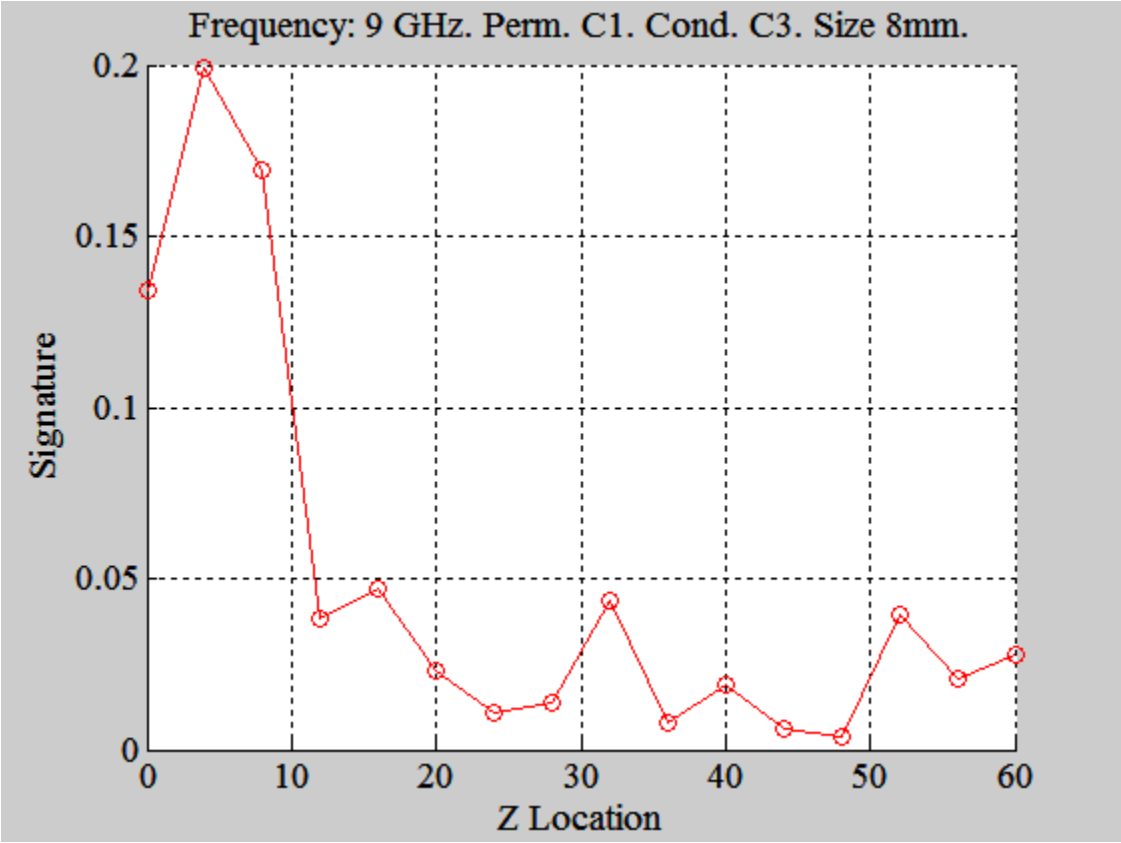

Figure 95: The signature present in equation (4) for a shift in the z location of the tumour. Relevant details are included in the plot title.

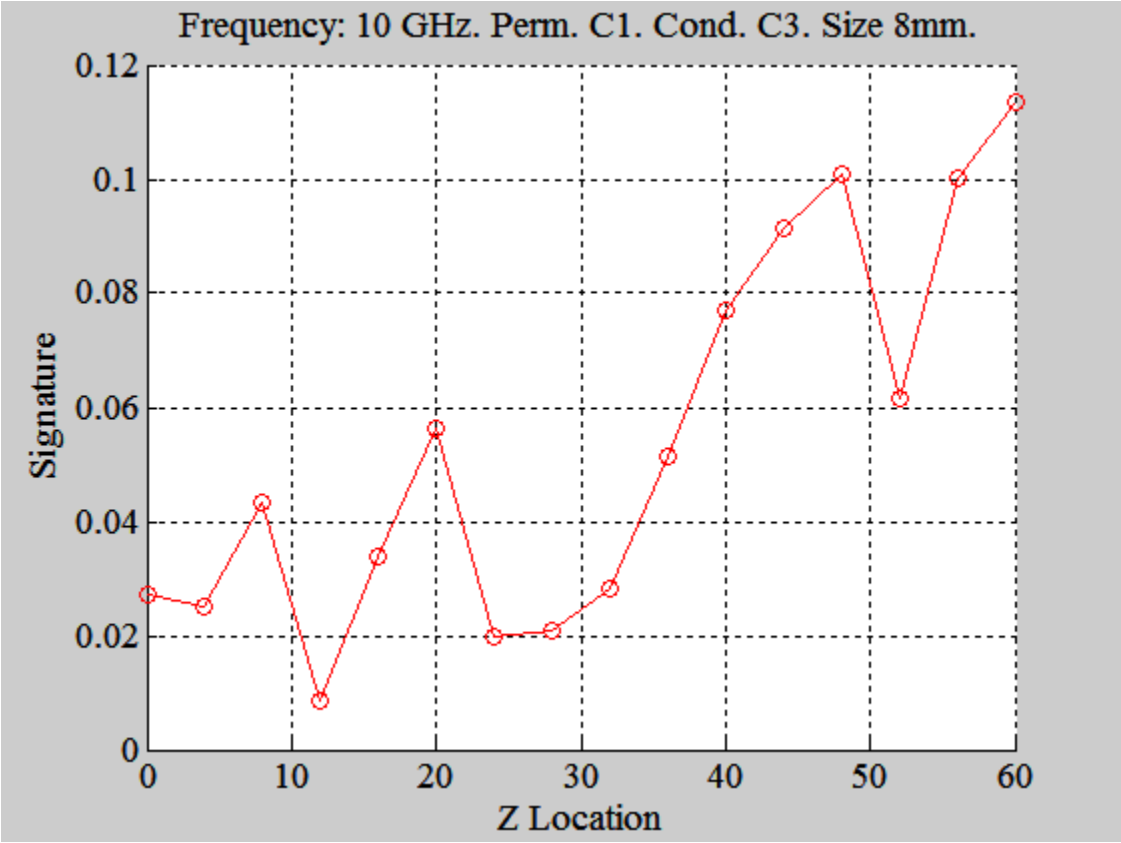

Figure 96: The signature present in equation (4) for a shift in the z location of the tumour. Relevant details are included in the plot title.

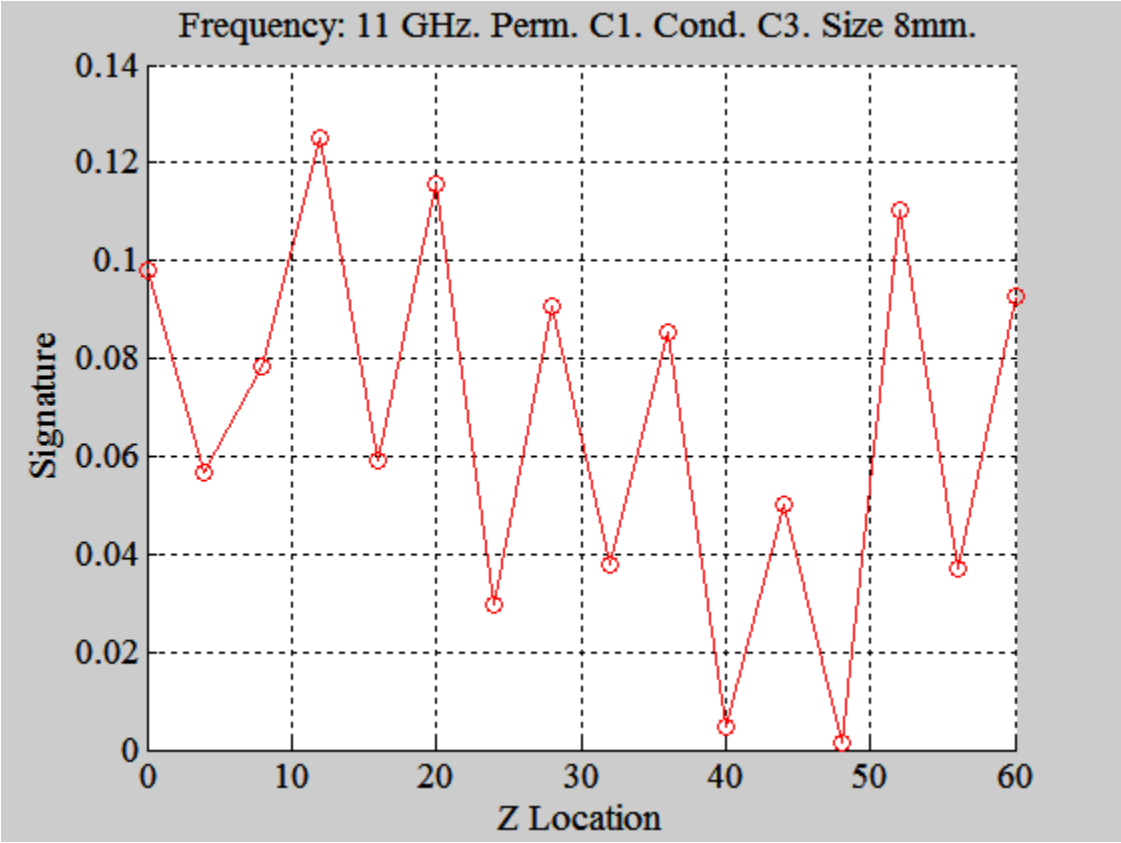

Figure 97: The signature present in equation (4) for a shift in the z location of the tumour. Relevant details are included in the plot title.

Again a sharp roll off is clearly visible in the signature at the frequencies of 3, 4, and 6 GHz, with the signal almost nothing by a shift of a mere 12 mm. Oddly, Figure 91, corresponding to 5 GHz, seems strongly corrupted by numerical noise. As of now the author has no explanation for this, though it is likely some flaw in the simulator software that is responsible. Regardless, the data can be excluded and the same conclusions drawn.

The phase data for the systems was also acquired in simulation. However, as it was not experimentally feasible to measure the phase, and because the author has not yet achieved a sufficient understanding of the implications of the phase, the data has been excluded as it is not pertinent to this report.

Experiments

Due to the difficulty and length of time that would be required in fabricating such a large amount of antennas with tumours required for the location and size experiments, it was decided to simply attempt to corroborate a single contrast situation with that of the simulations. Then, if there was a strong correlation between the two, it could be extrapolated that the simulations were a good predictor of what would occur in an experimental set up. After the phantoms were fabricated, the one port probe was used to determine their conductivity and permittivities. For the two phantoms that had a 9 cm diameter by 3 cm thickness, shown in Figure 11 a) and b), the dielectric properties are presented for the one with the tumour in Table 1, and the one without the tumour in Table 2.

Table 1: 9 cm diameter breast phantom with 8 mm by 8mm by 8mm tumour implanted inside.

Frequency, Hz	ε'(ω)	ε''(ω)	σ_{eff}	Frequency, Hz	ε'(ω)	ε''(ω)	σ_{eff}
3.00E+09	76.463	11.75	1.9611	7.16E+09	68.815	24.553	9.78
3.16E+09	76.43	12.072	2.1222	7.32E+09	68.262	24.925	10.15
3.32E+09	76.152	13.411	2.477	7.48E+09	67.999	25.335	10.543
3.48E+09	75.837	13.775	2.667	7.64E+09	67.942	25.598	10.88
3.64E+09	75.512	14.368	2.9096	7.80E+09	67.554	26.132	11.34
3.80E+09	75.355	14.582	3.0827	7.96E+09	66.885	26.56	11.761
3.96E+09	75.357	15.131	3.3334	8.12E+09	66.414	26.902	12.153
4.12E+09	75.125	15.856	3.6344	8.28E+09	66.326	27.178	12.519
4.28E+09	74.731	16.328	3.8878	8.44E+09	66.075	27.436	12.882
4.44E+09	74.238	16.81	4.1521	8.60E+09	65.493	27.979	13.386
4.60E+09	74.081	17.31	4.4298	8.76E+09	65.087	28.325	13.804
4.76E+09	74.08	17.967	4.7578	8.92E+09	64.516	28.468	14.127
4.92E+09	73.391	18.449	5.0498	9.08E+09	63.983	28.792	14.544
5.08E+09	72.881	18.874	5.3339	9.24E+09	64.04	29.114	14.966
5.24E+09	72.818	19.261	5.6148	9.40E+09	62.747	29.599	15.478
5.40E+09	72.725	19.646	5.902	9.56E+09	64.052	29.79	15.844
5.56E+09	72.507	20.272	6.2703	9.72E+09	62.785	30.006	16.225
5.72E+09	71.954	20.691	6.5843	9.88E+09	62.655	30.118	16.554
5.88E+09	71.374	21.22	6.9415	1.00E+10	62.031	30.317	16.934
6.04E+09	71.355	21.422	7.1982	1.02E+10	61.238	30.786	17.47
6.20E+09	71.15	22.017	7.5943	1.04E+10	60.889	31.021	17.879

6.36E+09	70.659	22.589	7.9926	1.05E+10	60.634	31.2	18.26
6.52E+09	70.107	22.984	8.3368	1.07E+10	60.56	31.296	18.595
6.68E+09	69.811	23.261	8.6445	1.08E+10	60.02	31.658	19.092
6.84E+09	69.684	23.713	9.0233	1.10E+10	59.372	32.008	19.588
7.00E+09	69.386	24.068	9.3726				

Table 2: 9 cm diameter breast phantom without tumour implanted inside.

Frequency, Hz	ε'(ω)	ε''(ω)	σ_{eff}	Frequency, Hz	ε'(ω)	ε''(ω)	σ_{eff}
3.00E+09	76.366	12.543	2.0934	7.16E+09	68.412	25.686	10.231
3.16E+09	76.663	12.098	2.1268	7.32E+09	67.287	26.158	10.652
3.32E+09	76.658	15.387	2.8419	7.48E+09	67.202	26.637	11.085
3.48E+09	75.991	15.38	2.9775	7.64E+09	68.019	26.393	11.218
3.64E+09	75.391	16.229	3.2864	7.80E+09	67.679	27.358	11.872
3.80E+09	75.235	15.521	3.2812	7.96E+09	66.261	28.101	12.444
3.96E+09	75.942	15.937	3.5109	8.12E+09	65.428	28.541	12.893
4.12E+09	75.877	17.057	3.9096	8.28E+09	66.072	28.497	13.127
4.28E+09	75.111	17.531	4.1743	8.44E+09	66.182	28.422	13.345
4.44E+09	73.902	18.139	4.4805	8.60E+09	65.166	29.603	14.163
4.60E+09	74.037	18.526	4.7411	8.76E+09	64.752	30.04	14.64
4.76E+09	74.904	19.439	5.1478	8.92E+09	63.444	29.819	14.797
4.92E+09	73.092	20.021	5.4799	9.08E+09	62.391	30.165	15.238
5.08E+09	71.933	20.41	5.7681	9.24E+09	63.824	30.3	15.575
5.24E+09	72.434	20.433	5.9566	9.40E+09	60.167	31.602	16.526
5.40E+09	72.897	20.435	6.139	9.56E+09	66.574	30.925	16.447
5.56E+09	73.011	21.373	6.6111	9.72E+09	62.355	31.617	17.097
5.72E+09	71.818	21.776	6.9294	9.88E+09	62.941	30.955	17.014
5.88E+09	70.481	22.721	7.4326	1.00E+10	61.615	30.984	17.306
6.04E+09	71.187	22.057	7.4117	1.02E+10	59.852	32.224	18.286
6.20E+09	71.422	23.005	7.935	1.04E+10	59.534	32.411	18.68
6.36E+09	70.594	23.982	8.4854	1.05E+10	59.531	32.335	18.924
6.52E+09	69.453	24.415	8.8558	1.07E+10	60.408	31.857	18.928
6.68E+09	69.13	24.302	9.0312	1.08E+10	59.537	32.632	19.679
6.84E+09	69.646	24.77	9.4255	1.10E+10	58.28	33.486	20.492
7.00E+09	69.497	24.892	9.6936				

We observe that there is minimal difference between the two observed general conductivity and permittivities.

Displays the conductivity and permittivity of the cancerous tissue phantom analog from which the tumour was extracted.

Table 3: Properties of the phantom that was created to represent the properties of cancerous tissue.

Frequency, Hz	ε'(ω)	ε''(ω)	σ_{eff}	Frequency, Hz	ε'(ω)	ε''(ω)	σ_{eff}
3.00E+09	74.354	22.645	3.7794	7.16E+09	62.91	33.249	13.244
3.16E+09	79.103	12.713	2.2348	7.32E+09	55.081	34.805	14.174
3.32E+09	73.256	33.8	6.2428	7.48E+09	55.296	39.494	16.435
3.48E+09	71.2	29.939	5.7962	7.64E+09	67.494	33.484	14.232
3.64E+09	66.954	35.343	7.157	7.80E+09	66.365	36.649	15.903
3.80E+09	71.287	25.769	5.4476	7.96E+09	57.441	38.582	17.085
3.96E+09	79.058	25.01	5.5098	8.12E+09	50.345	42.896	19.378
4.12E+09	77.924	29.005	6.6481	8.28E+09	61.082	42.48	19.568
4.28E+09	75.323	29.845	7.1063	8.44E+09	65.454	36.171	16.984
4.44E+09	66.321	31.883	7.8755	8.60E+09	59.162	40.573	19.412
4.60E+09	70.827	30.014	7.6808	8.76E+09	57.417	45.056	21.958
4.76E+09	79.255	32.749	8.6723	8.92E+09	48.892	41.263	20.477
4.92E+09	67.82	32.29	8.8381	9.08E+09	46.96	39.135	19.769
5.08E+09	57.546	32.02	9.0493	9.24E+09	60.791	36.941	18.989
5.24E+09	65.249	32.844	9.5745	9.40E+09	40.343	37.026	19.362
5.40E+09	73.018	28.541	8.5742	9.56E+09	103.48	45.257	24.07
5.56E+09	74.541	31.391	9.7097	9.72E+09	64.233	69.078	37.354
5.72E+09	68.054	30.472	9.6966	9.88E+09	65.108	38.694	21.268
5.88E+09	56.856	35.587	11.641	1.00E+10	58.158	34.732	19.4
6.04E+09	68.401	28.751	9.6611	1.02E+10	47.686	38.566	21.885
6.20E+09	71.831	31.744	10.949	1.04E+10	43.261	41.032	23.649
6.36E+09	66.826	34.599	12.242	1.05E+10	46.646	41.354	24.203
6.52E+09	59.934	34.865	12.646	1.07E+10	58.71	35.964	21.368
6.68E+09	60.137	34.166	12.697	1.08E+10	54.953	38.211	23.043
6.84E+09	67.35	34.946	13.298	1.10E+10	46.927	42.124	25.778
7.00E+09	69.075	31.324	12.199				

As one can observe, there is a conductivity and slight permittivity contrast between the host tissue and the tumour tissue. Table 4 is a calculation of the contrast, calculated by dividing the tumour tissue's properties by the host medium's properties. We can see that the tumour tissue actually has a lower permittivity than the host medium, and a higher conductivity. This is a disadvantage of the phantom fabrication process – a lack of specificity in the resulting properties. Figure 98 represents the signature in equation (4) obtained from in lab measurements of the two phantoms. The other signature can also be determined from the measurements however it provided no further insight into the situation.

Table 4: Contrast of Tumour Tissue

Frequency, Hz	ε'(ω)	σ_{eff}	Frequency, Hz	ε'(ω)	σ_{eff}
3.00E+09	0.97366	1.8054	7.16E+09	0.91958	1.2944
3.16E+09	1.0318	1.0508	7.32E+09	0.8186	1.3306
3.32E+09	0.95562	2.1967	7.48E+09	0.82282	1.4827
3.48E+09	0.93696	1.9466	7.64E+09	0.99228	1.2687
3.64E+09	0.88809	2.1778	7.80E+09	0.98059	1.3396
3.80E+09	0.94752	1.6603	7.96E+09	0.86688	1.373
3.96E+09	1.041	1.5693	8.12E+09	0.76946	1.5029
4.12E+09	1.027	1.7005	8.28E+09	0.92448	1.4907
4.28E+09	1.0028	1.7024	8.44E+09	0.989	1.2726
4.44E+09	0.89742	1.7577	8.60E+09	0.90787	1.3706
4.60E+09	0.95663	1.6201	8.76E+09	0.88672	1.4999
4.76E+09	1.0581	1.6847	8.92E+09	0.77064	1.3838
4.92E+09	0.92787	1.6128	9.08E+09	0.75268	1.2974
5.08E+09	0.79999	1.5688	9.24E+09	0.95247	1.2192
5.24E+09	0.90081	1.6074	9.40E+09	0.67051	1.1716
5.40E+09	1.0017	1.3967	9.56E+09	1.5543	1.4634
5.56E+09	1.021	1.4687	9.72E+09	1.0301	2.1848
5.72E+09	0.94758	1.3994	9.88E+09	1.0344	1.25
5.88E+09	0.80669	1.5662	1.00E+10	0.9439	1.121
6.04E+09	0.96087	1.3035	1.02E+10	0.79674	1.1968
6.20E+09	1.0057	1.3799	1.04E+10	0.72666	1.266
6.36E+09	0.94663	1.4427	1.05E+10	0.78355	1.2789
6.52E+09	0.86295	1.428	1.07E+10	0.97189	1.1289
6.68E+09	0.86992	1.4059	1.08E+10	0.923	1.1709
6.84E+09	0.96703	1.4108	1.10E+10	0.8052	1.258
7.00E+09	0.99393	1.2584			

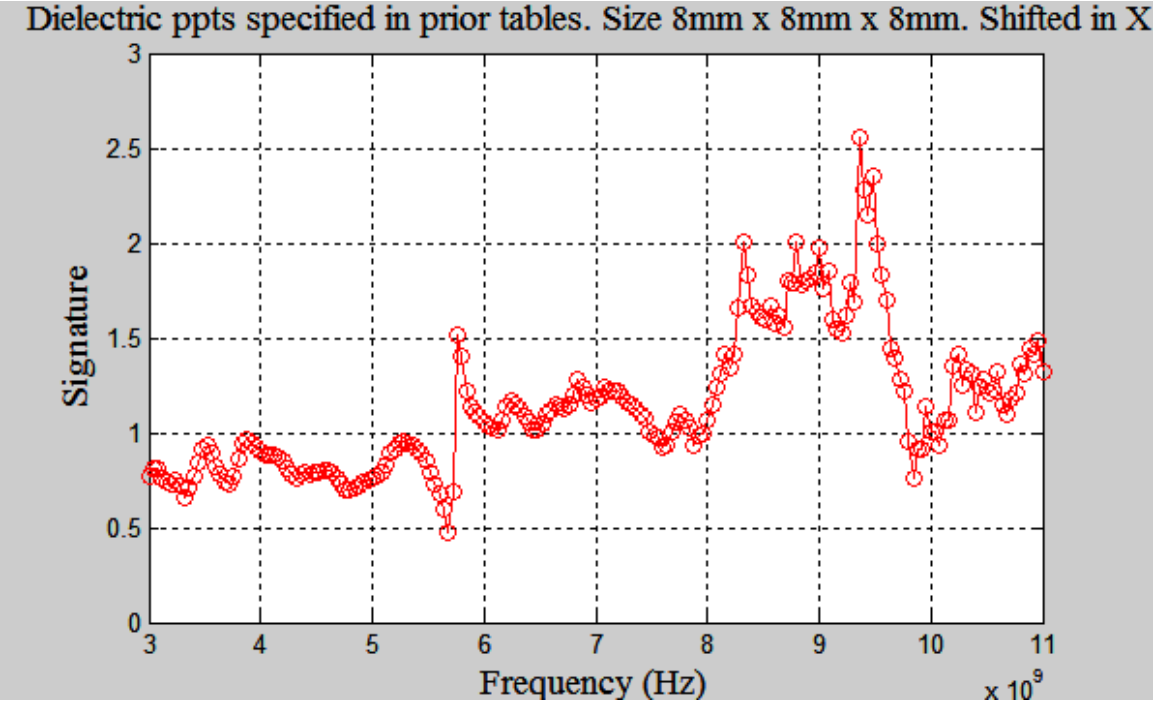

Figure 98: Measured signature according to equation (4). Dielectric properties specified in Table 1 and Table 2. Recall that a shift in the X direction has a completely negligible effect on the tumour signature.

The implications of this result will be discussed in the following section

Discussion

In order to qualify sensitivity, a certain threshold needs to be set. For the magnitude, this threshold was set at 1 dB for the signature present in equation (3), and 0.075 for the signature present in equation (4).

From the simulation data collected and presented in Figure 16 to Figure 24, regarding the S11 parameters with a permittivity contrast of 5 and a varying conductivity contrast, we may safely conclude that the S11 parameter is not sensitive enough to permit an extensive study, and as such it was disregarded for rest of the project.

From the simulation data collected and presented in Figure 25 to Figure 51, regarding the S21 parameters with the permittivity and conductivity contrast being varied, we may conclude that the antenna is sensitive in the frequency range of 3-6 GHz. We may also conclude that at high contrasts, the permittivity and conductivity have antagonistic effects, which may prove detrimental in future attempts at detecting tumours.

From the simulation data collected and presented in Figure 52 to Figure 60, we may conclude that the antenna is not sensitive at any frequency to tumours with sizes less than 6mm by 6mm by 6mm.

From the simulation data collected and displayed in Figure 61, regarding the X direction shift, we may conclude that a shift of the tumour in the X direction results in no change in the tumour signature.

From the simulation data collected and displayed in Figure 62 to Figure 79, regarding the Y direction shift, we may conclude that past a shift of 20mm there is no detectable signature from the tumour.

From the simulation data collected and displayed in Figure 80 to Figure 97, regarding the Z direction shift, we may conclude that past a shift of 20 mm there is assuredly no detectable tumour signature, but in the low frequency range of 3-6 GHz, this shift can be as low as 12mm.

The data collected regarding the Y and Z directional shifts correlates well with theoretical expectation. A main factor in the design of the antenna was the directivity of the power, discussed in more detail in the paper specifying its design [20]. Specifically, the antenna was designed to strongly focus its irradiated power into its frontal aperture. As such, it

makes sense that when the tumour is not in the area of the tissue targeted by the aperture that it be invisible to the antenna.

Comparing the experimental results with the simulations, we can see we have very good agreement in the lower frequency range. In the following comparisons, the experiment is compared to the simulation using a conductivity contrast of 2 and a permittivity contrast of 1. At 3 GHz, our simulation indicates we should have a contrast of approximately 0.073, and in our experiment we have a contrast of almost 0.075, a very close match. At 4 GHz, our simulation predicts we should have a contrast of approximately 0.0744, and we have an experimental contrast of 0.90316. At 5 GHz, our simulation predicts a contrast of 0.025035, and we have a contrast of 0.76034. At a frequency of 6 GHz, our simulation predicts a contrast 0.050059, and our experiments show a contrast of 1.059. At the further frequencies the simulations cannot be reliably trusted and as such no comparison is needed. As one can clearly see, there is very good agreement between the simulation and experiment at the lower frequencies of 3 and 4 GHz and decent agreement between the two at frequencies of 5 and 6 GHz.

An effective method that was used in order to more succinctly represent the data in the presentation was the l2 norm. This method simplified the large quantity of data and gave an easier impression of the sensitivity of the antenna.

Table 5, Table 6, and Table 7 contain the l2 norm that was publicized in the final oral presentation. The l2 norm was calculated using the following equation (7):

$$\left|E_k\right| = \frac{\left|S_{21} - S_{21_{\text{notumour}}}\right|}{\left|S_{21_{\text{notumour}}}\right|}$$
$$D_{mag} = \frac{1}{N}\sqrt{\sum_1^N E_k{}^2} \tag{5}$$

Table 5: l2 norm data for permittivity and conductivity contrasts

Varying Conductivity					
Varying Permittivity	**1**	**2**	**3**	**4**	**5**
1	0	5.77	6.82	7.17	7.92
2	4.51	4.41	6.60	7.56	8.14
3	5.82	5.94	6.90	7.77	8.26
4	5.63	7.37	8.15	8.73	8.85
5	8.50	10.35	10.00	9.75	9.56

Table 6: l2 norm data for Z location shift with a conductivity contrast of 3

Location (mm)	Error (%)	Location(mm)	Error (%)
0	4.88	32	0.45
4	4.36	36	0.44
8	2.44	40	0.44
12	1.13	44	0.39
16	0.33	48	0.56
20	0.3	52	0.55
24	0.32	56	0.54
28	0.5	60	0.5

Table 7: l2 norm data for Y location shift with a conductivity contrast of 3

Location(mm)	Error (%)
20	2.72
24	0.89
28	0.38
32	0.51
36	0.38
40	2.24
44	0.95
48	0.75
52	0.86
36	0.95
60	0.65

Conclusions and Recommendations

As has been shown in the prior discussion section, the antenna has a good sensitivity in its region of interest at low frequencies, such as 3-6 GHz, and can be relied upon to detect tumours with contrasts as low as 2, as shown in experimentation. Further work still needs to be performed in order to fully exploit the potential of the antenna array system. The phase can be a vital source of information, and a method of reliably measuring it in practice must be developed in order to fully take advantage of the potential benefits it offers. Furthermore, analyzing the tumour's effects on the antenna system when the two antennas are cross polarized may also lead to an even stronger sensitivity to tumours in the tissue. Potential designs for 3 or 4 antennas in an array should also be briefly considered, even though the preliminary results of this study indicate that the signal power received at the side antennas may not be sufficient to detect the tumour. Further work is currently being performed utilizing more heterogeneous breast phantoms in an effort to more accurately represent the breast. The results of this study give a solid foundation for the efficacy microwave imaging to detect breast cancer, specifically the effectiveness of the TEM horn antenna which has been designed for this purpose.

Appendix

Table 8: Design Parameters used for Antenna

Parameter	Value (mm)	Parameter	Value (mm)
l	39.6	w_3	38.0
w	31.2	x_1	8.0
h	22.6	x_2	21 .0
a	8.3	x_3	28 .0
b	5 .0	x_4	32.0
c	11.4	x_5	15.0
r	10.5	y_1	5.0
d	5.0	y_2	2.0
L	75.9	y_3	4.0
s	38.0	y_4	5.0
t	47.0	z_1	14.0
w_1	14.0	z_2	55.3
w_2	29.0	z_3	23.0

Table 9: Values for S11 parameters at a permittivity contrast of 5. 8mm x 8mm x 8mm. Unsuited.

	Frequency (GHz)								
Conductivity Contrast	3	4	5	6	7	8	9	10	11
1	0.333	0.253	0.146	0.200	0.356	0.102	0.061	0.370	0.353
2	0.333	0.254	0.145	0.201	0.358	0.096	0.070	0.384	0.346
3	0.333	0.254	0.145	0.201	0.358	0.097	0.072	0.382	0.345
4	0.333	0.254	0.144	0.201	0.359	0.096	0.073	0.384	0.347
5	0.333	0.254	0.144	0.201	0.359	0.097	0.073	0.385	0.346

Table 10: Values for S11 signature specified in equation (4). Permittivity contrast of 5. 8mm x 8mm x 8mm. Unshifted.

	Frequency (GHz)								
Conductivity Contrast	3	4	5	6	7	8	9	10	11
1	0.081	0.200	0.142	0.017	0.008	0.065	0.031	0.033	0.026
2	0.082	0.205	0.145	0.011	0.013	0.004	0.197	0.073	0.046
3	0.082	0.204	0.148	0.012	0.014	0.006	0.215	0.067	0.050
4	0.081	0.205	0.154	0.012	0.016	0.002	0.233	0.072	0.043
5	0.081	0.204	0.153	0.013	0.015	0.005	0.242	0.074	0.045

Table 11: Values for S21 parameter when no tumour is present in the tissue

	Frequency (GHz)								
	3	4	5	6	7	8	9	10	11
No Tumour	0.010646	0.005974	0.001472	0.001035	0.0002	7.34E-05	5.19E-05	3.60E-05	1.06E-05

References

[1] S. Gabriel, R. W. Lau, and C. Gabriel, "The dielectric properties of biological tissues—Part II: Measurement in the frequency range 10 Hz to 20 GHz," *Phys. Medicine Biol*., vol. 41, pp. 2251–2269, 1996.

[2] M. Lazebnik, L. McCartney, D. Popovic, C. B. Watkins, M. J. Lindstorm, J. Harter, S. Sewall, A. Magliocco, J. H. Brooske, M. Okoniewski and S. C. Lazebnik, " A large – scale study of the ultra wideband microwave dielectric properties of normal breast tissue obtained from reduction surgeries," *Phys. Med. Biol*., vol.52, pp.2637-2656, April 2007.

[3] Ahmedin Jemal, Rebecca Siegel, Elizabeth Ward, Yongping Hao, Jiaquan Xu, Taylor Murray and Michael J. Thun, "Cancer Statistics, 2008" *CA Cancer J Clin* 2008;58;71-96; originally published online Feb 20, 2008;

[4] AIHW Australian Institute of Health and Welfare & National Breast Cancer Centre 2006. "Breast cancer in Australia: an overview, 2006". Cancer series no. 34. cat. no. CAN 29. Canberra

[5] GLOBOCAN 2002: "Cancer Incidence, Mortality and Prevalence Worldwide", IARC CancerBase No. 5. version 2.0, IARCPress, Lyon, 2004

[6] National Research Council. Advisory Committee on the Biological Effects of Ionizing Radiations; Oak Ridge Associated Universities; Federal Coordinating Council for Science, Engineering, and Technology. Committee on Interagency Radiation Research and Policy Coordination, *Health effects of exposure to low levels of ionizing radiation*, National Academy Press, Washington, D.C., 1990..

[7] Feig S, Hendrick R. "Radiation risk from screening mammography of women aged 40-49 years". *J Natl Cancer Inst Monogr*: 119–24.

[8] Efficacy of MRI and Mammography for Breast-Cancer Screening in Women with a Familial or Genetic Predisposition, The New England Journal of Medicine

[9] Bancej C, Decker K, Chiarelli A, et al. "Contribution of clinical breast examination to mammography screening in the early detection of breast cancer". *J Med Screen* 2003; 10: 16–21

[10] Bobo JK, Lee NC, Thames SF. “Findings from 752,081 clinical breast examinations reported to a national screening program from 1995 through 1998”. *J Natl Cancer Inst* 2000; 92: 971–976.

[11] Oestreicher N, White E, Lehman CD, et al. “Predictors of sensitivity of clinical breast examination (CBE)”. *Breast Cancer Res Treatment* 2002; 76: 73–81.

[12] Elmore JG, Barton MB, Moceri VM, Polk S, Arena PJ, Fletcher SW. Ten-year risk of false positive screening mammograms and clinical breast examinations. N Engl J Med. 1998;338:1089-96. [PMID: 9545356]

[13] Semiglazov VF, Moiseyenko VM, Bavli JL, Migmanova NSh, Seleznyov NK, Popova RT, et al. “The role of breast self-examination in early breast cancer detection (results of the 5-years USSR/WHO randomized study in Leningrad)”. Eur J Epidemiol. 1992;8:498-502. [PMID: 1397215]

[14] Semiglazov VF, Moiseenko VM, Manikhas AG, Protsenko SA, Kharikova RS, Popova RT, et al. “Interim results of a prospective randomized study of self-examination for early detection of breast cancer (Russia/St.Petersburg/WHO)”. Vopr Onkol. 1999;45:265-71. [PMID: 10443229]

[15] Thomas DB, Gao DL, Self SG, Allison CJ, Tao Y, Mahloch J, et al. Randomized trial of breast self-examination in Shanghai: methodology and preliminary results. J Natl Cancer Inst. 1997;89:355-65. [PMID: 9060957]

[16] Joshua J. Fenton, Mary B. Barton, Ann M. Geiger, Lisa J. Herrinton, Sharon J. Rolnick, Emily L. Harris, William E. Barlow, Lisa M. Reisch, Suzanne W. Fletcher, Joann G. Elmore, Screening Clinical Breast Examination: How Often Does It Miss Lethal Breast Cancer?, *JNCI Monographs* 2005, vol. 2005: n 35: pp. 67-71;

[17] National Inventory of Selected Imaging Equipment, Canadian Coordinating Office for Health Technology Assessment (MRIs in hospitals, 1991–2001); National Survey of Selected Medical Imaging Equipment. Canadian Institute for Health Information (2003-2007), supplemented by information from provincial ministries of health.

[18] Rublee D. Medical technology in Canada, Germany and the United States. *Health Aff (Millwood)* 1994;13:113-7

[19] National Inventory of Selected Imaging Equipment, Canadian Coordinating Office for Health Technology Assessment (MRIs in hospitals, 1991–2001); National Survey of Selected Medical Imaging Equipment. Canadian Institute for Health Information (2003-2007), supplemented by information from provincial ministries of health.

[20] Reza's Antenna.

[21] Meaney, P. M., M. W. Fanning, T. Raynolds, C. J. Fox, Q. Fang, C. A. Kogel, S. P. Poplack, and K. D. Paulsen, "Initial clinical experience with microwave breast imaging in women with normal mammography," *Acad Radiol*., Vol. 14, No. 2, 207–218, February 2007.

[22] Sill, J. M. and E. C. Fear, "Tissue sensing adaptive radar for breast cancer detection: study of immersion liquids," *Electron. Lett.*, Vol. 41, No. 3, 113–115, 2005.

[23] Chung, K., S. Pyun, and J. Choi, "Design of an ultra wide-band TEM horn antenna with a microstrip-type balun," *IEEE Trans. Antennas and Propag.*, Vol. 53, No. 10, 3410–3413, October 2005.

[24] Y. Okano, K. Ito, and H. Kawai, "Solid phantom composed of glycerin and its application to SAR estimation," *IEICE Trans. Commun*. (Japanese Edition), vol.J83-B, no.4, pp.534–543, April 2000.

[25] Xing Yun, Elise C. Fear, Ronald H. Johnston, "Compact Antenna for Radar-Based Breast Cancer Detection" *IEEE Transactions on Antennas and Propagation*, vol. 53, no. 8, August 2005

[26] S. Nikolaou, G.E. Ponchak, J. Papapolymerou and M.M. Tentzeris, "CPW-fed Elliptical Slot UWB Antenna with a Tuning Uneven U-shape Stub on Liquid Crystal Polymer (LCP)", *Proc. Of the 2006 ACES Conference, Miami, FL, March 2006.*

[27] Tavassolian, N.; Nikolaou, S.; Tentzeris, M.M., "Microwave Tumor Detection Using a Flexible UWB Elliptical Slot Antenna with a Tuning Uneven

U-shape Stub on LCP", *Antennas and Propagation International Symposium*, 2007 IEEE, June 2007 pp. 257 - 260

Vitae

Alistair Johnson is currently a 4th year undergraduate student at McMaster university. His degree will be conferred in May of 2009.